Astronomy & Astrophysics manuscript no. f100
March 9, 2021

The SPHERE infrared survey for exoplanets (SHINE)*

I Sample definition and target characterization

S. Desidera[1], G. Chauvin[2], M. Bonavita[3,4,1], S. Messina[5], H. LeCoroller[6], T. Schmidt[7,8], R. Gratton[1], C. Lazzoni[1,9], M. Meyer[10,11], J. Schlieder[12,13], A. Cheetham[14,13], J. Hagelberg[14], M. Bonnefoy[2], M. Feldt[13], A-M. Lagrange[2], M. Langlois[6,15], A. Vigan[6], T.G. Tan[16], F.-J. Hambsch[17], M. Millward[18], J. Alcalá[19], S. Benatti[20], W. Brandner[13], J. Carson[21,13], E. Covino[19], P. Delorme[2], V. D'Orazi[1], M. Janson[13,22], E. Rigliaco[1], J.-L. Beuzit[6], B. Biller[3,4,13], A. Boccaletti[8], C. Dominik[23] F. Cantalloube[13], C. Fontanive[24,1], R. Galicher[8], Th. Henning[13], E. Lagadec[25], R. Ligi[26], A-L. Maire[27,13], F. Menard[2], D. Mesa[1], A. Müller[13], M. Samland[13], H.M. Schmid[11], E. Sissa[1], M. Turatto,[1], S. Udry[14], A. Zurlo[28,29,6] R. Asensio-Torres[13], T. Kopytova[13,30,31], E. Rickman[14], L. Abe[25], J. Antichi[32], A. Baruffolo[1], P. Baudoz[8], J. Baudrand[8], P. Blanchard[6], A. Bazzon[11], T. Buey[8], M. Carbillet[25], M. Carle[6], J. Charton[2], E. Cascone[1], R. Claudi[1], A. Costille[6], A. Deboulbé[2], V. De Caprio[19], K. Dohlen[6], D. Fantinel[1], P. Feautrier[2], T. Fusco[33], P. Gigan[8], E. Giro[1,26], D. Gisler[11], L. Gluck[2], N. Hubin[34], E. Hugot[6], M. Jaquet[6], M. Kasper[34,2], F. Madec[6], Y. Magnard[2], P. Martinez[25], D. Maurel[2], D. Le Mignant[6], O. Möller-Nilsson[13], M. Llored[6], T. Moulin[2], A. Origné[6], A. Pavlov[13], D. Perret[8], C. Petit[33], J. Pragt[35], P. Puget[2], P. Rabou[2], J. Ramos[13], F. Rigal[23], S. Rochat[2], R. Roelfsema[35], G. Rousset[8], A. Roux[2], B. Salasnich[1], J.-F. Sauvage[33], A. Sevin[8], C. Soenke[33], E. Stadler[2], M. Suarez[33], L. Weber[14], F. Wildi[14]

(Affiliations can be found after the references)

ABSTRACT

Context. Large surveys with new-generation high-contrast imaging instruments are needed to derive the frequency and properties of exoplanet populations with separations from ∼5 to 300 au. A careful assessment of the stellar properties is crucial for a proper understanding of when, where, and how frequently planets form, and how they evolve. The sensitivity of detection limits to stellar age makes this a key parameter for direct imaging surveys.
Aims. We describe the SpHere INfrared survey for Exoplanets (SHINE), the largest direct imaging planet-search campaign initiated at the VLT in 2015 in the context of the SPHERE Guaranteed Time Observations of the SPHERE consortium. In this first paper we present the selection and the properties of the complete sample of stars surveyed with SHINE, focusing on the targets observed during the first phase of the survey (from February 2015 to February 2017). This early sample composed of 150 stars is used to perform a preliminary statistical analysis of the SHINE data, deferred to two companion papers presenting the survey performance, main discoveries, and the preliminary statistical constraints set by SHINE.
Methods. Based on a large database collecting the stellar properties of all young nearby stars in the solar vicinity (including kinematics, membership to moving groups, isochrones, lithium abundance, rotation, and activity), we selected the original sample of 800 stars that were ranked in order of priority according to their sensitivity for planet detection in direct imaging with SPHERE. The properties of the stars that are part of the early statistical sample were revisited, including for instance measurements from the GAIA Data Release 2. Rotation periods were derived for the vast majority of the late-type objects exploiting TESS light curves and dedicated photometric observations.
Results. The properties of individual targets and of the sample as a whole are presented.

Key words. Stars: fundamental parameters - Stars: rotation - Stars: activity - Stars: pre-main sequence - Stars: kinematics and dynamics - (Stars:) binaries: general

1. Introduction

Today's success in direct imaging of exoplanets is intimately connected to the pioneering work in the previous decades to develop adaptive optics (AO) systems, infrared detectors, coronagraphs, and differential imaging techniques for ground-based telescopes (Mawet et al. 2012; Chauvin 2018). With the advent of dedicated instruments on 5-10 m telescopes (e.g., LBT, Palomar, Subaru, Keck, VLT, Gemini, and Magellan), high-contrast imaging (HCI) demonstrated the ability to detect and characterize exoplanets and planetary systems, confirming that ground-based instrumentation may reach performance levels that could compete with those from space. Early large systematic surveys of young nearby stars led to the discovery of the first planetary-mass companions at large separations (> 100 au) or with a low mass ratio relative to their stellar host (Chauvin et al. 2004, 2005b; Neuhäuser et al. 2005; Luhman et al. 2006; Lafrenière et al. 2008), followed by

* Tables 5-11 are only available in electronic form at the CDS via anonymous ftp to cdsarc.u-strasbg.fr (130.79.128.5) or via http://cdsweb.u-strasbg.fr/cgi-bin/qcat?J/A+A/

the breakthrough discoveries of closer planetary-mass companions such as HR 8799 bcde (Marois et al. 2008, 2010), β Pictoris b Lagrange et al. (2009), κ And b (Carson et al. 2013), HD 95086 b (Rameau et al. 2013a), and GJ 504 b (Kuzuhara et al. 2013). This allowed a first systematic characterization of the giant planet population with separations typically $\geq$ 20-30 au (e.g., Biller et al. 2007; Lafrenière et al. 2007; Heinze et al. 2010; Chauvin et al. 2010; Vigan et al. 2012; Rameau et al. 2013b; Nielsen et al. 2013; Wahhaj et al. 2013; Brandt et al. 2014; Chauvin et al. 2015; Galicher et al. 2016; Bowler 2016; Vigan et al. 2017). These early results confirmed that direct imaging is an important complementary technique in terms of discovery space with respect to other planet hunting techniques like radial velocity, transit, μ-lensing and astrometry (e.g., Johnson et al. 2010; Howard et al. 2010; Mayor et al. 2011; Sumi et al. 2011; Cassan et al. 2012; Bonfils et al. 2013; Meyer et al. 2018; Fernandes et al. 2019). Nowadays, direct imaging brings a unique opportunity to explore the outer part of exoplanetary systems with separations beyond ~5 au to complete our view of planetary architectures, and to explore the properties of relatively cool giant planets. The advent of the new generation of extreme-AO planet imagers like SPHERE (Beuzit et al. 2019) and GPI (Macintosh et al. 2014) connected to systematic surveys of hundreds young nearby stars led to new discoveries like 51 Eri b (Macintosh et al. 2015), HIP 65426 b (Chauvin et al. 2017b), and PDS 70 b and c (Keppler et al. 2018; Haffert et al. 2019; Mesa et al. 2019). However, the low rate of discoveries despite the unprecedented gain in detection performance achieved with SPHERE and GPI showed that massive giant planets with an orbital semi-major axis beyond 10 au are rare (Nielsen et al. 2019).

On the other hand, the gain in performance allows a much better characterization of exoplanetary systems and exoplanets themselves. In direct imaging the exoplanet's photons can indeed be spatially resolved and dispersed to directly probe the atmospheric properties of exoplanets and brown dwarf companions. In comparison to generally older free-floating substellar objects, exoplanets discovered by high-contrast imaging are younger, hotter, and brighter. Their atmospheres show low-gravity features, and the presence of clouds and non-equilibrium chemistry processes. These physical conditions are very different and complementary to those observed in the atmospheres of hot Jupiters (observed in transmission or via secondary-eclipse). A large number of young brown dwarf and exoplanet atmospheres have been systematically characterized to test our current understanding of the processes at play in the atmospheres of substellar objects and to test evolutionary models including HR 8799 bcde (Ingraham et al. 2014; Bonnefoy et al. 2016; Greenbaum et al. 2018), 51 Eri b (Rajan et al. 2017; Samland et al. 2017), β Pictoris b (Chilcote et al. 2017), HD 95086 b (De Rosa et al. 2016; Chauvin et al. 2018), HIP 65426 b (Chauvin et al. 2017b; Cheetham et al. 2019), HIP 64892 B (Cheetham et al. 2018), and PDS 70 b and c (Müller et al. 2018; Mesa et al. 2019).

Regarding planetary architectures, relative astrometry at 1-2 mas precision with SPHERE and GPI opens up a new parameter space to carry out a precise monitoring of the orbital motion of a handful of exoplanets and brown dwarfs. This constrains their orbital properties and allows the exploration of the dynamical stability of the whole architecture. Examples of systems for which this analysis was done include β Pictoris (Wang et al. 2016; Lagrange et al. 2019), HR 8799 (Wang et al. 2018), HD 95086 (Rameau et al. 2016; Chauvin et al. 2018), HR 2562 (Maire et al. 2018), 51 Eri (Maire et al. 2019; De Rosa et al. 2020), and GJ 504 (Bonnefoy et al. 2018).

The current instrumentation does not yet allow us to detect mature planets reflecting star light, except perhaps for the closest and brightest stars. The focus of direct imaging programs is therefore on thermal emission from young planets because they are expected to be brighter than their older counterparts. For this same reason they are very useful to directly probe the presence of planets within the environment where they form, the circumstellar disks. This allows us to connect the spatially resolved structures of circumstellar disks (e.g., warp, cavity, rings, vortices) with imaged or unseen exoplanets. This is a fundamental and inevitable path to understand the formation of giant planets, and more generally planetary architectures favorable to the formation of smaller rocky planets with suitable conditions to host life (Barbato et al. 2018; Bryan et al. 2019). Studying the demographics of exoplanets is particularly important in order to understand the architecture and the formation and evolution of exoplanets. Giant planets dominate the architecture of planetary systems from a dynamical point of view, with impact on the subsequent formation and evolution of smaller planets, the distribution of water in the system, and thus the chances for habitability.

Within this framework, we planned the SpHere INfrared survey for Exoplanets (SHINE; Chauvin et al. 2017a). This survey uses a total of 200 nights that were allocated in visitor mode (typically affected by 20% of poor conditions for AO) and makes up a large fraction of the SPHERE consortium Guaranteed Time Observations allocated by ESO for the design and construction of the SPHERE instrument (Beuzit et al. 2019). SHINE has been designed by the SPHERE consortium to: (i) identify new planetary and brown dwarf companions and provide a first-order characterization; (ii) study the architecture of planetary systems (multiplicity and dynamical interactions); (iii) investigate the link between the presence of planets and disks (in synergy with the GTO program aimed at disk characterization); (iv) determine the frequency of giant planets with semi-major axes beyond 5 au; and (v) investigate the impact of stellar mass (and even age if possible) on the frequency and characteristics of planetary companions over the range ~0.5 to 3.0 $M_{\odot}$.

SHINE started in February 2015 and is planned to be completed by July 2021, with observation of a total of about 500 young nearby stars. This is the first in a series of three papers describing early results obtained from the analysis of about one-third of this very large sample, in which we consider only those targets whose first observation was done before February 2017. We chose this cut-off date as second-epoch observations with time separations of 1-2 years were required for a large number of candidates to vet physical companions from field stars (mainly background). This sample, hereafter referred to as F150 (as it consists of 150 stars), is already large enough for a first statistical discussion of the incidence of massive planets at a separation $\geq$ 5 au, and to have a first indication of the formation scenarios for giant planets. This paper describes the general characteristics of the survey and the observed sample. A second paper (Langlois et al. 2020, A&A, in press; Paper II) describes the observations and analysis methods, and presents the results in terms of detection and upper limits, while a third paper (Vigan et al. 2020, Paper III) presents the statistical analysis and a discussion of the implications, as derived from the F150 sample.

The paper is organized as follows: Section 2 describes the SHINE survey, its science goals, and the target selection criteria. Section 3 presents the selection of the complete SHINE sample and the priority ranking. Section 4 describes the F150 subsample used for the early statistical analysis. In Sect. 5 we derive the most relevant parameters of individual targets and in Sect. 6 we present the ensemble properties of the sample. Section 7 summarizes the results. Appendix A includes notes on individual targets.

2. Design of the SHINE survey

In order to achieve its scientific goals, the design and selection of the SHINE sample was of prime importance to optimally exploit a total of 200 nights of Guaranteed Time Observations with SPHERE at VLT dedicated to this campaign. Since massive planets at large separations are rare with a typical frequency of a few percent (see, e.g. Vigan et al. 2017; Nielsen et al. 2019), several hundred targets must be surveyed in order to lead to new discoveries and set precise constraints on the occurrence of giant planets beyond 5 au. Having a sample that is complete (in terms of distance, age, or limiting magnitude) likely implies a low efficiency. On the other hand, a proper statistical discussion requires well-defined selection criteria. The approach we considered to combine these apparently conflicting issues was to start from a very large sample of potential targets for which a wide set of properties, including magnitude, distance, mass, and age, was known (determined by us). We then divided them into priority groups according to a figure of merit (FoM) determined from these properties. A higher value for this FoM implies a higher probability that a star has a planet possibly detectable by SPHERE according to a specified model describing the planet distribution. To reduce the possibility that results will be poor because the selected model is not appropriate, the final priority list was actually obtained combining rankings given by two completely different models (see Sect. 2.3). This approach allows a reasonably high efficiency in detecting planets combined with the requirement of well-defined selection criteria, that can be finally considered in the statistical analysis.

The survey design included the optimization of the number of visits versus observing time per visit. We adopted as a compromise a visit of about 1.5 hours including pointing and AO setup overheads. This ensures a field rotation of $\geq$ 30 degrees for most declinations in the case of observations including the meridian passage, allowing good removal of the speckle patterns using angular differential imaging (ADI; Marois et al. 2006). Longer exposures provide little improvement because of the limited additional field rotation. Shorter exposures would allow us to observe more targets, but would imply significant degradation of the achievable contrast for individual observations. Considering that the available number of high-merit targets (nearby very young stars) is not particularly large (see below), this would imply a smaller number of expected detections.

In the original survey design we planned to devote 70% of the time to first-epoch observations, 20% to second epochs for common proper motion confirmation, and 10% to additional characterization observations, exploiting the variety of observing modes available for SPHERE. The estimate of the amount of time needed for second-epoch observations was based on predictions of the background star contamination rate in the SPHERE field of view using Galactic population models (e.g., Robin & Creze 1986) and our target coordinates.

The selected setup for the survey used the IRDIFS mode, allowing simultaneous observations in YJ range ($0.95 - 1.35\,\mu m$ using IFS (Claudi et al. 2008) over a small field of view ($1.77'' \times 1.77''$) and observations in two narrowband filters in H-band using IRDIS (Dohlen et al. 2008) over a $11'' \times 11''$ field of view. The two narrowband filters (H2 and H3, Vigan et al. 2010) were selected for their sensitivity to methane-dominated objects (H2-H3 $\leq$ 0.0 mag) and to very red, late L objects (H2-H3 $\sim$ 0.0-0.5 mag). Field stars have an H2-H3 color close to zero, allowing the implementation of a robust priority scheme for the confirmation of the candidates (see Paper II for details).

2.1. The SHINE database

Over the past ten years we assembled a large sample of young stars with the main goal of preparing the SHINE survey. This work included the determination of several stellar properties, either from the analysis of new observations or from the literature. The database was also used to select samples for other programs, such as the NaCo Large Program for Exoplanet Imaging (NaCo-LP; Chauvin et al. 2015), the SPOTS survey for circumbinary planets (Asensio-Torres et al. 2018), the HARPS Large Program for planets around young stars (Grandjean et al. 2020), the search for planets around young stars in the framework of the GAPS program at TNG (Carleo et al. 2020), and several other programs.

The determination of target parameters is mostly based on the methods described in the NaCo-LP target characterization paper (Desidera et al. 2015). Briefly, stellar ages were obtained from a combination of age methods (membership to groups, lithium, rotation, activity, kinematics, isochrone fitting). Moving groups (MGs) membership was taken from Torres et al. (2008), with updates from the literature in the following years. Ages of moving groups were those adopted by Desidera et al. (2015) (their Table 8). Stellar distances were taken from Hipparcos trigonometric parallax when available (van Leeuwen 2007), otherwise the (age-dependent) photometric distances derived as done in Desidera et al. (2015) were adopted. Stellar masses were derived following the Reid et al. (2002) calibrations. The original values of stellar mass, distance, and age are listed in Table 11. Comparison with the updated values derived in this paper (Sect. 5) shows a nice agreement for the distance (mean difference 3.7 pc, rms 9.4 pc), a small offset in stellar age (0.13 dex with rms 0.21 dex, with the original ages being younger), and a systematic difference in stellar masses above 1.8-2.0 $M_{\odot}$ (the original mass being smaller) and a fairly good agreement below this value. This last difference has some impact on the actual upper limit in mass for the sample (see below), but otherwise the use of the original parameters with respect to the updated ones derived in this paper should have a minor impact on the target selection and the priority scheme defined below. Originally the sample was limited to distances closer than 100 pc; it was complemented with stars in the Sco-Cen OB association (e.g., de Zeeuw et al. 1999) to reach a suitable number of young, early-type stars (from early F to late B) at slightly larger distances.

For the final selection of the SHINE sample, we first identified some general selection criteria, driven by the characteristics of the SPHERE instrument (coordinates of the site; magnitude limit for good performance of the AO system) or by the science goals described above. The following selection criteria were set:

1. Declination limits between -84 and +21 degrees to ensure observations at airmass values of less than 2;
2. Wavefront sensor (WFS) flux[1] > 5 e-/subpup/frame or $R \leq 11.5$ (to ensure good quality of AO correction, being on the conservative side of estimates from the SPHERE performance simulations available at the time of target selection);
3. Exclusion of known spectroscopic and close visual binaries (projected separation < 6 arcsec, i.e., within the IRDIS field of view)[2]. This is motivated by the technical limitations of AO working and ADI processing for spatially resolved binaries and by our scientific choice of having a homogeneous sample of single stars or components of wide binaries without the complications of the severe dynamical influence of stellar companions or of uncertain process of planet formation and evolution in circumbinary disks;
4. Age $<$ 800 Myr because planets are too faint at older ages for wavelengths $< 2.3\mu m$;
5. Distance $<$ 100 pc to probe the smallest physical separations, except for Sco-Cen members, as this region is rich in young early-type stars;
6. $M_{*} < 3\ M_{\odot}$. This limit was set because the frequency of planets detected using radial velocities (RV) appears to drop above this mass (Reffert et al. 2013). We did not set any explicit lower-mass cutoff, though an implicit limit was set by the requirement on AO flux. Our survey then covers the full range 0.5 to 3.0 $M_{\odot}$, which allows us to explore the influence of stellar mass.

The sample has no explicit biases related to the presence of disks nor to metallicity. At young ages metallicity determinations are quite sparse (Biazzo et al. 2012; Viana Almeida et al. 2009). The available results point toward a metallicity close to solar for stars younger than ∼200 Myr in the solar vicinity. The metallicity dispersion becomes significant for older stars, which constitute a very small fraction of our sample.

The resulting list satisfying the above criteria at the time of freezing the SHINE sample (May-August 2014) included 1224 targets; this is larger by about 50% with respect to the sample to be selected (800 stars), which in turn is almost twice the number of stars that could be effectively observed.

2.2. Target priorities

A well-defined priority scheme is necessary in order to run an efficient survey on a sample of several hundred targets because the potential for exoplanet discovery is very different from star to star, depending on age, distance, mass, and magnitude. Ideal targets are very young stars close to the Sun. Simulations described in Sect. 2.3 were performed on this extended list in order to estimate the potential for planet detectability of each target and drive the final target selection.

The priority assignment applied to the SHINE database is the following:

1. Build a FoM that allows the stars to be ranked according to the probability that they host planets potentially detectable by SPHERE. To estimate this probability, we used *i)* planet population models based on power laws in planet mass and separation, with cutoffs at large separations; combined with stellar ages this enables the planet luminosity to be estimated via suitable evolution models; *ii)* the MESS code (Multi-purpose Exoplanet Simulation System, see Bonavita et al. 2012, 2013, for details)[3] that allows the planet position to be projected on the sky at the epoch of observation; and *iii)* expected contrast limits appropriate for each star given the stellar properties (distance, age, magnitude). These three different aspects of the construction of the FoM are described in the next subsection.
2. Sort the parent sample according to this FoM and construct an optimal 400 star sample as high priority (List 400), and complete it with additional targets to fill in according to rank order, lower priority, up to 100% oversubscription (List 400+). The final sample reaches 800 stars[4].
3. Check that this optimized-for-detections sample covers a reasonably wide distribution in stellar mass.
4. Consider some adaptions of this sample, such as *i)* inclusion of homogeneous subsamples, as volume-limited members of nearby young moving groups and *ii)* limiting the number of Sco-Cen members to 20% of the sample because these stars have a limited span in right ascension, and the background contamination is often large due to their low galactic latitude, which has a severe impact on the expected need for second-epoch observations.

2.3. Simulations of planet detectability

In order to define the FoM to be used to select the final SHINE sample, we estimated the expected survey yield as a function of the target list as well as the assumptions on the underlying characteristics of the planet population. For this purpose we used the MESS (see Bonavita et al. 2012, for details) code to evaluate the probability of detecting a companion given the expected instrument performance. The synthetic companions were generated according to two different models, both based on the one described by Cumming et al. (2008), that is, adopting power-law distributions for the companion mass and semi-major axis.

[1] Flux as seen by the SPHERE WFS sensor; see Beuzit et al. (2019) for details.

[2] Preparatory observations of part of the sample were performed with FEROS (Mouillet et al. 2010; Desidera et al. 2015) and with AstraLux (Hormuth et al. 2008).

[3] An updated version of the MESS code, now called Exoplanet Detection Map Calculator (Exo-DMC Bonavita 2020), is available for download at https://github.com/mbonav/Exo_DMC

[4] This is significantly larger than the sample size allowed by the available observing time, but we decided to oversize the sample in order to have enough flexibility on the scheduling, considering the requirement of observing the targets including the meridian passage.

Both models are defined so that the resulting frequency of companions F is consistent with the value of the fraction of planets per star retrieved by Cumming et al. (2008) ($F_0 = 0.0394$) if calculated over the same parameter space (mass: $1 - 13\ M_{Jup}$, semi-major axis: $0.3 - 2.5$ au, stellar mass: $0.7 - 1.6\ M_\odot$, [Fe/H]: $-0.5 - +0.5$.). This implies the use of a normalization factor C_0 defined as follows:

$$F_0 = C_0 \int_{0.7M_\odot}^{1.6M_\odot} dM * \int_{1M_{Jup}}^{13M_{Jup}} m^{-1.3}\ dm \int_{0.3au}^{2.5au} a^{-0.61}\ da \tag{1}$$

The companion mass range was fixed at $m_{max} = 75\ M_{jup}$ for all the targets in the first model (hereafter Mod01). For the second model (hereafter Mod02) we instead adopted $m_{max} = 0.03 \times M_* \frac{M_{Jup}}{M_\odot}$. Mod02 also includes a dependency on the stellar mass for the expected value of the frequency. For this model the normalization factor is in fact expressed as $C_0 f(M_*)$, where $f(M_*)$ is a mass function that ensures that the resulting number of companions increases linearly with stellar masses up to 2 $M_\odot$, and is zero for stellar masses higher than 3 $M_\odot$, following the findings of Reffert et al. (2013) for close-in planets.

The main difference between the two models is therefore that for Mod02 the properties of the generated planet population are not fixed, but change for each target. For this reason, a ranking based only on Mod02 would introduce a bias towards A-F stars. The use of both models combined instead supports the selection of a more balanced sample, which is necessary to assess the dependence of planet frequency on stellar mass, which is one of the main scientific drivers of the survey.

For all the stars in the initial list we evaluated the expected SPHERE detection limits, expressed in terms of luminosity contrast versus projected separation (shown in the left panel of Fig. 1), using the method described in Mesa et al. (2015). The models of Baraffe et al. (2003) were then used to estimate the corresponding minimum detectable companion mass M_{lim} [5] (see Fig. 1, right panel), under the assumption that any companion would be coeval with its host star, hence using the age of the star to select the appropriate evolutionary track. To take into account the fact that the detection limits are expressed in projected separation, while the models produces semi-major axis values, the code evaluates the probability that a companion with a given semi-major axis can have a projected separation which would put it inside the field of view (FoV). This is done assuming a random orbital phase and eccentricity drawn from a Gaussian distribution (see Bonavita et al. 2012, for details).

For each model we performed six MESS runs, using the list of 1244 targets from the SHINE database, but changing the following parameters:

- the value of the age used for the magnitude to mass conversion of the detection limits (the adopted age of each star, as well as the minimum and maximum values) in order to properly estimate the impact of the uncertainty on the age on the survey results.
- the cutoff of the semi-major axis distribution, which was set at 15 or 30 au (a value of 50 au was used for the Sco-Cen members to take into account the larger distance of this region with respect to the other targets in the list).[6]

Table 1 summarizes the outcome of the simulations, in terms of expected detection yield, assuming a sample made of the best 400 targets ranked according to each model. The values obtained using the 15 au and the 30 au cutoff values are both shown, and those obtained using the minimum and maximum values of the stellar age for the magnitude to mass conversion of all the detection limits.

Table 1: Summary of the expected detection yield for the best 400 targets ranked according to the different models. The same values obtained considering the minimum and maximum estimated age of each target are also shown. The number of Sco-Cen members (for which the cutoff is always 50 au) is reported in the last column.

Model, cutoff	Number of expected detections			Sco-Cen
	adopt. age	min. age	max age	Members
Mod01, 15 au	24.73	28.29	22.41	15
Mod01, 30 au	48.27	53.65	44.82	35
Mod02, 15 au	16.12	18.89	14.25	2
Mod02, 30 au	30.22	34.25	27.12	12

The expected number of detections in Table 1 is larger than the actual number (although the final number of detection from SHINE is not yet available, pending the completion of the second-epoch observations). This indicates that some of the assumptions we made in the simulations are not adequate. The dependency of planet frequency on semi-major axis is likely the most prominent case. There were already hints at the time of the sample selection that the extrapolations of RV-based power laws with outer cutoff are not ideal, considering both the few individual detections at very wide separations, and low frequency of substellar companions resulting from various surveys. However, alternative distributions such the log-normal distribution by Meyer et al. (2018) were published a few years later. Therefore, we were expecting the outcome of our simulations to be overestimating the number of new discoveries since the beginning of the survey, and in this perspective we planned only a limited amount of time for characterization observations in the original survey design (see Sect. 2). In spite of these limitations, we consider our simulations

[5] Alternative sets of models available at the time of sample building were considered but not used because of the lack of grid covering our space of parameters of our interest and/or because of counter-examples already available at that time against some of these models, such as the extreme cold-start scenario by Marley et al. (2007).

[6] This allowed us a proper ranking of the Sco-Cen targets, which would not be reliable for closer cutoff values. A cutoff as large as 50 au was already ruled out at the time of the sample selection for solar-type stars. The situation was less clear for more massive stars, with possible scaling of planet distribution in mass (following the mass ratio) and in separation (following the loction of the snow line). Considering the roughly flat sensitivity curve of SPHERE at separation larger than 0.3”, this simulation was roughly equivalent from the point of view of the ranking the Sco-Cen targets to a more realistic one with a low-frequency but broad distribution at wide separation. This inhomogeneity has no consequences in the final sample selection, considering that we included a fixed number of Sco-Cen targets for each priority bin (see Sect. 3).

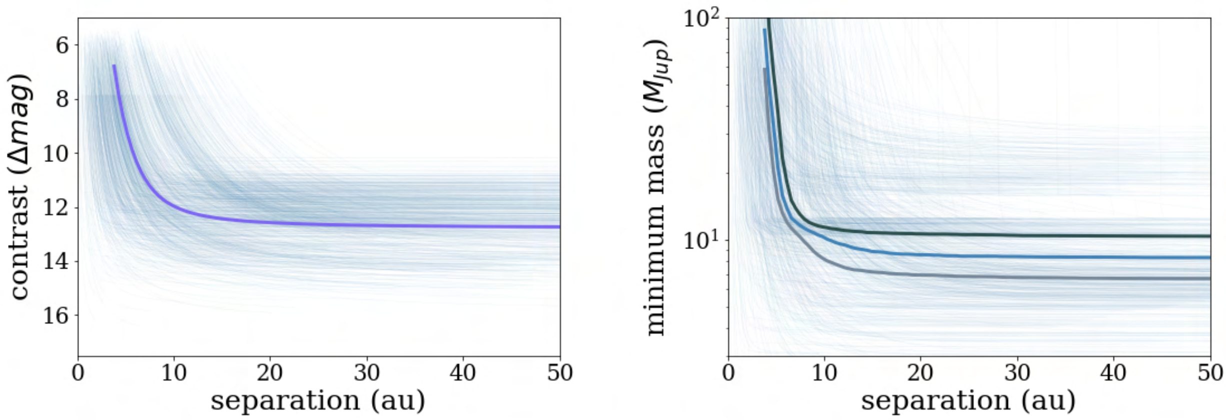

Fig. 1: Expected IFS detection limits (light blue curves), evaluated using the method described in Mesa et al. (2015), expressed in terms of contrast (left panel) or minimum companion mass (right panel, calculated assuming the best age for each target). The solid blue line shows the average over the full input sample. The light and dark gray curves in the right panel show the average mass limit obtained adopting the minimum and maximum values of the age, respectively.

appropriate for the main aim of the priority ranking, which is to build a good sample to answer our scientific questions (e.g., including a broad range of stellar masses).

3. The final SHINE target list

After the simulations described above, the SHINE list is composed of 800 stars rank ordered following the proposed scheme for two bins of masses Bin-1 (early-type; $\geq 1.5\ M_{\odot}$) and Bin-2 (low-mass $\leq 1.5\ M_{\odot}$) as summarized in Table 2. For operational reasons linked to the scheduling of the observations, we choose to have four priority classes, which we labeled P1 (highest priority), P2, P3, and P4 (lowest priority), rather than individual priorities that are different for each target. We considered the relevance of members of nearby young MGs, aiming at a complete sample of members, and considering the lower errors in stellar age compared to isolated objects and the better availability of information in the literature. For this reason, in a few cases we overruled the priority ranking resulting from simulations to have well-defined distance limit for MG members in the first two priority bins. We also limited the number of Sco-Cen targets to fulfill observational constraints. Overall, 200 targets were included in each bin, as detailed below.

P1 sample:

- all the known members of nearby young MGs (β Pic, Tucana, Columba, Carina, TW Hya, Argus, AB Dor) within 60 pc;
- the known members of the youngest groups (those listed above except AB Dor, which is significantly older) between 60 to 80 pc and the two early-type members of η Cha cluster;
- the first 40 Sco-Cen stars from ranking of the simulation performed using the 50 au outer cutoff;
- the remaining stars to achieve the planned size of the sample (about 20 stars) taken from the ranking of the 15 and 30 au simulations, taking stars alternatively from the two lists sorted according to planet detection probabilities.

P2 sample:

- all the known members of nearby young MGs (β Pic, Tucana, Columba, Carina, TW Hya, Argus, AB Dor) in the distance range between 80 to 100 pc;
- the known members of AB Dor MG from 60 to 80 pc;
- a handful of stars whose membership status in the above MGs is controversial in the literature;
- the next 40 Sco-Cen stars from ranking of the simulation performed using the 50 au outer cutoff;
- the remaining stars to achieve the planned size of the sample taken from the ranking of the 15 and 30 au simulations, taking stars alternatively from the two lists sorted according to planet detection probabilities.

P3 sample:

- the next 40 Sco-Cen stars from ranking of the simulation performed using the 50 au outer cutoff;
- the remaining stars to achieve the planned size of the sample (160 stars) taken from the ranking of the 15 and 30 au simulations, taking stars alternatively from the two lists sorted according to planet detection probabilities.

P4 sample:

- the next 40 Sco-Cen stars from ranking of the simulation performed using the 50 au outer cutoff;
- the remaining stars to achieve the planned size of the sample (160 stars) taken from the ranking of the 15 and 30 au simulations, taking stars alternatively from the two lists sorted according to planet detection probabilities.

We also selected bright targets to be observed with short observations in case of bad weather conditions or short gaps in the schedule (labeled P5 targets). They include known binary systems of specific interest for orbit determinations (Rodet et al. 2018) and stars with known RV planets to

Table 2: Priority distribution of the SHINE sample

Priority	Early-type	Solar and Low-mass
P0	Special targets	
P1	20 MGs + 40 ScoCen	120 MGs + 20 Field
P2	20 Field + 40 ScoCen	50 MGs + 90 Field
P3	20 Field + 40 ScoCen	140 Field
P4	20 Field + 40 ScoCen	140 Field
P5	Bad weather backup or filler	

look for stellar companions (Hagelberg et al., in preparation.). They are not intended to be deep enough to allow us the detection of planetary companions and will not be considered in this paper.

3.1. New targets added after the original definition

After evaluating of the actual on-sky performances of SPHERE, the results of which showed a reasonably good performance on stars as faint as R $\sim$ 12 (Beuzit et al. 2019, see their Fig. 7), the original sample was complemented starting from ESO period P98 (April-September 2016) with about 50 M-type objects proposed as members of young moving groups. The targets were assigned to priority bins P1 and P2 following the distance limits for individual groups, as defined above.

3.2. Special targets

A number of special targets were identified and promoted to higher priority for observation, defined as P0 priority. The science motivation for special priority is related to the known presence of planets or brown dwarfs, amenable to detailed characterization studies (e.g., Bonavita et al. 2017; Lagrange et al. 2019), stars with spatially resolved disks, especially when the disk properties suggest the presence of planets (e.g., PDS 70 Keppler et al. 2018; Mesa et al. 2019), or stars with long-period RV planets potentially detectable with SPHERE (Zurlo et al. 2018).

Other targets were promoted as P0 during the survey, thanks to results of observations of other components of the SPHERE-GTO (DISK program) or discoveries by other groups (e.g 51 Eri after planet detection, Macintosh et al. 2015). Targets that were not included in the original statistical sample, as defined above, are not considered in this paper as their inclusion would considerably bias the overall frequency of substellar objects. This is, for instance, the case of PDS 70 not originally selected given its distance, but observed in the context of a SHINE follow-up of the DISK program. Only targets included in the original statistical sample are kept for the present analysis. Nevertheless, some bias is still present, as the increase in priority implied a greater probability of being actually observed. This is further discussed in Paper III (Vigan et al. 2020).

Table 3 lists the targets in the F150 sample promoted to P0, the original priority class, the motivation for the priority upgrade, and the reference to individual papers based on SHINE data, if any. η Tel and CD-35 2722 were not flagged as special objects in spite of the previously known BD companions.

4. The F150 sample

The aim of the present series of papers is to present a preliminary statistical analysis from the first half of targets observed in the SHINE survey. The resulting sample is then necessarily incomplete. The optimal observing procedure for ground-based direct imaging surveys requires the target to be observed at meridian to maximize field rotation. A dedicated program to optimize the scheduling of an extended list of targets over individual nights or runs and even full semesters considering the actual time allocation has been built and is routinely used to prepare the SHINE observing nights (Lagrange et al. 2016). As a result, the actual targets included in the schedule is a compromise between the scientific priorities, the constraints of meridian passage, and the maximization of the number of targets to be observed.

To build the sample considered in the present paper, we included targets observed until February 2017 (the first two years of the survey), considering only the targets that are part of the statistical sample, as defined in Sect. 3. Targets observed in poor conditions (not validated following quantitative criteria of achieved contrast with respect to the expected level considering stellar magnitude and declination) were removed. Details on data reduction are provided in Paper II (Langlois et al.).

We also removed targets identified as new close visual binaries from SPHERE observations in order to be homogeneous with the original selection of single stars or members of wide binaries[7]. The new binaries will be presented in a dedicated paper (Bonavita et al. 2020, submitted).

We removed four targets (HIP 37288, HIP 39826, HIP 64792=GJ504, HIP 82588) which resulted to be older than 1 Gyr from the revised age analysis described in Sect. 5.9. Finally, we removed four targets (HD 100546, TW Hya, MP Mus, and EP Cha) because of the presence of gas-rich disks. Planets may still be forming in these disks, but are probably heavily obscured by disk features. The case of HD 100546, formally in our sample, is probably the best example of this (Sissa et al. 2018).

The sample built as described above is then formed by 150 targets, listed in Table 5, together with available broadband photometry in several filters.

5. Updated stellar properties

The target parameters were determined using the methods and procedures described in Desidera et al. (2015). A major improvement is the availability of Gaia DR2 astrometric parameters (Gaia Collaboration et al. 2016, 2018). As a result, all the targets have trigonometric parallaxes.

5.1. Distance and proper motion

Trigonometric parallaxes and proper motions were mostly taken from Gaia DR2. For two very bright stars not in-

[7] In some cases the physical link between the central star and the companion remains to be demonstrated, but the chance of background objects is small because of the bright magnitude of the candidates. Details will be presented in Bonavita et al., in preparation. Cases of very low-mass star companion candidates were analyzed with special care. A common proper motion test was performed, and stars with moderately bright background objects were kept in the F150 sample.

Table 3: Stars in the SHINE statistical sample observed as special targets (highest priority). The original priority in the selection of the statistical sample, the motivation for priority upgrade, and the references to discovery papers and individual SPHERE papers are listed. SAM stands for sparse aperture masking (e.g., Tuthill et al. 2006).

Target	Priority	Remarks	Discovery paper	SPHERE paper
β Pic	P1	known planet and disk	Lagrange et al. (2009)	Lagrange et al. (2019)
HR 8799	P1	known planet	Marois et al. (2008)	Zurlo et al. (2016)
HD 95086	P1	known planet	Rameau et al. (2013b)	Chauvin et al. (2018)
Fomalhaut	P2	known planet and disk	Kalas et al. (2008)	–
FomalhautB	P3	companion to P0 star	–	–
PZ Tel	P1	known brown dwarf	Biller et al. (2010)	Maire et al. (2016)
HIP 107412	P4	known brown dwarf	Milli et al. (2017)	Delorme et al. (2017); Grandjean et al. (2019)
51 Eri	P1	known planet	Macintosh et al. (2015)	Samland et al. (2017); Maire et al. (2019)
AB Pic	P1	known brown dwarf	Chauvin et al. (2005b)	–
TYC 8047-0232-1	P1	known brown dwarf	Chauvin et al. (2005a)	–
HIP 78530	P1	known brown dwarf	Lafrenière et al. (2011)	–
HD 61005	P1	known disk	Hines et al. (2007)	Olofsson et al. (2016)
HR 4796	P1	known disk	Schneider et al. (1999)	Milli et al. (2017, 2019)
AU Mic	P1	known disk	Liu (2004)	Boccaletti et al. (2015, 2018)
HD 30477	P1	known disk	Soummer et al. (2014)	
TWA 7	P1	known disk	Choquet et al. (2016)	Olofsson et al. (2018)
HD 141943	P2	known disk	Soummer et al. (2014)	Boccaletti et al. (2019)
ζ Lep	P2	known disk	Moerchen et al. (2010)	
ρ Vir	P1	known disk	Booth et al. (2013)	–
HIP 71724	P3	known low-mass comp.	Hinkley et al. (2015)	–
HIP 73990	P3	known low-mass comp.	Hinkley et al. (2015)	–
HD 115600	P3	known disk	Currie et al. (2015)	–
HD 377	P2	known disk	Choquet et al. (2016)	–

cluded in Gaia DR2 (Fomalhaut and β Leo), we used the Hipparcos results derived by van Leeuwen (2007) (hereafter VL07). For an additional 13 very bright stars (V< 5), the VL07 errors are smaller than the Gaia DR2 values. We adopted VL07 parallaxes and proper motions for these targets; they are listed in Table 6, together with other kinematic parameters.

5.2. Radial velocity

Radial velocity (RV) is a key input for the kinematic assignment (membership to groups) and for checking multiplicity. RV measurements were mostly taken from the literature (sources listed in Table 6). We obtained new RVs for 32 stars from spectra available in public archives. For 31 stars observed with HARPS we exploited the reduced spectra and RVs provided by the instrument pipeline available on the ESO archive[8]. The mean value was adopted when multiple epochs were available[9]. For one star (HIP 69989) we took the RV from public observations obtained with SOPHIE, available in the archive of the Haute Provence Observatory (Moultaka et al. 2004)[10].

5.3. Multiplicity

As discussed above, objects with known stellar companions (mass > 75 M_{Jup}) within 6 arcsec (approximate size of IRDIS field of view) were removed from the sample, including the previously unknown binaries discovered by our observations. The multiplicity search was based on the SPHERE images themselves, Gaia DR2, and other recent literature, including the evaluation of RV variability.

We opted to be conservative in the removal of targets due to binarity, aiming at avoiding spurious rejections in our sample. For this reason, a few stars with low-amplitude RV variability or indication of multiplicity derived only from the $\Delta\mu$ signature[11] were kept in the sample. RV variability of up to 1-2 km/s may be linked to stellar activity for our very young targets (e.g., Carleo et al. 2018; Brems et al. 2019) or to pulsations for early-type stars (e.g., Lagrange et al. 2009), or, when combining data from different instruments, due to zero-point offsets. The $\Delta\mu$ signature has instead some ambiguity in terms of physical mass and orbital parameters responsible for the dynamical signature. We also checked non-coronagraphic images taken with SPHERE at the beginning and end of the observing sequence, looking for the presence of stellar companions (Engler et al. 2020). Some ambiguous cases are discussed individually in Appendix A. It should be noted that several targets in our sample lack RV monitoring, making the rejection of spectroscopic binaries incomplete.

In order to have a more complete view of the properties of the targets in the sample, we also looked for companions at projected separations larger than 6 arcsec from our targets (outside the IRDIS field of view). They are listed in Table 10. Dedicated checks using Gaia DR2 have been performed to confirm the physical association of previously known companions and to look for new ones through the evaluation of the parallax and proper motion of individual objects. Forty-one targets are found to have companions outside the IRDIS field of view. In two cases (HIP 95270/η

[8] http://archive.eso.org/wdb/wdb/adp/phase3_spectral/form

[9] In a few cases the RVs available on the ESO archive were obtained with different masks for the same star. In these cases we adopted the value obtained from the mask that is closer to our adopted spectral type.

[10] http://atlas.obs-hp.fr/sophie/

[11] Proper motion difference between Gaia DR2 and other catalogs such as Gaia Dr1, Hipparcos, and Tycho2.

Tel and Fomalhaut/Fomalhaut B) we observed both components of the system. Two stars, namely HN Peg and β Cir, have brown dwarf companions at wide separation. For MG members, especially for the well-populated Sco-Cen groups, there is some ambiguity between very wide binaries and co-moving members of the associations. We opted to be conservative and then inclusive in Table 10, requiring tight common proper motion and parallax values (within 2 mas/yr and 1 mas, respectively). We note some cases of extremely wide binaries in our sample, with separation even larger than the typical limit for bound objects adopted in the literature ($\sim$ 20 000 au, Abt 1988; Allen et al. 2000). However, at young ages the occurrence of multiple systems at wider separations is expected (Caballero 2009). Among the extremely wide multiple systems not previously noted in the literature we mention HIP 22226 + 2MASS J04463413-262755 (the latter being itself a close binary) at a projected separation of about 50 000 au.

The presence of wide companions, an important environmental property of our targets, is also a useful resource for age dating systems when complementary diagnostics can be applied to the individual components, depending on their spectral types.

5.4. Kinematics and moving group membership

We exploited the updated kinematic data, particularly the high-accuracy parallaxes and proper motions from Gaia DR2, to evaluate the membership of our targets in young moving groups. We derived the space velocities U, V, W following prescriptions by Johnson & Soderblom (1987), and we exploited the BANYAN Σ tool[12] (Gagné et al. 2018a). Unambiguous assignment to groups or field can be made for nearly all targets thanks to the improved kinematics data and group definition. There are a few cases of different membership assignment with respect to the literature, mostly a few exchanges between Tuc-Hor and Columba and Carina or between Sco-Cen subgroups. A few targets classified in the literature as members of AB Dor MG have low membership probability according to BANYAN Σ. However, their properties (lithium, activity, rotation; see below) are fully consistent with those of confirmed members. Targets worthy of individual discussion are included in Appendix A.

5.5. Chromospheric and coronal activity

X-ray luminosities for all the targets were derived from the ROSAT All Sky Catalogs (Voges et al. 1999, 2000) using the calibration by Hünsch et al. (1999); 89 stars in the sample have detected X-ray emission. Chromospheric emission was retrieved from the literature or measured by us on archive HARPS spectra as in Desidera et al. (2015). Overall $\log R^{'}_{HK}$ is available for 46 stars. Both quantities are reported in Table 7. These indicators have limited dependency on stellar age below the Pleiades age (for G-K stars). Therefore, low weight was assigned to these indicators to quantify the age of very young stars, while for older objects we relied on the Mamajek & Hillenbrand (2008) calibrations. The possibility of old active stars misclassified as young being tidally locked binaries or because of the occurrence of some kind of accretion of angular momentum is unlikely, considering the complementary age diagnostics (e.g. lithium) and the search for close binaries.

[12] http://www.exoplanetes.umontreal.ca/banyan/banyansigma.php

5.6. Lithium

The equivalent width of the available age-sensitive diagnostic Li 6707 AA was gathered from the literature and included in Table 7, to be used as an age diagnostic.

5.7. Photometric variability and rotation period

In our sample 103 stars have spectral type later than A. They are all young, and exhibit clear evidence of magnetic activity and photometric variability. The last property is exploited to make measurement of the stellar rotation period and of the level of magnetic activity.

As the first step in our rotation period study, we explored the literature for all 103 stars and found existing measurements of the rotation period for 64 stars (62%). As the second step we explored the public photometric time series archives of all 103 stars and found (mostly in the TESS archive) suitable data for rotation period search for 58 stars (56%). Finally, we planned and collected our own photometric time series data for the remaining targets lacking suitable data and measured the rotation period for six of them. Observations were carried out at the Remote Observatory Atacama Desert (ROAD) in Chile, the Perth Exoplanet Survey Telescope Observatory (PEST) in Australia, and the York Creek Observatory (YCO) in Tasmania.

As the results of our study we obtained the rotation period for 101 of the 103 late-type stars in F150. They are reported in Table 7, together with amplitude of the photometric rotational modulation.

Ages from rotation were estimated comparing the observed rotation period with that of stars of similar colors in groups or clusters of known age, considering those compiled by Desidera et al. (2015) and more recent literature results (e.g., Rebull et al. (2016) for the Pleiades and Messina et al. (2017) for β Pic MG). The ambiguity in rotation age due to the non-monotonic evolution of the rotation (minimum period reached close to the zero age main sequence, ZAMS) can usually be eliminated by considering additional indicators such as the Li equivalent width (EW) and the position on the color-magnitude diagram (CMD) because very young stars that are in the acceleration phase are above the ZAMS. The number of targets involved in these ambiguities is small, considering the large fraction of members of moving groups, especially at young ages. The additional ambiguity represented by the small fraction of very fast rotators ("C" sequence in the nomenclature by Barnes 2007) is more subtle. As the majority of these fast rotators are found in binary systems (e.g., Messina et al. 2017), which are rejected in our study, and considering the low fraction of such targets in well-studied clusters and the help of the other age diagnostics, we expect a very limited impact on our age classification.

5.7.1. Period search methods

We followed the approach outlined in Messina et al. (2010, 2011), to search for the stellar rotation period of our targets.

Briefly, the period search was carried out by computing the Lomb−Scargle periodogram (LS; Press et al. 2002; Scargle 1982; Horne & Baliunas 1986) and the CLEAN algorithm (Roberts et al. 1987). The false alarm probability (FAP) that a peak of given height in the periodogram is caused by statistical variations was computed through Monte Carlo simulations, by generating 1000 artificial light curves obtained from the real light curve, keeping the time sampling but permuting the magnitude values (see, e.g., Herbst et al. 2002). We considered only rotation periods that were measured with FAP $< 0.01\%$. Only a very few targets with FAP in the range 0.01–1% had their rotation periods confirmed by independent measurements, for example from the literature.

When data from more observation seasons (or sectors in the case of TESS) were available, we computed LS and CLEAN periodograms for each season(sector); the most accurate results were reported as adopted values, and they are shown in Figs. A.1–A.85. We followed the method used by Lamm et al. (2004) to compute the errors associated with the period determinations (see, e.g., Messina et al. 2010 for details). To derive the light curve amplitude, we fit the data with a sinusoidal function whose period is equal to the stellar rotation period. As a result of our photometric analysis we obtained our own rotation period measurements and photometric variability amplitudes for 82 of the 103 target stars: 76 from data of one or more public archives and 6 from our own photometry. We confirmed 44 previously known rotation periods. Finally, we adopted the rotation periods retrieved from the literature for 18 targets (of which 8 periods were retrieved from Messina et al. 2010, 2011, 2017). We produced plots for all the photometric time series (either new or from archives) analyzed in this work. These plots are available as online material in Figs. A.1–A.85.

5.8. Isochrone fitting

Isochronal ages were derived using the models by Bressan et al. (2012) and the web interface PARAM [13]. For this determination, we used the V-band magnitude listed in Table 5, the effective temperature listed in Table 8, the parallax listed in Table 6, and adopted solar metallicity. The effective temperatures were obtained through Casagrande et al. (2010) for late-type stars, using the combination of colors adopted in Desidera et al. (2015), and through the Mamajek tables Pecaut & Mamajek (2013) for early-type stars. A few cases of ambiguities between pre-main sequence and post-main sequence evolution (see, e.g. Bonnefoy et al. 2018) are discussed individually in the Appendix. The availability of other indicators allows us to solve the ambiguity between the two alternatives. In addition to the systematic uncertainties in the stellar models, possible biases of the isochrone method are linked to photometric variability of most of the late-type targets and to the possibility of unrecognized binaries. The first item is included in the error bar of the input parameters. For the second item, the sensitivity of our SPHERE observations to stellar companions, especially those bright enough to bias the photometry, allows us to rule out cases at separations larger than a few tens of mas. For closer companions we inspected the available data for spectroscopic binaries, although a significant fraction of the targets lack suitable RV monitoring. Finally, after Gaia Dr2, parallax is no longer the dominant source of uncertainty for isochrone age determination.

[13] Version 1.3 available at http://stev.oapd.inaf.it/cgi-bin/param_1.3

5.9. Adopted ages

The primary age method adopted in this work is the group membership because the age of an ensemble is usually better determined than any individual measurement. For bona fide members the group age was adopted. The ages for the MG and their errors are those described in Bonavita et al. (2016) and were also adopted by Vigan et al. (2017). They are summarized in Table 4[14]. The Bonavita et al. (2016) MG ages were mostly taken from Bell et al. (2015). The main motivation for this choice is to ensure the best homogeneity for the whole list of targets as no comparable studies were published in the following years. For groups not included in Bell et al. (2015), we checked (using indirect methods such as lithium and rotation) that our adopted age ranking is correct. Improved ages for individual groups have been published (e.g., Miret-Roig et al. 2020, for β Pic MG), but adopting them without revision for other groups would imply inconsistencies in the relative ages, which we want to avoid, We have started to work on comprehensive updates of the MG ages in the perspective of the final analysis of the SHINE sample.

We recognize that there are indications for a significant age spread in some of these groups, such as the Sco-Cen association (Pecaut & Mamajek 2016). However, a common age is adequate for the statistical purposes of this series of papers. In addition, the errors associated with the age determination for individual stars are usually comparable or even larger than the age dispersion of the groups. Finally, possible members with ages that are somewhat discrepant from the bulk of an association are often subject to a dedicated analysis as typically their kinematic membership probability is lower (see, e.g., the case HD 95086 discussed in Appendix A). For late-type bona fide members, lithium, rotation, and secondary rotation-activity indicators are typically consistent with the age assigned to the MGs.

Table 4: Adopted MG ages

Group	Age (Myr)	Min (Myr)	Max (Myr)
TW Hya (TWA)	10	7	13
η Cha OC (ETAC)	11	8	14
Upper Scorpius (US)	11	4	12
Lower Centaurus-Crux (LCC)	16	12	20
Upper Centaurus-Lupus (UCL)	17	15	20
β Pic (BPIC)	24	19	29
Columba (COL)	42	35	50
Tuc-Hor (TUC)	45	35	50
Carina (CAR)	45	35	50
Argus (ARG)	50	40	70
AB Doradus (ABDO)	149	100	180

[14] In our sample there are no members of Octans, Octans-Near, Carina-Near, or Pisces-Eridanus MG, and is why these groups are not included in Table 4.

For field objects, the age determination is based on isochrone fitting for early-type stars (spectral type earlier than mid-F), while for late-type stars (spectral type later than mid-F) it is based on indirect methods (lithium, rotation, chromospheric activity, X-ray emission), complemented by isochrone fitting and kinematic evaluation when applicable. The indirect estimates are based on comparison with the locus of members of nearby moving groups and open clusters, as done in Desidera et al. (2015).

For stars with ambiguous membership to groups, we opted for a conservative approach. In the case of objects with probable membership, we adopted the group age but extended the possible range of values (minimum and maximum values in Table 9) to include the values resulting from the analysis based on other methods, applied depending on the spectral type of the star. Object with a low probability of membership were considered field objects, adapting the age limits to the group age in the adopted range.

The adopted ages are listed in Table 9. Further details on individual targets are provided in Appendix A.

5.10. Stellar masses

Stellar masses were derived using the PARSEC isochrones Bressan et al. (2012) models and the PARAM interface (see above). As done in Desidera et al. (2015) for the objects with ages derived from moving group membership or indirect methods, we restricted the allowed age range for the determination of the stellar mass, assuming uniform prior in the selected age range. This allowed us to consider, among the overlapping isochrones within the error bars of the input parameters, only those consistent with the age estimate. This effect is small but not negligible (typically a few hundredths of a solar mass). For stars with M spectral type the resulting stellar masses appear rather low. This is likely due to issues in the atmospheric models for cool objects in the PARSEC tracks (Chen et al. 2014b). Therefore, for these stars we derived the stellar masses from the models by Baraffe et al. (2015) for the appropriate age of the star. The masses are listed in Table 8.

5.11. Presence of disks

We also checked in the literature for the presence of dusty disks surrounding the stars in the sample. Of the 150 objects, 73 show infrared (IR) excesses, interpreted as the clear presence of dust in the system. Twenty-nine of these were detected and spatially resolved with instruments such as HST/NICMOS, VLT/SPHERE, Gemini/GPI, Herschel/PACS, and ALMA (see Table 8). Disks identified as double-belts from SED fitting (Chen et al. 2014a) have a special flag in Table 8. Finally, seven objects were classified as potential disk hosts since the IR excesses were only marginally detected, while in two cases there are indications that the observed emission is likely associated with contaminants (background sources). The absolute frequency of stars with disks in our sample, in particular those with spatially resolved disks, appears higher than typically found in the literature. The priority enhancement for some stars with disks described in Sect. 3.2 is certainly one of the reasons for such a high occurrence. Our selection of well-isolated objects (single stars or components of wide binaries) with broad dynamical room for extended disks is another likely reason [15]. It should be considered that our flag includes the detection of IR excess at any wavelength, then including a large variety of disk temperatures and configurations. Finally, while our original selection criteria do not concern the presence of disks, it is also possible that some indirect bias is at work. This may happen if stars with IR excess were more carefully scrutinized for youth and membership in moving groups and then more likely to be included in our target list. This may be the case for a few individual targets; however, most of the main sources of our original target compilations (e.g., Torres et al. 2006; Wright et al. 2004) are completely unrelated to the presence of IR excesses or resolved disks, so we think this bias is minor, if present at all.

6. Sample properties

Figures 2-4 show the distributions for some of the key astrophysical parameters for our F150 sample. Figures 5, 7, and 8 show the cumulative distributions along with the comparison with the GPIES sample (Sect. 6.1).

The bumps in the age distribution are due to the large fraction of members in young MGs. The median age value is 45 Myr, with 90% limits of 11 and 450 Myr. The adopted ages are typically similar to those originally considered in the sample selection process, although improved thanks to the availability of data on individual targets and better ages of the MGs. Only in a handful of cases were the revised ages found to be $>$ 1 Gyr. These targets were removed from the present work, being old interlopers in the original sample (tidallylocked binaries, Li-rich giants, or stars with badly measured age indicators; details will be provided in forthcoming works).

The median mass is 1.15 $M_{\odot}$, with 90% limits of 0.57 and 2.37 $M_{\odot}$. Most of the early-type stars (mass $\geq 1.5 M_{\odot}$) are members of Sco-Cen groups. The broad mass range of the sample will allow us to investigate in Paper III the mass dependence of the frequency and properties of substellar companions. The analysis will be extended to higher stellar masses by the BEAST survey, targeting B-type stars in Sco-Cen (Janson et al. 2019).

The median distance is 48 pc, with 90% limits of 11 and 137 pc. The peak in the distance distribution between 100 and 150 pc is due to the inclusion of Sco-Cen members. At 150 pc, the inner working angle of SPHERE allows us to access separation of $\geq$ 20 au for the presence of planetary companions.

The stars with resolved disks and detectable IR excess have a different mass distributions with respect to those without these features, being more massive (median values 1.41 versus 0.94 $M_{\odot}$), while the age distributions of stars with and without disks are similar. Considering the inhomogeneity of our census of disks concerning, for example, the wavelengths of the observations, sensitivity to IR excess with respect to the stellar photosphere, and sensitivity to spatially resolved disks, we do not investigate the origin of these features. While our original survey sample has no specific biases linked to the presence of disks or IR excess, which were never considered in the selection process, some

[15] The frequency of stars with detected IR excess is much lower (below 10%) in the sample of 78 new binaries detected in the whole SHINE survey (Bonavita et al., submitted).

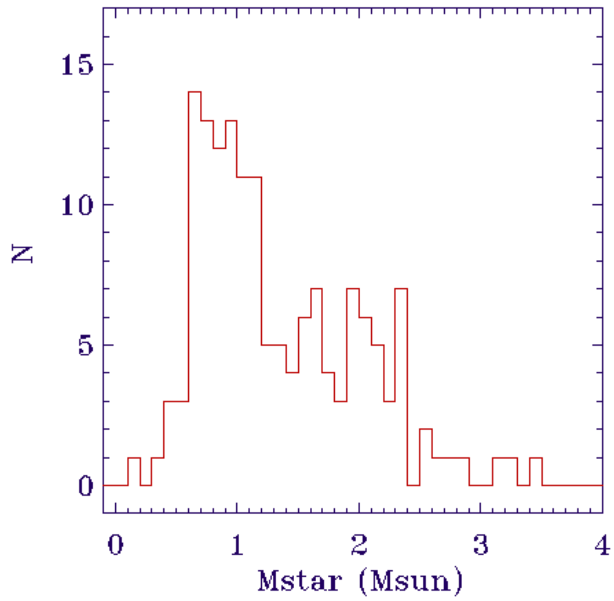

Fig. 2: Histogram of stellar masses for the F150 sample

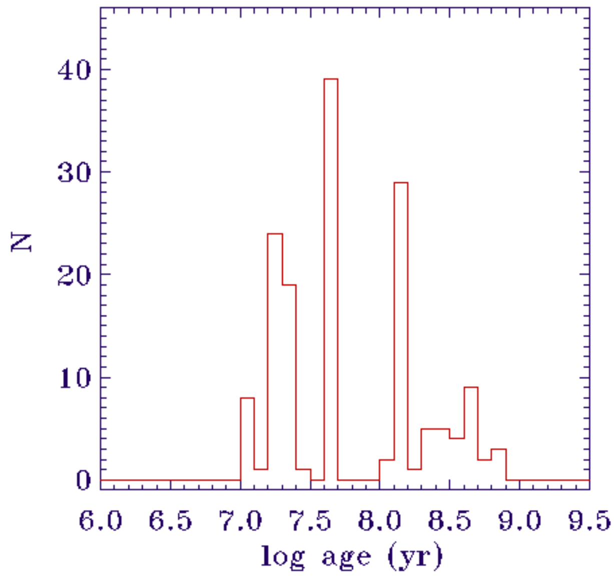

Fig. 4: Histogram of stellar ages for the F150 sample

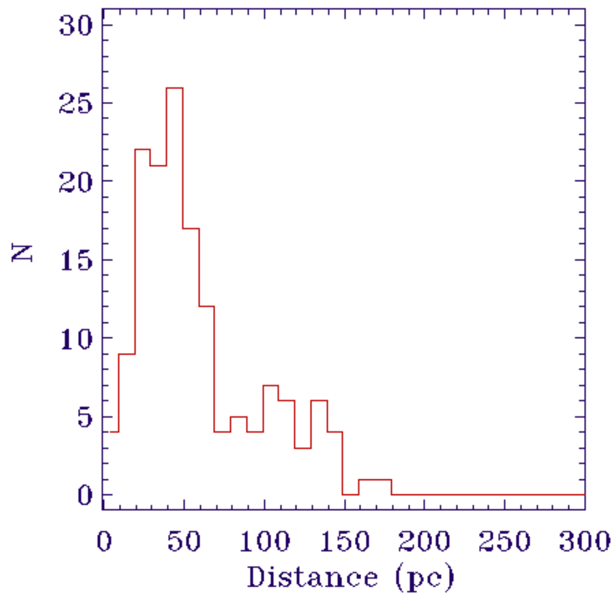

Fig. 3: Histogram of distances for the F150 sample

of the stars with disks were observed with increased priority because of the presence of the disks themselves (see Sect. 3.2). This effect will be mitigated by the end of the survey, allowing more robust statistical inferences.

As already noted in Vigan et al. (2017), the majority of young nearby stars have metallicity values close to solar, making the sample of stars searched for planets via direct imaging somewhat different with respect to those considered by RVs and transits, which span a broader range of age and metallicity. The available data (e.g., Viana Almeida et al. 2009) suggest a slightly subsolar metallicity for stars in nearby young associations, at odds with expectations from galactic chemical evolution models. Recent results indicate that the standard chemical abundance analysis might be biased for young stars, because of an overestimation of microturbulent velocities somewhat linked to stellar activity (Reddy & Lambert 2017; Baratella et al. 2020; Spina et al. 2020). Since a new analysis of chemical composition of members in various moving groups with these new methods is not yet available, we assumed in the following a solar metallicity for all the targets.

6.1. Comparison with GPIES and other surveys

6.1.1. Properties of individual targets

In the F150 sample, 67 out of 150 stars were also observed with GPI and were included in the GPIES early statistical analysis (Nielsen et al. 2019). In Fig. 9 we compare the adopted ages; 49 of the 67 overlapping targets are members of moving groups, for which the adopted individual age is equal (TW Hya, η Cha, Tuc-Hor, Columba, Carina, Argus, AB Dor MG) or differ by a very small amount, 1 or 2 Myr (β Pic MG, Sco-Cen groups). As a result, the median age difference is equal to zero, and we can infer that the age scales in the two studies are very similar. Nevertheless, there are moderately large discrepancies for some individual field objects, for which ages are more uncertain. In a few cases for which the membership to groups is ambiguous (see Appendix A for details on individual objects), we adopted the stellar age derived independently of the group membership constraints (typically much older than the group ages) with lower limits encompassing the group ages. In most of these cases, Nielsen et al. (2019) adopted the membership to the groups and the corresponding ages, resulting in fairly large discrepancies. We also note that the ages adopted in Nielsen et al. (2019) for the components in the Fomalhaut system (749 Myr for A and 200 Myr for B) bracket our adopted common value for the system (440 Myr).

The comparison of the adopted masses in Fig. 10 also shows fairly good agreement over the whole range of masses considered by the programs. There is a small systematic difference, median delta of 0.03 $M_{\odot}$ with our masses being smaller. There is perfect agreement for the adopted distances, derived from the same sources (Gaia DR2 and Hipparcos).

6.1.2. Sample comparison

After the comparison of the individual stellar parameters, we compared the distributions, in order to reveal differences between the two samples. A first highly significant difference concerns the stellar magnitude (Fig. 5). This can be understood due to the differences between the AO systems of GPI and SPHERE, the latter working well to fainter magnitudes. This allowed us to choose a fainter magnitude limit. As a result, our sample includes a larger fraction of low-mass stars and extends to slightly larger distances (Fig. 6). The median masses of SHINE-F150 and GPIES being 1.15 and 1.34 $M_{\odot}$, respectively, with stars below 1 $M_{\odot}$ representing 40% of the sample for SHINE and just 19% for GPIES (Fig. 7). Additional differences concern the high-mass tail, where we stopped at about 3 $M_{\odot}$. There are only three stars with masses higher than this value in our final determination, (i.e., 2% of the sample, with a maximum value of 3.48 $M_{\odot}$). On the other hand, GPIES extends up to 9 $M_{\odot}$ with 4.5% of the targets more massive than 3 $M_{\odot}$.

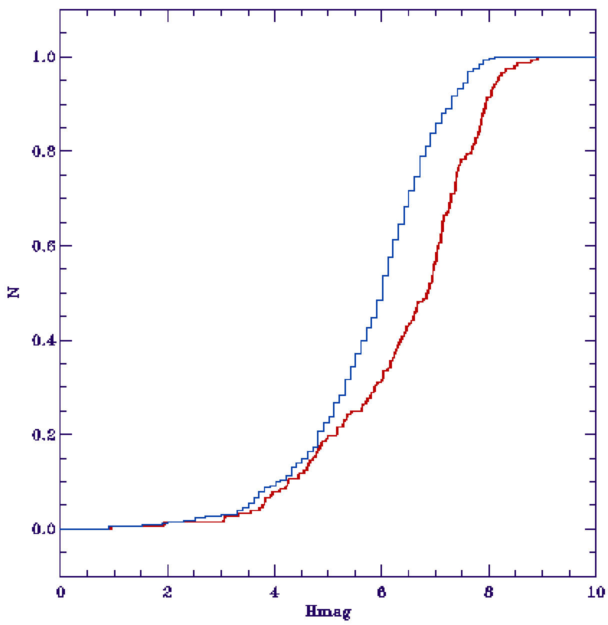

Fig. 5: Cumulative distribution of H-band magnitude for the stars in our sample (red line) and that of Nielsen et al. (2019) (blue line).

There are also some differences in the age distribution (median ages of 45 Myr for SHINE and 125 Myr for GPIES, Fig. 8) . The age difference is mostly explained by the larger fraction of field early-type stars (typically intermediate age) in the GPIES sample and by the larger fraction of young low-mass MG members in our sample, due to the fainter magnitude limit.

Both teams avoided close visual binaries within the field of view of the high-contrast instruments. As the field of view of GPIES is smaller with respect to SHINE/SPHERE, binaries with 3-6 arcsec projected separation, not present in our sample, are included in GPIES. Finally, GPIES included in their statistics a sample of spatially unresolved binaries. The corresponding planets searched in these systems are circumbinary. Instead, we excluded these systems from the present study, although unrecognized spectroscopic binaries might still be present because of the lack of RV monitoring for a fraction of our targets. As spectroscopic binaries represent about 10% of the GPIES sample, this difference could have some impact on the statistical results.

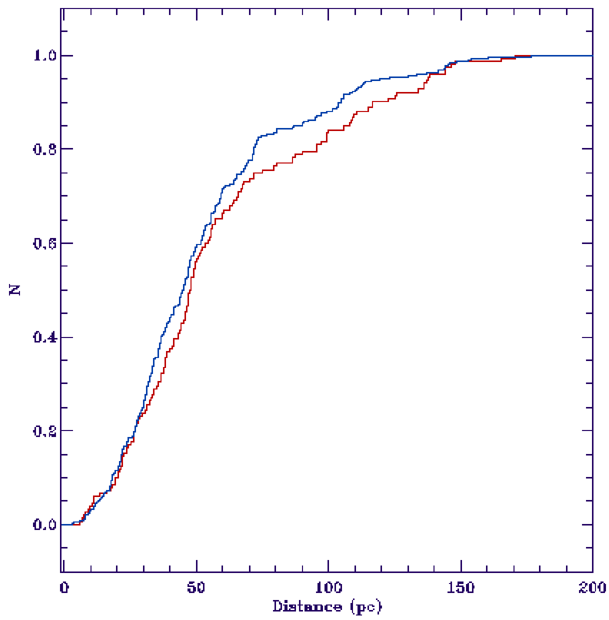

Fig. 6: Cumulative distribution of distance for the stars in our sample (red line) and that of Nielsen et al. (2019) (blue line).

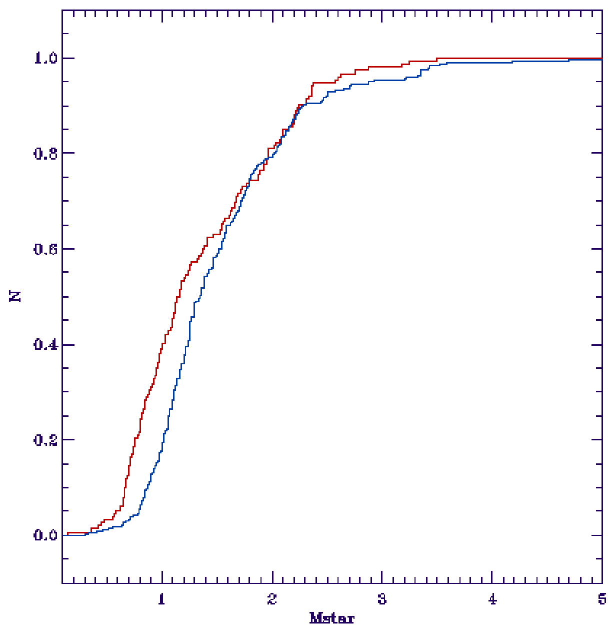

Fig. 7: Cumulative distribution of masses for the stars in our sample (red line) and that of Nielsen et al. (2019) (blue line).

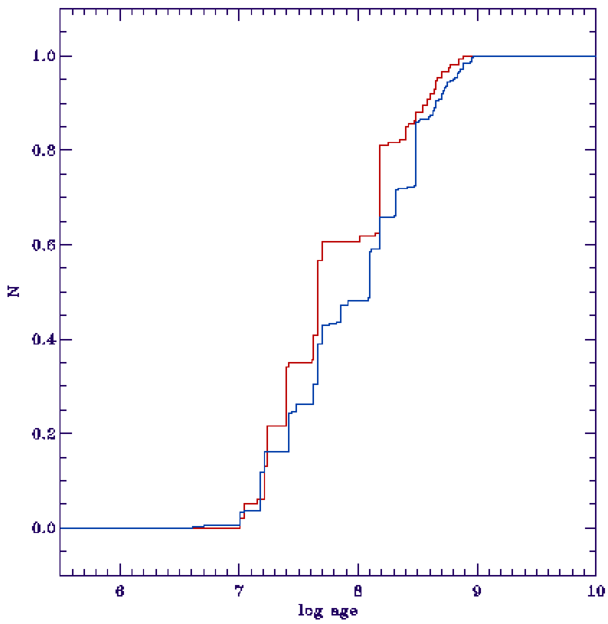

Fig. 8: Cumulative distribution of log (age) for the stars in our sample (red line) and that of Nielsen et al. (2019) (blue line).

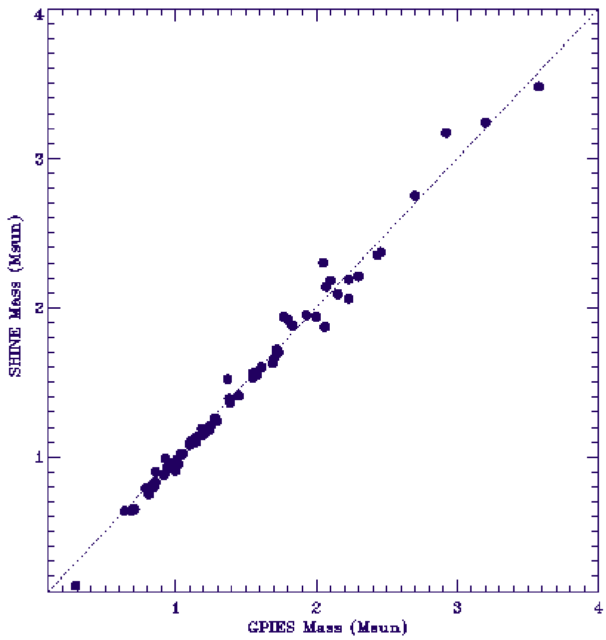

Fig. 10: Comparison of stellar masses derived in the present work and in Nielsen et al. (2019).

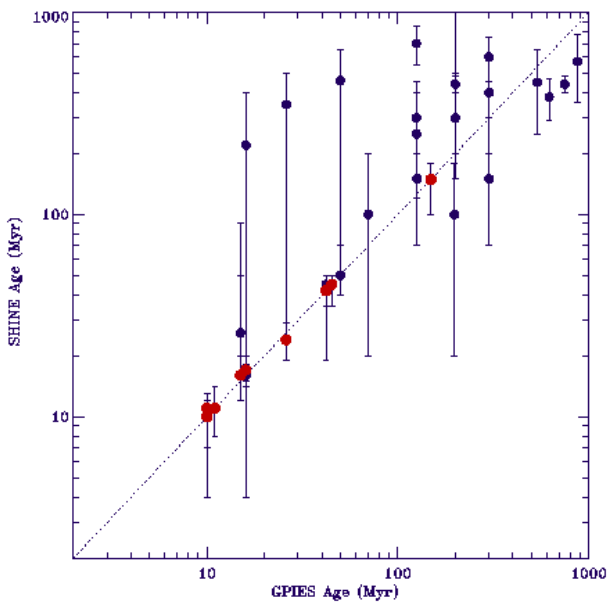

Fig. 9: Comparison of ages derived in the present work and in Nielsen et al. (2019). Black circles refer to individual stars and red circles to moving groups (typically several targets for each group). The error bars refer to the minimum and maximum age values from Table 9

.

7. Summary and conclusions

We described SHINE, the largest direct imaging survey for exoplanets at VLT performed as part of SPHERE GTO. We detailed the process of sample selection and the priority ranking scheme. The survey is focused on young nearby stars, with spectral types from A to M. Known binaries within the field of view of the SPHERE-IRDIS camera (6 arcsec) are excluded, as are all known spectroscopic binaries (though not all targets were thoroughly searched).

A subsample of 150 stars with first epoch observations done before February, 2017 was defined for a preliminary statistical assessment of the frequency of planets and brown dwarfs in wide orbits (5-300 au). This paper presents the characterization of the individual targets and of this subsample as a whole. The companion paper (Langlois et al., in press) presents the observations, data processing, identification, and classification of companion candidates, while Vigan et al. (2020) presents the statistical analysis of the frequency of substellar companions and its dependence on stellar mass.

We exploited a variety of methods (kinematics and membership to groups, isochrone, lithium, rotation, and activity) to infer the stellar age and other stellar parameters. The median age value is 45 Myr, with 90% limits of 11 and 450 Myr. The median stellar mass is 1.15 $M_{\odot}$, with 90% limits of 0.57 and 2.37 $M_{\odot}$. A comparison with GPIES early statistical analysis (Nielsen et al. 2019) shows no large systematic differences in the age scales between the two studies, but significant differences in the mass distribution and binary properties.

Acknowledgements. SPHERE is an instrument designed and built by a consortium consisting of IPAG (Grenoble, France), MPIA (Heidelberg, Germany), LAM (Marseille, France), LESIA (Paris, France), Laboratoire Lagrange (Nice, France), INAF - Osservatorio di Padova (Italy), Observatoire de Genève (Switzerland), ETH Zürich (Switzerland), NOVA (Netherlands), ONERA (France) and ASTRON (Netherlands) in collaboration with ESO. SPHERE was funded by ESO, with additional contributions from CNRS (France), MPIA (Germany), INAF (Italy), FINES (Switzerland) and NOVA (Netherlands). SPHERE also received funding from the European Commission Sixth and Seventh Framework Programmes as part of the Optical Infrared Coordination Network for Astronomy (OPTICON) under grant number RII3-Ct-2004-001566 for FP6 (2004–2008), grant number 226604 for FP7 (2009–2012) and grant number 312430 for FP7 (2013–2016).

This research has made use of the SIMBAD database and Vizier services, operated at CDS, Strasbourg, France and of the Washington Double Star Catalog maintained at the U.S. Naval Observatory. This work has made use of data from the European Space Agency (ESA) mission *Gaia* (https://www.cosmos.esa.int/gaia), processed by the *Gaia* Data Processing and Analysis Consortium (DPAC, https://www.cosmos.esa.int/web/gaia/dpac/consortium). Funding for the DPAC has been provided by national institutions, in particular the institutions participating in the *Gaia* Multilateral Agreement. This paper includes data collected with the TESS mission, obtained from the MAST data archive at the Space Telescope Science Institute (STScI). Funding for the TESS mission is provided by the NASA Explorer Program. STScI is operated by the Association of Universities for Research in Astronomy, Inc., under NASA contract NAS 5–26555. This paper has made use of data products available in ESO archive. Program ID: 60.A-9036(A); 072.C-0488(E) (PI Mayor), 074.C-0364(A) (PI Robichon), 074.C-0037(A) (PI Gunther), 075.C-0202(A) (PI Gunther), 075.C-0689(A) (PI Galland), 076.C-0010(A) (PI Gunther), 077.C-0012(A) (PI Gunther), 077.C-0295(D) (PI Galland), 078.D-0245(C) (PI Dall), 079.C-0046(A) (PI Gunther), 080.D-0151(A) (PI Hatzes), 080.C-0712(A) (PI Desort), 180.C-0886(A) (PI Bonfils), 082.C-0718(B) (PI Bonfils), 082.C-0427(A) (PI Doellinger), 082.C-0390(A) (PI Weise), 183.C-0437(A) (PI Bonfils), 083.C-0794(A) (PI Chauvin), 084.C-1039(A) (PI Chauvin), 184.C-0815(B) (PI Desort), 089.C-0732(A) (PI Lo Curto), 191.C-0873(D) (PI Bonfils), 192.C-0224(A) (PI Lagrange), 097.C-0864(B) (PI Lannier), 098.C-0739(A) (PI Lagrange), 099.C-0205(A) (PI Lagrange), 099.C-0458(A) (PI Lo Curto), 1101.C-0557(A) (PI Lagrange). We have used data from the WASP public archive in this research. The WASP consortium comprises of the University of Cambridge, Keele University, University of Leicester, The Open University, The Queen's University Belfast, St. Andrews University and the Isaac Newton Group. Funding for WASP comes from the consortium universities and from the UK's Science and Technology Facilities Council. Based on data retrieved from the SOPHIE archive at Observatoire de Haute-Provence (OHP), available at http://atlas.obs-hp.fr/sophie/

S.D., V.D., D.M. and R.G. acknowledge the support by INAF/Frontiera through the "Progetti Premiali" funding scheme of the Italian Ministry of Education, University, and Research. AV acknowledges funding from the European Research Council (ERC) under the European Union's Horizon 2020 research and innovation programme (grant agreement No. 757561). AML acknowledges funding from Agence Nationale de la Recherche (France) under contract number ANR-14-CE33-0018. JC was supported by SC Space Grant and Fulbright Colombia. M.B. acknowledges funding by the UK Science and Technology Facilities Council (STFC) grant no. ST/M001229/1.

References

Abt, H. A. 1988, ApJ, 331, 922
Allen, C., Poveda, A., & Herrera, M. A. 2000, A&A, 356, 529
Anderson, E. & Francis, C. 2012, Astronomy Letters, 38, 331
Asensio-Torres, R., Janson, M., Bonavita, M., et al. 2018, A&A, 619, A43
Baliunas, S. L., Donahue, R. A., Soon, W. H., et al. 1995, ApJ, 438, 269
Baraffe, I., Chabrier, G., Barman, T. S., Allard, F., & Hauschildt, P. H. 2003, A&A, 402, 701
Baraffe, I., Homeier, D., Allard, F., & Chabrier, G. 2015, A&A, 577, A42
Baratella, M., D'Orazi, V., Carraro, G., et al. 2020, A&A, 634, A34
Barbato, D., Sozzetti, A., Desidera, S., et al. 2018, A&A, 615, A175
Barenfeld, S. A., Bubar, E. J., Mamajek, E. E., & Young, P. A. 2013, ApJ, 766, 6
Barnes, J. R. 2005, MNRAS, 364, 137
Barnes, S. A. 2007, ApJ, 669, 1167
Barrado y Navascues, D. 1998, A&A, 339, 831
Bell, C. P. M., Mamajek, E. E., & Naylor, T. 2015, MNRAS, 454, 593
Beuzit, J. L., Vigan, A., Mouillet, D., et al. 2019, A&A, 631, A155
Biazzo, K., D'Orazi, V., Desidera, S., et al. 2012, MNRAS, 427, 2905
Biller, B. A., Close, L. M., Masciadri, E., et al. 2007, ApJS, 173, 143
Biller, B. A., Liu, M. C., Wahhaj, Z., et al. 2010, ApJ, 720, L82
Biller, B. A., Liu, M. C., Wahhaj, Z., et al. 2013, ApJ, 777, 160
Boccaletti, A., Sezestre, E., Lagrange, A.-M., et al. 2018, A&A, 614, A52
Boccaletti, A., Thalmann, C., Lagrange, A.-M., et al. 2015, Nature, 526, 230
Boccaletti, A., Thébault, P., Pawellek, N., et al. 2019, A&A, 625, A21
Boesgaard, A. M., Budge, K. G., & Burck, E. E. 1988, ApJ, 325, 749
Bonavita, M. 2020, Exo-DMC: Exoplanet Detection Map Calculator
Bonavita, M., Chauvin, G., Desidera, S., et al. 2012, A&A, 537, A67
Bonavita, M., de Mooij, E. J. W., & Jayawardhana, R. 2013, PASP, 125, 849
Bonavita, M., Desidera, S., Thalmann, C., et al. 2016, A&A, 593, A38
Bonavita, M., D'Orazi, V., Mesa, D., et al. 2017, A&A, 608, A106
Bonfils, X., Delfosse, X., Udry, S., et al. 2013, A&A, 549, A109
Bonnefoy, M., Chauvin, G., Lagrange, A. M., et al. 2014, A&A, 562, A127
Bonnefoy, M., Perraut, K., Lagrange, A. M., et al. 2018, A&A, 618, A63
Bonnefoy, M., Zurlo, A., Baudino, J. L., et al. 2016, A&A, 587, A58
Booth, M., Kennedy, G., Sibthorpe, B., et al. 2013, MNRAS, 428, 1263
Borgniet, S., Lagrange, A.-M., Meunier, N., et al. 2019, A&A, 621, A87
Bowler, B. P. 2016, PASP, 128, 102001
Brandt, T. D., McElwain, M. W., Turner, E. L., et al. 2014, ApJ, 794, 159
Brems, S. S., Kürster, M., Trifonov, T., Reffert, S., & Quirrenbach, A. 2019, A&A, 632, A37
Bressan, A., Marigo, P., Girardi, L., et al. 2012, MNRAS, 427, 127
Bryan, M. L., Knutson, H. A., Lee, E. J., et al. 2019, AJ, 157, 52
Busko, I. C. & Torres, C. A. O. 1978, A&A, 64, 153
Caballero, J. A. 2009, A&A, 507, 251
Caballero, J. A. 2010, A&A, 514, A98
Cantat-Gaudin, T. & Anders, F. 2020, A&A, 633, A99
Carleo, I., Benatti, S., Lanza, A. F., et al. 2018, A&A, 613, A50
Carleo, I., Malavolta, L., Lanza, A. F., et al. 2020, arXiv e-prints, arXiv:2002.10562
Carson, J., Thalmann, C., Janson, M., et al. 2013, ApJL, 763, L32
Casagrande, L., Ramírez, I., Meléndez, J., Bessell, M., & Asplund, M. 2010, A&A, 512, A54
Cassan, A., Kubas, D., Beaulieu, J. P., et al. 2012, Nature, 481, 167
Chauvin, G. 2018, in Society of Photo-Optical Instrumentation Engineers (SPIE) Conference Series, Vol. 10703, Proc. SPIE, 1070305
Chauvin, G., Desidera, S., Lagrange, A. M., et al. 2017a, in SF2A-2017: Proceedings of the Annual meeting of the French Society of Astronomy and Astrophysics, ed. C. Reylé, P. Di Matteo, F. Herpin, E. Lagadec, A. Lançon, Z. Meliani, & F. Royer, Di
Chauvin, G., Desidera, S., Lagrange, A.-M., et al. 2017b, A&A, 605, L9
Chauvin, G., Gratton, R., Bonnefoy, M., et al. 2018, A&A, 617, A76
Chauvin, G., Lagrange, A. M., Bonavita, M., et al. 2010, A&A, 509, A52
Chauvin, G., Lagrange, A. M., Dumas, C., et al. 2004, A&A, 425, L29
Chauvin, G., Lagrange, A. M., Lacombe, F., et al. 2005a, A&A, 430, 1027
Chauvin, G., Lagrange, A. M., Zuckerman, B., et al. 2005b, A&A, 438, L29
Chauvin, G., Vigan, A., Bonnefoy, M., et al. 2015, A&A, 573, A127
Cheetham, A., Bonnefoy, M., Desidera, S., et al. 2018, A&A, 615, A160
Cheetham, A. C., Samland, M., Brems, S. S., et al. 2019, A&A, 622, A80
Chen, C. H., Mamajek, E. E., Bitner, M. A., et al. 2011, ApJ, 738, 122
Chen, C. H., Mittal, T., Kuchner, M., et al. 2014a, ApJS, 211, 25
Chen, Y., Girardi, L., Bressan, A., et al. 2014b, MNRAS, 444, 2525
Chilcote, J., Pueyo, L., De Rosa, R. J., et al. 2017, AJ, 153, 182
Choquet, É., Perrin, M. D., Chen, C. H., et al. 2016, ApJ, 817, L2
Chugainov, P. F. 1974, Izvestiya Ordena Trudovogo Krasnogo Znameni Krymskoj Astrofizicheskoj Observatorii, 52, 3
Claudi, R. U., Turatto, M., Gratton, R. G., et al. 2008, in Society of Photo-Optical Instrumentation Engineers (SPIE) Conference Series, Vol. 7014, Proc. SPIE, 70143E
Cumming, A., Butler, R. P., Marcy, G. W., et al. 2008, PASP, 120, 531
Currie, T., Lisse, C. M., Kuchner, M., et al. 2015, ApJ, 807, L7
Cutispoto, G., Messina, S., & Rodonò, M. 2003, A&A, 400, 659
Cutispoto, G., Pastori, L., Tagliaferri, G., Messina, S., & Pallavicini, R. 1999, A&AS, 138, 87
da Silva, L., Torres, C. A. O., de La Reza, R., et al. 2009, A&A, 508,

833
Damiani, F., Prisinzano, L., Pillitteri, I., Micela, G., & Sciortino, S. 2019, A&A, 623, A112
David, T. J. & Hillenbrand, L. A. 2015, ApJ, 804, 146
De Rosa, R. J., Esposito, T. M., Hirsch, L. A., et al. 2019, AJ, 158, 225
De Rosa, R. J., Nielsen, E. L., Wang, J. J., et al. 2020, AJ, 159, 1
De Rosa, R. J., Rameau, J., Patience, J., et al. 2016, ApJ, 824, 121
de Zeeuw, P. T., Hoogerwerf, R., de Bruijne, J. H. J., Brown, A. G. A., & Blaauw, A. 1999, AJ, 117, 354
Delorme, P., Schmidt, T., Bonnefoy, M., et al. 2017, A&A, 608, A79
Desidera, S., Covino, E., Messina, S., et al. 2015, A&A, 573, A126
Desidera, S., Covino, E., Messina, S., et al. 2011, A&A, 529, A54
Dohlen, K., Langlois, M., Saisse, M., et al. 2008, in Society of Photo-Optical Instrumentation Engineers (SPIE) Conference Series, Vol. 7014, Proc. SPIE, 70143L
Donahue, R. A., Saar, S. H., & Baliunas, S. L. 1996, ApJ, 466, 384
Duflot, M., Fehrenbach, C., Mannone, C., Burnage, R., & Genty, V. 1995, A&AS, 110, 177
Eisenbeiss, T., Ammler-von Eiff, M., Roell, T., et al. 2013, A&A, 556, A53
Elliott, P., Bayo, A., Melo, C. H. F., et al. 2014, A&A, 568, A26
Engler, N., Boccaletti, A., Schmid, H. M., et al. 2019, A&A, 622, A192
Engler, N., Lazzoni, C., Gratton, R., et al. 2020, A&A, 635, A19
Erspamer, D. & North, P. 2003, A&A, 398, 1121
Esposito, S., Mesa, D., Skemer, A., et al. 2013, A&A, 549, A52
Evans, D. S. 1967, in IAU Symposium, Vol. 30, Determination of Radial Velocities and their Applications, ed. A. H. Batten & J. F. Heard, 57
Favata, F., Micela, G., & Sciortino, S. 1997, A&A, 322, 131
Fernandes, R. B., Mulders, G. D., Pascucci, I., Mordasini, C., & Emsenhuber, A. 2019, ApJ, 874, 81
Fernández, D., Figueras, F., & Torra, J. 2008, A&A, 480, 735
Folsom, C. P., Petit, P., Bouvier, J., et al. 2016, MNRAS, 457, 580
Frasca, A., Guillout, P., Klutsch, A., et al. 2018, A&A, 612, A96
Gagné, J., Mamajek, E. E., Malo, L., et al. 2018a, ApJ, 856, 23
Gagné, J., Roy-Loubier, O., Faherty, J. K., Doyon, R., & Malo, L. 2018b, ApJ, 860, 43
Gaia Collaboration, Brown, A. G. A., Vallenari, A., et al. 2018, A&A, 616, A1
Gaia Collaboration, Brown, A. G. A., Vallenari, A., et al. 2016, A&A, 595, A2
Gaidos, E. J., Henry, G. W., & Henry, S. M. 2000, AJ, 120, 1006
Galicher, R., Marois, C., Macintosh, B., et al. 2016, A&A, 594, A63
Goldman, B., Röser, S., Schilbach, E., Moór, A. C., & Henning, T. 2018, ApJ, 868, 32
Gontcharov, G. A. 2006, Astronomy Letters, 32, 759
Grandjean, A., Lagrange, A. M., Beust, H., et al. 2019, A&A, 627, L9
Grandjean, A., Lagrange, A. M., Keppler, M., et al. 2020, A&A, 633, A44
Gray, R. O., Corbally, C. J., Garrison, R. F., et al. 2006, AJ, 132, 161
Gray, R. O., Corbally, C. J., Garrison, R. F., McFadden, M. T., & Robinson, P. E. 2003, AJ, 126, 2048
Greenbaum, A. Z., Pueyo, L., Ruffio, J.-B., et al. 2018, AJ, 155, 226
Guenther, E. W., Esposito, M., Mundt, R., et al. 2007, A&A, 467, 1147
Guenther, E. W., Neuhäuser, R., Huélamo, N., Brandner, W., & Alves, J. 2001, A&A, 365, 514
Haffert, S. Y., Bohn, A. J., de Boer, J., et al. 2019, Nature Astronomy, 3, 749
Heinze, A. N., Hinz, P. M., Kenworthy, M., et al. 2010, ApJ, 714, 1570
Henry, T. J., Soderblom, D. R., Donahue, R. A., & Baliunas, S. L. 1996, AJ, 111, 439
Herbst, W., Bailer-Jones, C. A. L., Mundt, R., Meisenheimer, K., & Wackermann, R. 2002, A&A, 396, 513
Hines, D. C., Schneider, G., Hollenbach, D., et al. 2007, ApJ, 671, L165
Hinkley, S., Kraus, A. L., Ireland, M. J., et al. 2015, ApJ, 806, L9
Hojjatpanah, S., Figueira, P., Santos, N. C., et al. 2019, A&A, 629, A80
Hormuth, F., Hippler, S., Brandner, W., Wagner, K., & Henning, T. 2008, in Society of Photo-Optical Instrumentation Engineers (SPIE) Conference Series, Vol. 7014, Proc. SPIE, 701448
Horne, J. H. & Baliunas, S. L. 1986, ApJ, 302, 757
Howard, A. W., Marcy, G. W., Johnson, J. A., et al. 2010, Science, 330, 653
Hünsch, M., Schmitt, J. H. M. M., Sterzik, M. F., & Voges, W. 1999, A&AS, 135, 319
Ingraham, P., Marley, M. S., Saumon, D., et al. 2014, ApJ, 794, L15
Isaacson, H. & Fischer, D. 2010, ApJ, 725, 875
Janson, M., Asensio-Torres, R., André, D., et al. 2019, A&A, 626, A99
Janson, M., Carson, J. C., Lafrenière, D., et al. 2012, ApJ, 747, 116
Jeffers, S. V., Schöfer, P., Lamert, A., et al. 2018, A&A, 614, A76
Jenkins, J. S., Jones, H. R. A., Tinney, C. G., et al. 2006, MNRAS, 372, 163
Jenkins, J. S., Murgas, F., Rojo, P., et al. 2011, A&A, 531, A8
Johnson, D. R. H. & Soderblom, D. R. 1987, AJ, 93, 864
Johnson, J. A., Aller, K. M., Howard, A. W., & Crepp, J. R. 2010, PASP, 122, 905
Kalas, P., Fitzgerald, M. P., & Graham, J. R. 2007, ApJ, 661, L85
Kalas, P., Graham, J. R., Chiang, E., et al. 2008, Science, 322, 1345
Keppler, M., Benisty, M., Müller, A., et al. 2018, A&A, 617, A44
King, J. R. & Schuler, S. C. 2005, PASP, 117, 911
King, J. R., Villarreal, A. R., Soderblom, D. R., Gulliver, A. F., & Adelman, S. J. 2003, AJ, 125, 1980
Kiraga, M. 2012a, Acta Astron., 62, 67
Kiraga, M. 2012b, Acta Astron., 62, 67
Kiss, L. L., Moór, A., Szalai, T., et al. 2011, MNRAS, 411, 117
Koen, C. & Eyer, L. 2002, MNRAS, 331, 45
Kraus, A. L., Shkolnik, E. L., Allers, K. N., & Liu, M. C. 2014, AJ, 147, 146
Kunder, A., Kordopatis, G., Steinmetz, M., et al. 2017, AJ, 153, 75
Kuzuhara, M., Tamura, M., Kudo, T., et al. 2013, ApJ, 774, 11
Lafrenière, D., Doyon, R., Marois, C., et al. 2007, ApJ, 670, 1367
Lafrenière, D., Jayawardhana, R., Janson, M., et al. 2011, ApJ, 730, 42
Lafrenière, D., Jayawardhana, R., & van Kerkwijk, M. H. 2008, ApJL, 689, L153
Lagrange, A. M., Boccaletti, A., Langlois, M., et al. 2019, A&A, 621, L8
Lagrange, A.-M., Desort, M., Galland, F., Udry, S., & Mayor, M. 2009, A&A, 495, 335
Lagrange, A.-M., Rubini, P., Brauner-Vettier, N., et al. 2016, in Proc. SPIE, Vol. 9910, Observatory Operations: Strategies, Processes, and Systems VI, 991033
Lamm, M. H., Bailer-Jones, C. A. L., Mundt, R., Herbst, W., & Scholz, A. 2004, A&A, 417, 557
Lawler, S. M., Greenstreet, S., & Gladman, B. 2015, ApJ, 802, L20
Lawson, W. A. & Crause, L. A. 2005, MNRAS, 357, 1399
Lazzoni, C., Desidera, S., Marzari, F., et al. 2018, A&A, 611, A43
Lee, J. & Song, I. 2019, MNRAS, 489, 2189
Liu, M. C. 2004, Science, 305, 1442
Lowrance, P. J., Schneider, G., Kirkpatrick, J. D., et al. 2000, ApJ, 541, 390
Luhman, K. L., Wilson, J. C., Brandner, W., et al. 2006, ApJ, 649, 894
Macintosh, B., Graham, J. R., Barman, T., et al. 2015, Science, 350, 64
Macintosh, B., Graham, J. R., Ingraham, P., et al. 2014, Proceedings of the National Academy of Science, 111, 12661
Madsen, S., Dravins, D., & Lindegren, L. 2002, A&A, 381, 446
Maire, A.-L., Bonnefoy, M., Ginski, C., et al. 2016, A&A, 587, A56
Maire, A. L., Rodet, L., Cantalloube, F., et al. 2019, A&A, 624, A118
Maire, A. L., Rodet, L., Lazzoni, C., et al. 2018, A&A, 615, A177
Malo, L., Artigau, É., Doyon, R., et al. 2014, ApJ, 788, 81
Malo, L., Doyon, R., Lafrenière, D., et al. 2013, ApJ, 762, 88
Mamajek, E. E. 2012, ApJ, 754, L20
Mamajek, E. E., Bartlett, J. L., Seifahrt, A., et al. 2013, AJ, 146, 154
Mamajek, E. E. & Hillenbrand, L. A. 2008, ApJ, 687, 1264
Mamajek, E. E., Lawson, W. A., & Feigelson, E. D. 1999, ApJ, 516, L77
Marley, M. S., Fortney, J. J., Hubickyj, O., Bodenheimer, P., & Lissauer, J. J. 2007, ApJ, 655, 541
Marois, C., Lafrenière, D., Doyon, R., Macintosh, B., & Nadeau, D. 2006, ApJ, 641, 556
Marois, C., Macintosh, B., Barman, T., et al. 2008, Science, 322, 1348
Marois, C., Zuckerman, B., Konopacky, Q. M., Macintosh, B., & Barman, T. 2010, Nature, 468, 1080
Marsden, S. C., Jardine, M. M., Ramírez Vélez, J. C., et al. 2011, MNRAS, 413, 1939
Marsden, S. C., Petit, P., Jeffers, S. V., et al. 2014, MNRAS, 444, 3517
Martínez-Arnáiz, R., Maldonado, J., Montes, D., Eiroa, C., & Montesinos, B. 2010, A&A, 520, A79
Mawet, D., Pueyo, L., Lawson, P., et al. 2012, in Society of Photo-Optical Instrumentation Engineers (SPIE) Conference Series,

Vol. 8442, Space Telescopes and Instrumentation 2012: Optical, Infrared, and Millimeter Wave. Proceedings of the SPIE, Volume 8442, article id. 844204, 21 pp. (2012)., 844204
Mayor, M., Marmier, M., Lovis, C., et al. 2011, arXiv e-prints, arXiv:1109.2497
Mesa, D., Gratton, R., Zurlo, A., et al. 2015, A&A, 576, A121
Mesa, D., Keppler, M., Cantalloube, F., et al. 2019, A&A, 632, A25
Messina, S., Desidera, S., Lanzafame, A. C., Turatto, M., & Guinan, E. F. 2011, A&A, 532, A10
Messina, S., Desidera, S., Turatto, M., Lanzafame, A. C., & Guinan, E. F. 2010, A&A, 520, A15
Messina, S., Millward, M., Buccino, A., et al. 2017, A&A, 600, A83
Messina, S., Rodonò, M., & Guinan, E. F. 2001, A&A, 366, 215
Meyer, M. R., Amara, A., Reggiani, M., & Quanz, S. P. 2018, A&A, 612, L3
Milli, J., Engler, N., Schmid, H. M., et al. 2019, A&A, 626, A54
Milli, J., Vigan, A., Mouillet, D., et al. 2017, A&A, 599, A108
Miret-Roig, N., Galli, P. A. B., Brandner, W., et al. 2020, A&A, 642, A179
Moerchen, M. M., Telesco, C. M., & Packham, C. 2010, ApJ, 723, 1418
Moerchen, M. M., Telesco, C. M., Packham, C., & Kehoe, T. J. J. 2007, ApJ, 655, L109
Montes, D., López-Santiago, J., Gálvez, M. C., et al. 2001, MNRAS, 328, 45
Montesinos, B., Eiroa, C., Krivov, A. V., et al. 2016, A&A, 593, A51
Mora, A., Merín, B., Solano, E., et al. 2001, A&A, 378, 116
Mosser, B., Michel, E., Appourchaux, T., et al. 2009, A&A, 506, 33
Mouillet, D., Beuzit, J. L., Desidera, S., et al. 2010, in In the Spirit of Lyot 2010, E50
Moultaka, J., Ilovaisky, S. A., Prugniel, P., & Soubiran, C. 2004, PASP, 116, 693
Mugrauer, M., Vogt, N., Neuhäuser, R., & Schmidt, T. O. B. 2010, A&A, 523, L1
Müller, A., Keppler, M., Henning, T., et al. 2018, A&A, 617, L2
Nakajima, T. & Morino, J.-I. 2012, AJ, 143, 2
Neuhäuser, R., Guenther, E. W., Wuchterl, G., et al. 2005, A&A, 435, L13
Nidever, D. L., Marcy, G. W., Butler, R. P., Fischer, D. A., & Vogt, S. S. 2002, ApJS, 141, 503
Nielsen, E. L., De Rosa, R. J., Macintosh, B., et al. 2019, AJ, 158, 13
Nielsen, E. L., Liu, M. C., Wahhaj, Z., et al. 2013, ApJ, 776, 4
Nordström, B., Mayor, M., Andersen, J., et al. 2004, A&A, 418, 989
Noyes, R. W., Hartmann, L. W., Baliunas, S. L., Duncan, D. K., & Vaughan, A. H. 1984, ApJ, 279, 763
Oelkers, R. J., Rodriguez, J. E., Stassun, K. G., et al. 2018, AJ, 155, 39
Olofsson, J., Samland, M., Avenhaus, H., et al. 2016, A&A, 591, A108
Olofsson, J., van Holstein, R. G., Boccaletti, A., et al. 2018, A&A, 617, A109
Pallavicini, R., Pasquini, L., & Randich, S. 1992, A&A, 261, 245
Pecaut, M. J. & Mamajek, E. E. 2013, ApJS, 208, 9
Pecaut, M. J. & Mamajek, E. E. 2016, MNRAS, 461, 794
Pecaut, M. J., Mamajek, E. E., & Bubar, E. J. 2012, ApJ, 746, 154
Perrot, C., Thebault, P., Lagrange, A.-M., et al. 2019, A&A, 626, A95
Plavchan, P., Barclay, T., Gagné, J., et al. 2020, Nature, 582, 497
Press, W. H., Teukolsky, S. A., Vetterling, W. T., & Flannery, B. P. 2002, Numerical recipes in C++ : the art of scientific computing (Cambridge University Press)
Pribulla, T., Sebastian, D., Ammler-von Eiff, M., et al. 2014, MNRAS, 443, 2815
Rajan, A., Rameau, J., De Rosa, R. J., et al. 2017, AJ, 154, 10
Rameau, J., Chauvin, G., Lagrange, A.-M., et al. 2013a, ApJL, 772, L15
Rameau, J., Chauvin, G., Lagrange, A. M., et al. 2013b, A&A, 553, A60
Rameau, J., Nielsen, E. L., De Rosa, R. J., et al. 2016, ApJ, 822, L29
Rebull, L. M., Stapelfeldt, K. R., Werner, M. W., et al. 2008, ApJ, 681, 1484
Rebull, L. M., Stauffer, J. R., Bouvier, J., et al. 2016, AJ, 152, 113
Reddy, A. B. S. & Lambert, D. L. 2017, ApJ, 845, 151
Reffert, S., Bergmann, C., Quirrenbach, A., Trifonov, T., & Künstler, A. 2013, in Protostars and Planets VI Posters, 28
Reid, I. N., Gizis, J. E., & Hawley, S. L. 2002, AJ, 124, 2721
Reiners, A., Joshi, N., & Goldman, B. 2012, AJ, 143, 93
Reiners, A. & Schmitt, J. H. M. M. 2003, A&A, 412, 813
Rizzuto, A. C., Ireland, M. J., & Robertson, J. G. 2011, MNRAS, 416, 3108
Roberts, D. H., Lehar, J., & Dreher, J. W. 1987, AJ, 93, 968
Robin, A. & Creze, M. 1986, A&A, 157, 71
Rodet, L., Bonnefoy, M., Durkan, S., et al. 2018, A&A, 618, A23
Rodriguez, D. R., Duchêne, G., Tom, H., et al. 2015, MNRAS, 449, 3160
Royer, F., Grenier, S., Baylac, M. O., Gómez, A. E., & Zorec, J. 2002, A&A, 393, 897
Royer, F., Zorec, J., & Gómez, A. E. 2007, A&A, 463, 671
Samland, M., Mollière, P., Bonnefoy, M., et al. 2017, A&A, 603, A57
Scargle, J. D. 1982, ApJ, 263, 835
Schneider, A. C., Shkolnik, E. L., Allers, K. N., et al. 2019, AJ, 157, 234
Schneider, G., Smith, B. A., Becklin, E. E., et al. 1999, ApJ, 513, L127
Scholz, A., Coffey, J., Brandeker, A., & Jayawardhana, R. 2007, ApJ, 662, 1254
Schröder, C., Reiners, A., & Schmitt, J. H. M. M. 2009, A&A, 493, 1099
Sissa, E., Gratton, R., Garufi, A., et al. 2018, A&A, 619, A160
Skelly, M. B., Unruh, Y. C., Collier Cameron, A., et al. 2008, MNRAS, 385, 708
Smith, L. C., Lucas, P. W., Contreras Peña, C., et al. 2015, MNRAS, 454, 4476
Soummer, R., Perrin, M. D., Pueyo, L., et al. 2014, ApJ, 786, L23
Spina, L., Nordlander, T., Casey, A. R., et al. 2020, arXiv e-prints, arXiv:2004.09771
Stauffer, J., Rebull, L. M., Cody, A. M., et al. 2018, AJ, 156, 275
Su, K. Y. L., Rieke, G. H., Stansberry, J. A., et al. 2006, ApJ, 653, 675
Sumi, T., Kamiya, K., Bennett, D. P., et al. 2011, Nature, 473, 349
Takeda, Y. & Kawanomoto, S. 2005, PASJ, 57, 45
Tanner, A., Plavchan, P., Bryden, G., et al. 2020, arXiv e-prints, arXiv:2004.12597
Tokovinin, A. 2008, MNRAS, 389, 925
Torres, C. A. O., Quast, G. R., da Silva, L., et al. 2006, A&A, 460, 695
Torres, C. A. O., Quast, G. R., Melo, C. H. F., & Sterzik, M. F. 2008, in Handbook of Star Forming Regions, Volume II, ed. Reipurth, B., 757
Tuthill, P., Lloyd, J., Ireland, M., et al. 2006, in Society of Photo-Optical Instrumentation Engineers (SPIE) Conference Series, Vol. 6272, Proc. SPIE, 62723A
Udry, S., Mayor, M., Naef, D., et al. 2000, A&A, 356, 590
Uesugi, A. & Fukuda, I. 1970, Catalogue of rotational velocities of the stars (University, Kwasan Observatory, Institute of Astrophysics)
van Leeuwen, F. 2007, A&A, 474, 653
Viana Almeida, P., Santos, N. C., Melo, C., et al. 2009, A&A, 501, 965
Vican, L. 2012, AJ, 143, 135
Vigan, A., Bonavita, M., Biller, B., et al. 2017, A&A, 603, A3
Vigan, A., Fontanive, C., Meyer, M., et al. 2020, arXiv e-prints, arXiv:2007.06573
Vigan, A., Moutou, C., Langlois, M., et al. 2010, MNRAS, 407, 71
Vigan, A., Patience, J., Marois, C., et al. 2012, A&A, 544, A9
Voges, W., Aschenbach, B., Boller, T., et al. 1999, A&A, 349, 389
Voges, W., Aschenbach, B., Boller, T., et al. 2000, IAU Circ., 7432, 3
Wahhaj, Z., Liu, M. C., Biller, B. A., et al. 2011, ApJ, 729, 139
Wahhaj, Z., Liu, M. C., Nielsen, E. L., et al. 2013, ApJ, 773, 179
Wang, J. J., Graham, J. R., Dawson, R., et al. 2018, AJ, 156, 192
Wang, S., Liu, J., Qiu, Y., et al. 2016, ApJS, 224, 40
White, R. J., Gabor, J. M., & Hillenbrand, L. A. 2007, AJ, 133, 2524
Wichmann, R., Schmitt, J. H. M. M., & Hubrig, S. 2003, A&A, 399, 983
Wright, J. T., Marcy, G. W., Butler, R. P., & Vogt, S. S. 2004, ApJS, 152, 261
Wright, N. J., Drake, J. J., Mamajek, E. E., & Henry, G. W. 2011, ApJ, 743, 48
Wright, N. J. & Mamajek, E. E. 2018, MNRAS, 476, 381
Zickgraf, F. J., Krautter, J., Reffert, S., et al. 2005, A&A, 433, 151
Zorec, J. & Royer, F. 2012, A&A, 537, A120
Zuckerman, B. 2019, ApJ, 870, 27
Zuckerman, B., Rhee, J. H., Song, I., & Bessell, M. S. 2011, ApJ, 732, 61
Zuckerman, B. & Song, I. 2004, ARA&A, 42, 685
Zuckerman, B. & Song, I. 2012, ApJ, 758, 77
Zuckerman, B., Song, I., Bessell, M. S., & Webb, R. A. 2001, ApJ, 562, L87
Zurlo, A., Mesa, D., Desidera, S., et al. 2018, MNRAS, 480, 35

Zurlo, A., Vigan, A., Galicher, R., et al. 2016, A&A, 587, A57

Appendix A: Notes on individual objects

Together with relevant notes on individual targets, i Figs A.1– A.85 we summarize the results of our periodogram analysis. In the top left panel we plot magnitude versus TESS Julian Date, unless differently specified. In th top middle panel we plot the Lomb−Scargle periodogra with the spectral window function (red dotted line) an power level corresponding to FAP = 0.01% and 0.1% (horizontal dashed line), and we indicate the peak corresponding to the rotation period. In the top right panel we plo the CLEAN periodogram. In the bottom panel we plot th light curve phased with the rotation period. The solid lin represents the sinusoidal fit.

HIP 490 = HD 105 We measured for the first time the rotation period from the TESS photometric time series (Fig. A.1). The light curve exhibits a significant evolution of amplitude in subsequent rotation cycles.

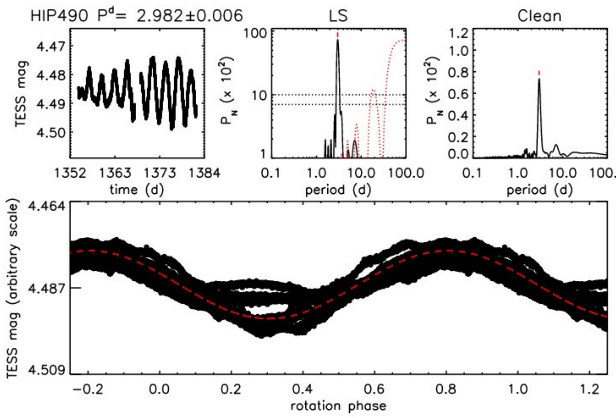

Fig. A.1: Photometric time sequence and periodogram for HIP490 = HD 105

HIP 682 = HD 377 Star with resolved debris disk (Choquet et al. 2016). We measured for the first time the rotation period from the All Sky Automated Survey (ASAS) photometric time series (Fig. A.2). This allowed us to refine the age estimate of the target, which results very close to that of the Pleiades. The star does not result as a member of any known young moving group. The inclination estimated from rotation period, $v \sin i$, and stellar radius is compatible within the error with that of the disk (85±5°). It was set as P0 target for disk characterization purposes.

HIP 1113 = HD 987 The photometric rotation period first measured by Messina et al. (2010) is confirmed by our analysis of the TESS data (Fig. A.3). The TESS data revealed one flare event superimposed on a quite stable light curve.

2MASS J00172353-6645124 The photometric rotation period first measured by Messina et al. (2017) is confirmed by our analysis of the TESS data (Fig. A.4). The TESS data revealed, superimposed on a quite stable light curve, the presence of multiple flare events, that support the young age estimated for this M-type star.

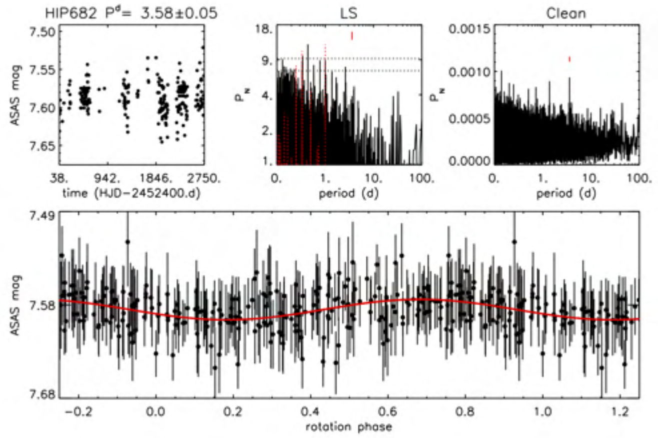

Fig. A.2: Photometric time sequence and periodogram for HIP682 = HD 377

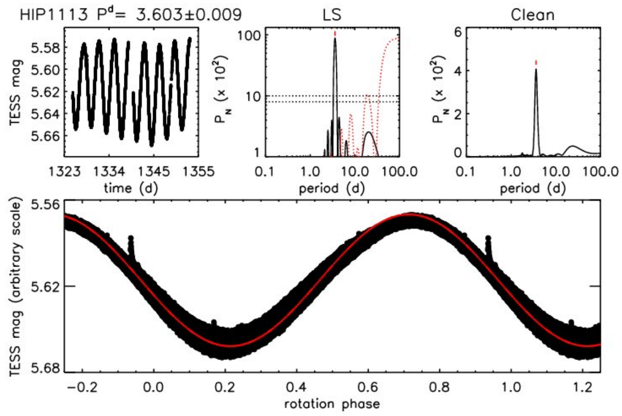

Fig. A.3: Photometric time sequence and periodogram for HIP1113

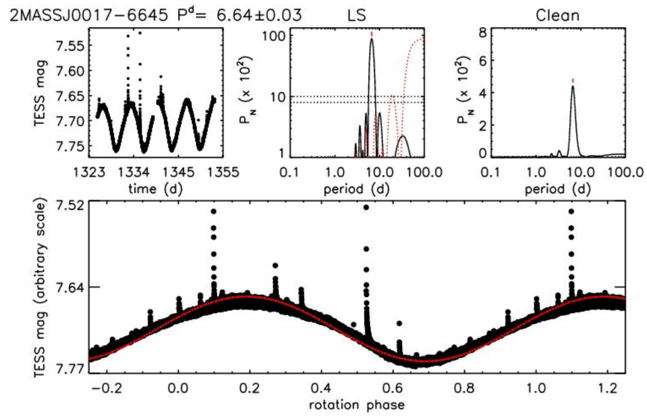

Fig. A.4: Photometric time sequence and periodogram for 2MASSJ0017-6645

HIP 1481 = HD 1466 We measured for the first time the rotation period from the TESS photometric time series (Fig. A.5).

HIP 1993 = CT Tuc The photometric rotation period first measured by Messina et al. (2010) is confirmed by our analysis of the TESS data (Fig. A.6). The

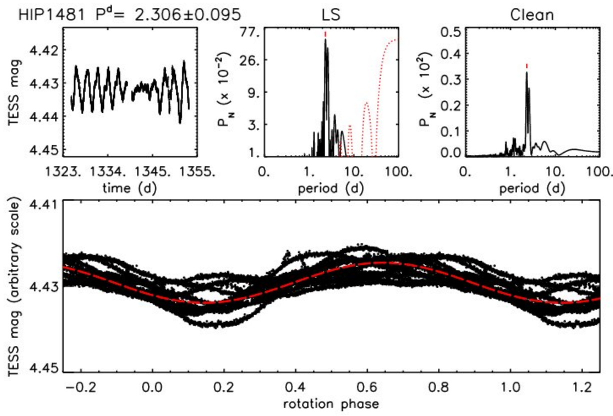

Fig. A.5: Photometric time sequence and periodogram for HIP1481

TESS data revealed, superimposed on a quite stable light curve, the presence of multiple flare events, that support the young age estimated for this M-type star.

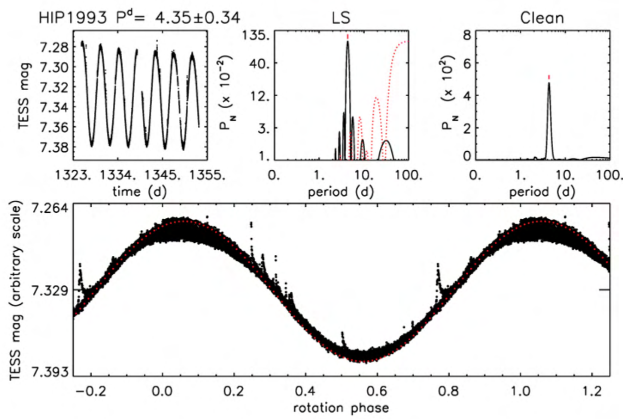

Fig. A.6: Photometric time sequence and periodogram for HIP1993

HIP 2578 = HD 3003 Member of Tuc-Hor association. It is comoving with the quadruple system HIP 2484+HIP 2487 (both of which are also visual binaries) at 25350 au projected separation. Masses of the components in Table 10 taken from Tokovinin (2008).

HIP 6276 = BD-12 243 We measured for the first time the rotation period from the TESS photometric time series (Fig. A.7), which is in rough agreement with the earlier measurement (P = 6.40 d) by Wright et al. (2011). TESS data revealed, superimposed on a quite stable light curve, the presence of multiple flare events.

HIP 6485 = HD 8558 The photometric rotation period first measured by Messina et al. (2010) is confirmed by the TESS data (Fig. A.8) and is in agreement with the measurements by Oelkers et al. (2018). TESS data reveal signficant evolution of light curve amplitude and numerous flare events.

HIP 6856 = HD 9054 We measured for the first time the rotation period from the TESS photometric time series (Fig. A.9), which revealed numerous flare events.

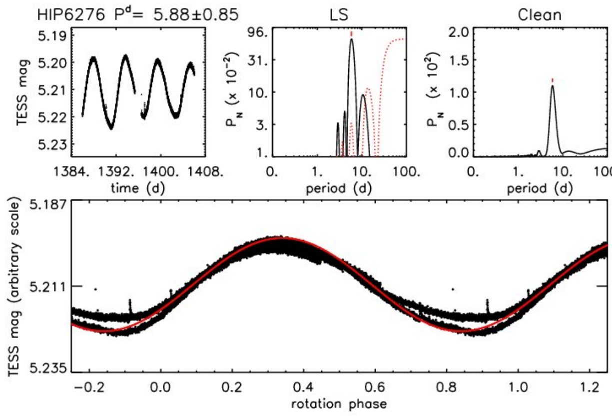

Fig. A.7: Photometric time sequence and periodogram for HIP6276

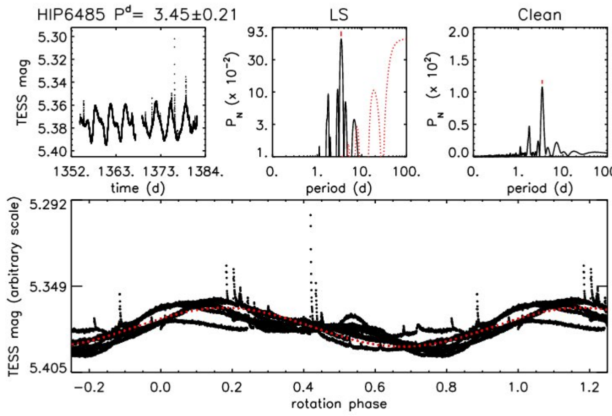

Fig. A.8: Photometric time sequence and periodogram for HIP6485

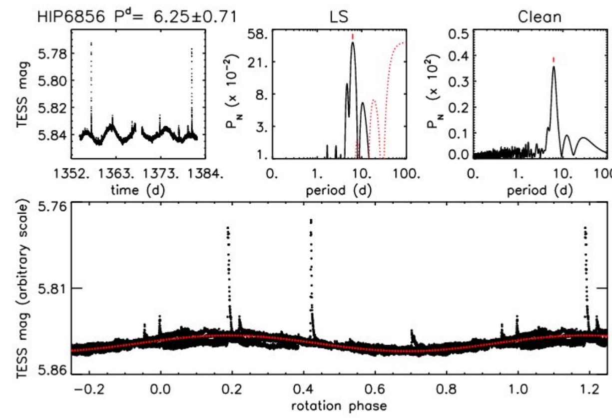

Fig. A.9: Photometric time sequence and periodogram for HIP6856

TYC 8047-0232-1 Star with brown dwarf companion discovered by Chauvin et al. (2005a). The photometric rotation period first measured by Messina et al. (2010) is confirmed by our analysis of the TESS data (Fig. A.10).

HIP 11360 = HD 15115 The revised RV from Desidera et al. (2015) supports the membership to the Tuc-Hor association (93.7% using BANYAN). The star has a spa-

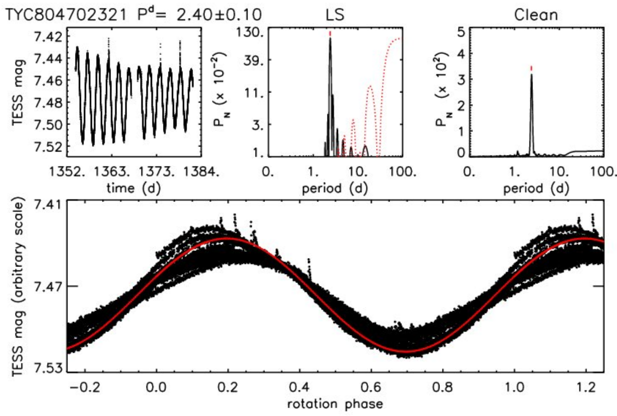

Fig. A.10: Photometric time sequence and periodogram for TYC 8047-0232-1

tially resolved edge-on debris disk (Kalas et al. 2007; Engler et al. 2019). We measured for the first time the rotation period from the TESS photometric time series (Fig. A.11).

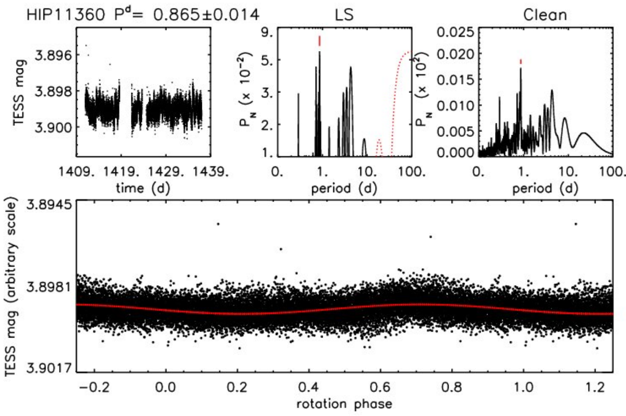

Fig. A.11: Photometric time sequence and periodogram for HIP11360

HIP 13402 = HD 17925 = EP Eri Flagged as RS CVn variable, with spectral types K1+K2 and period 6.85d in Rodriguez et al. (2015). However, HARPS observations available in ESO archive allow us to rule out the presence of close stellar companions (rms = 28 m s^{-1} from 42 RVs over 1200 days). We then kept the star in the sample. The photometric rotation period first measured by Messina et al. (2001) is confirmed by our analysis of the TESS data (Fig. A.12).

HIP 14551 = HD 19545 Originally classified as a member of Tuc-Hor (Zuckerman et al. 2011), the updated analysis indicates membership in the Columba association. The wide companion, UCAC4 311-003056, has been also classified as a member of the Columba association (Gagné et al. 2018b). The small but formally significant differences in parallax and proper motion make it possible that the two stars do not form a true binary system and are only projected very close on the sky (59 arcsec).

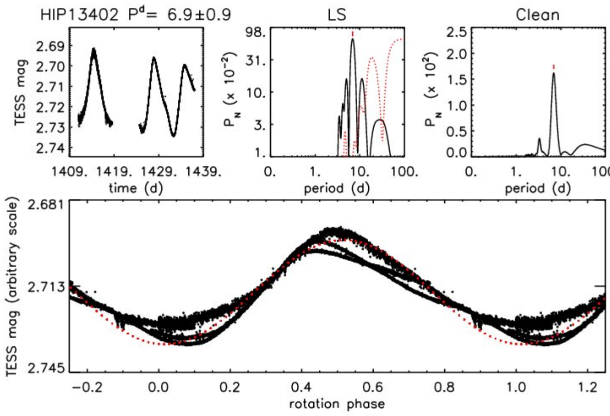

Fig. A.12: Photometric time sequence and periodogram for HIP13402

TYC 7026-0325-1 The photometric rotation period first measured by Messina et al. (2010) is confirmed by our analysis of the TESS data (Fig. A.13).

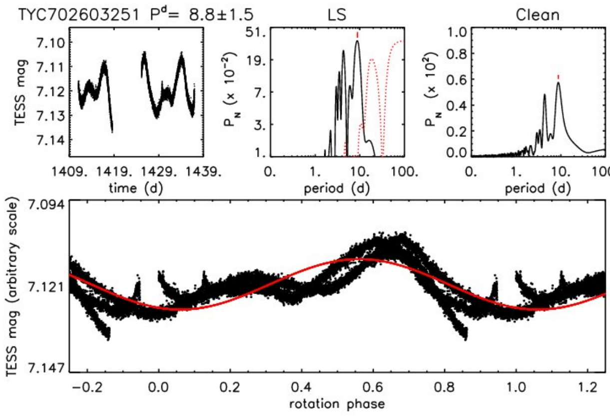

Fig. A.13: Photometric time sequence and periodogram for TYC 7026-0325-1

HIP 15457 = HD 20630 = κ Cet The photometric rotation period first measured by Messina et al. (2001) is confirmed by our analysis of the TESS data (Fig. A.14). The presence of numerous flare events are detected.

TYC 8060-1673-1 The photometric rotation period first measured by Messina et al. (2010) is confirmed by our analysis of the TESS data (Fig. A.15).

HIP 17764 = HD 24636 We measured for the first time the rotation period from the TESS photometric time series (Fig. A.16).

HD 25284B We measured for the first time the rotation period from the TESS photometric time series (Fig. A.17). We note that according to SIMBAD coordinates, HD 25284A and B are unresolved in the TESS photometry. As shown in the figure, both Lomb−Scargle and Clean detected three significant periods that are in order of decreasing power P = 4.54 d, P = 2.26 d, and P = 0.31 d. Considering that HD 25284B has $v \sin i$ = 6.9 km s^{-1}, its rotation period should be P = 4.54 d to reconcile with stellar radius and projected rotational velocity. Following similar reasoning, considering that

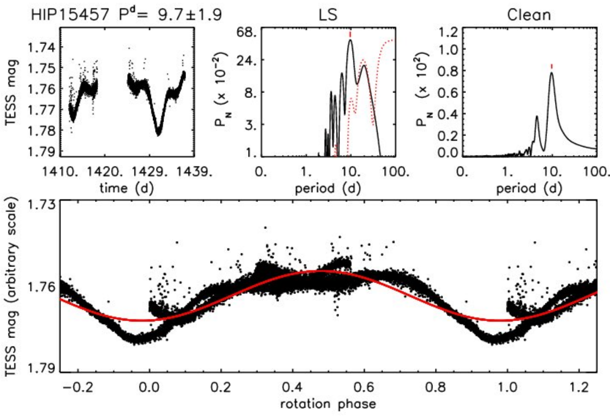

Fig. A.14: Photometric time sequence and periodogram for HIP15457 (κ Cet)

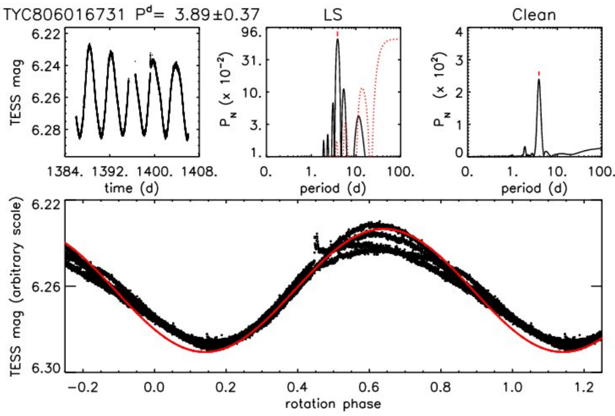

Fig. A.15: Photometric time sequence and periodogram for TYC 8060-1673-1

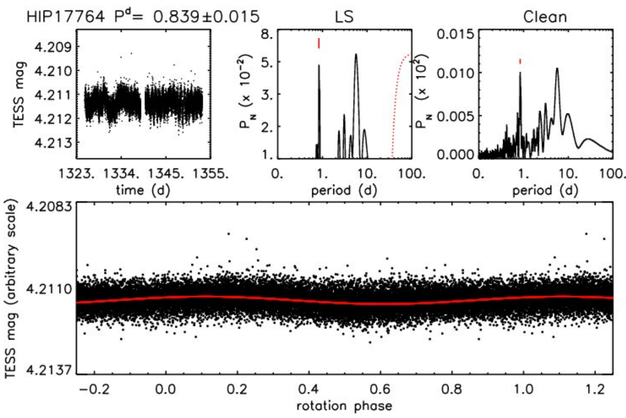

Fig. A.16: Photometric time sequence and periodogram for HIP17764

HD 25284A has $v \sin i = 69.8\,\mathrm{km\,s^{-1}}$, its rotation period should be P = 0.31 d. The remaining period P = 2.26 d, half of the primary period, may arise from the double-dip shape of the light curve.

TYC 5882-1169-1 = BD-15 705 Originally classified as a member of the Columba association, the updated analysis indicates membership in the Tuc-Hor association. The photometric rotation period first measured by Messina et al. (2010) is confirmed by our analysis of the TESS data (Fig. A.18). More flare events are detected in the TESS time series.

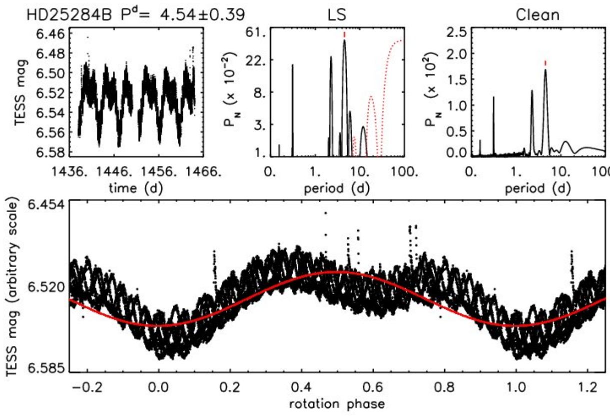

Fig. A.17: Photometric time sequence and periodogram for HD25284B

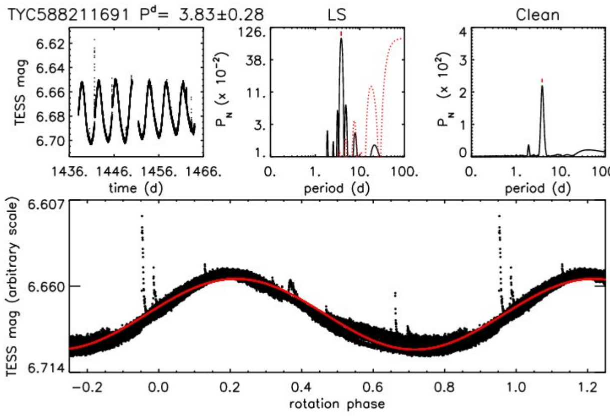

Fig. A.18: Photometric time sequence and periodogram for TYC 5882-1169-1

51 Eri = HIP 21547 The star has a planetary companion discovered by Macintosh et al. (2015). The periodogram analysis of the TESS data shows evidence of multi-periodicity with the most powerful peak at P = 1.84±0.06 d and the secondary power peak in agreement with the early rotation period measurement by Koen & Eyer (2002) (Fig. A.19-A.20-A.21). Considering the F0IV spectral type, it is likely that most periodicities arise from pulsations rather than variability induced by undiscovered close companions.

HIP 22226 = HD 30447 Star with debris disk spatially resolved by Soummer et al. (2014). The star has a close pair of faint comoving companions with very similar astrometric parameters at 622″ = 50100 au projected separation (Gaia DR2 4881308710762664576 and Gaia DR2 4881308710764495744, unique entry in 2MASS, 2MASS J04463413-2627559, ΔG=0.15 mag). The very wide separation is larger than the typical limit for binaries. These objects were flagged as members of Columba in Gagné et al. (2018b). The masses of the two compo-

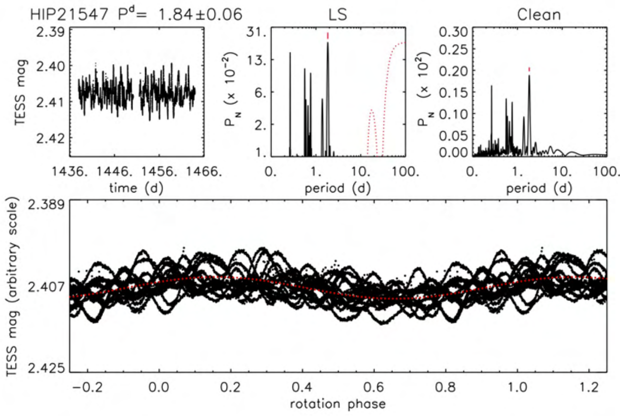

Fig. A.19: Photometric time sequence and periodogram for 51 Eri (HIP21547)

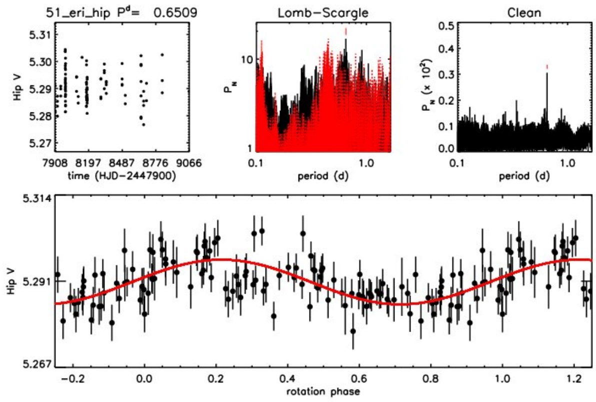

Fig. A.20: Photometric time sequence and periodogram for 51 Eri (HIP21547) (from Hipparcos)

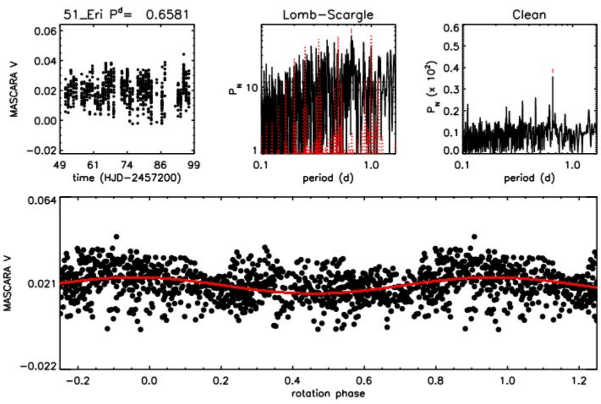

Fig. A.21: Photometric time sequence and periodogram for 51 Eri (HIP 21547) (from the Mascara survey)

nents are close to 0.2 $M_{\odot}$. We measured for the first time the rotation period from the TESS photometric time series (Fig. A.22).

HIP 22295 The photometric rotation period first measured by Kiraga (2012a) is confirmed by our analysis of the TESS data (Fig. A.23). The TESS data show a rapidly evolving double-dip light curve.

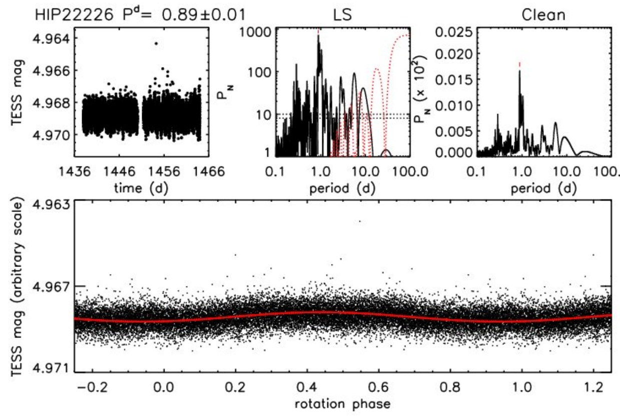

Fig. A.22: Photometric time sequence and periodogram for HIP 22226

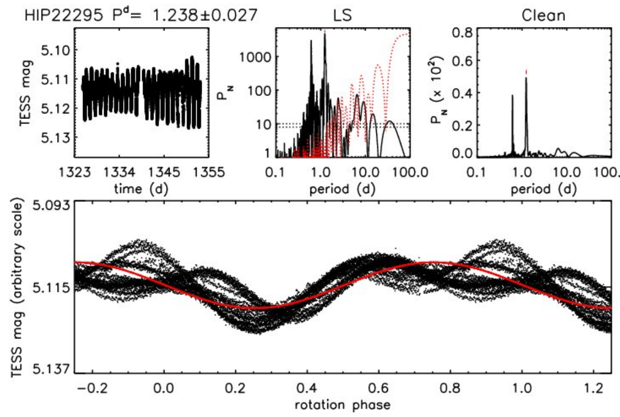

Fig. A.23: Photometric time sequence and periodogram for HIP 22295

TYC 5899-0026-1 We measured for the first time the rotation period from the TESS photometric time series (Fig. A.24). The TESS data reveal TYC 5899-0026-1 to be an M3 star with very intense flare activity.

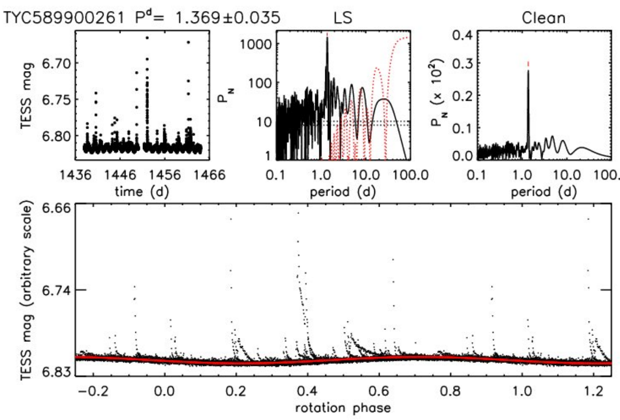

Fig. A.24: Photometric time sequence and periodogram for TYC 5899-0026-1

HIP 23200 The photometric rotation period first measured by Messina et al. (2010) is confirmed by our analysis of the TESS data (Fig. A.25). The TESS data reveal more flare events superimposed on a very stable light curve.

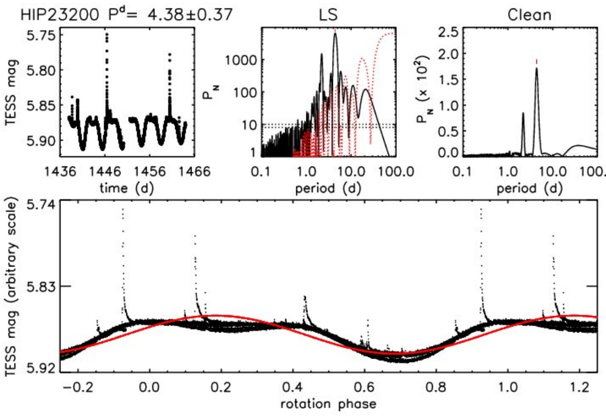

Fig. A.25: Photometric time sequence and periodogram for HIP 23200

HIP 23309 The photometric rotation period first measured by Messina et al. (2010) is confirmed by our analysis of the TESS data. (Fig. A.26). The TESS data reveal more flare events.

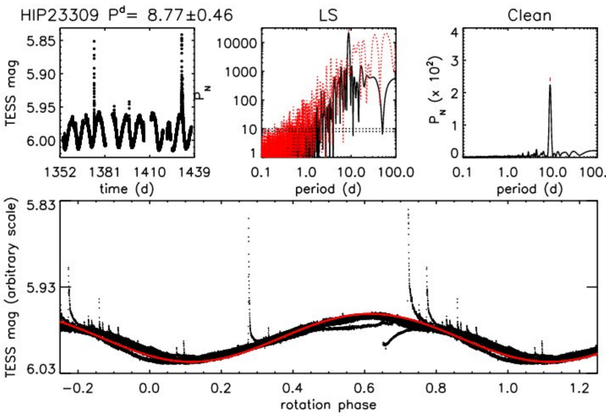

Fig. A.26: Photometric time sequence and periodogram for HIP 23309

HIP 24947 We measured for the first time the rotation period from the TESS photometric time series. (Fig. A.27).

HIP 25283 The photometric rotation period first measured by Messina et al. (2010) is confirmed by our analysis of the TESS data. (Fig. A.28).

HIP 25544 = HD 36435 Age indicators (Li, rotation period, R_X, $R^{'}_{HK}$) converge on an age similar to or possibly slightly older than the Hyades. We adopted 700±150 Myr. The photometric rotation period first measured by Koen & Eyer (2002) is confirmed by our analysis of the TESS data (Fig. A.29). The light curve exhibits a significant evolution from single-dip to double-dip shape.

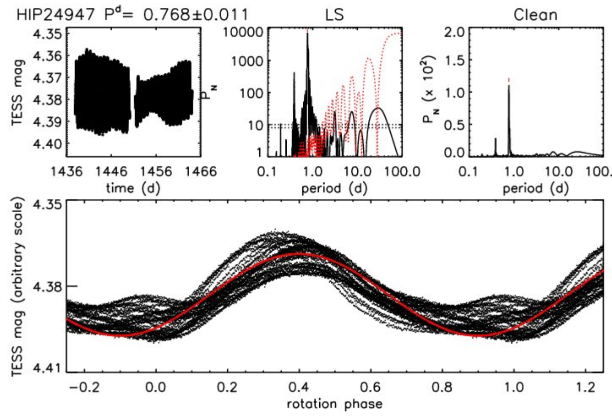

Fig. A.27: Photometric time sequence and periodogram for HIP 24947

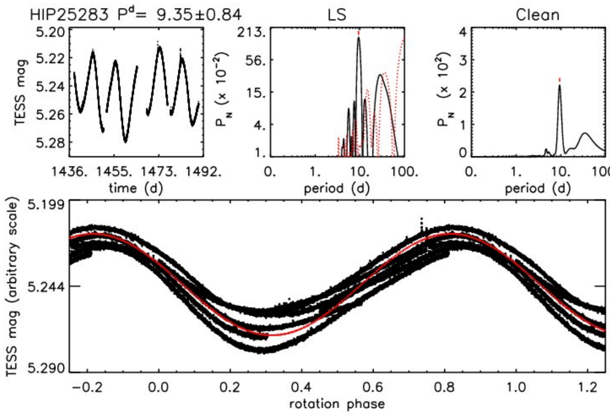

Fig. A.28: Photometric time sequence and periodogram for HIP 25283

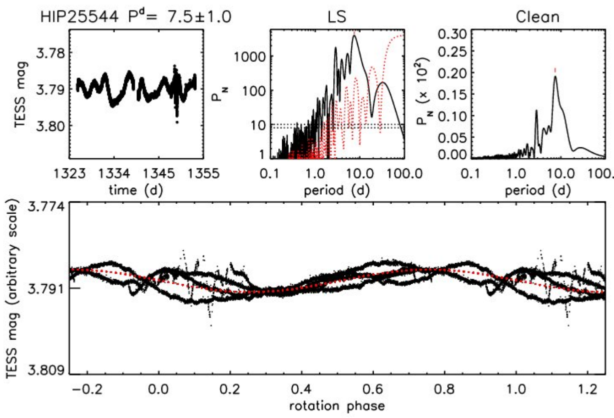

Fig. A.29: Photometric time sequence and periodogram for HIP 25544

ζ Lep = HIP 27288 = HD 38678 Early-type star with spatially resolved debris disk (Moerchen et al. 2007). It was proposed as a member of Castor MG by Barrado y

Navascues (1998). An age of few hundred Myr was derived from isochrone fitting by several authors (e.g., Su et al. 2006; David & Hillenbrand 2015). However, the star was also proposed as a member of β Pic MG by Nakajima & Morino (2012). The β Pic membership and age was also adopted by Nielsen et al. (2019). BANYAN Σ returns a membership probability of 26.9% with the van Leeuwen (2007) astrometric parameters (adopted because of the lower errors with respect to Gaia due to very bright magnitude; Gaia values yield a similar value, 24.6%). We then considered the β Pic membership uncertain, and we adopted the age from isochrones, extending the minimum age to include the β Pic MG age.

TYC 7084-0794-1 = CD-35 2722 Star with BD companion (Wahhaj et al. 2011). The star was not moved to special targets (P0). The photometric rotation period first measured by Messina et al. (2010) is confirmed by our analysis of the TESS data (Fig. A.30). Numerous flare events are detected in the TESS time series.

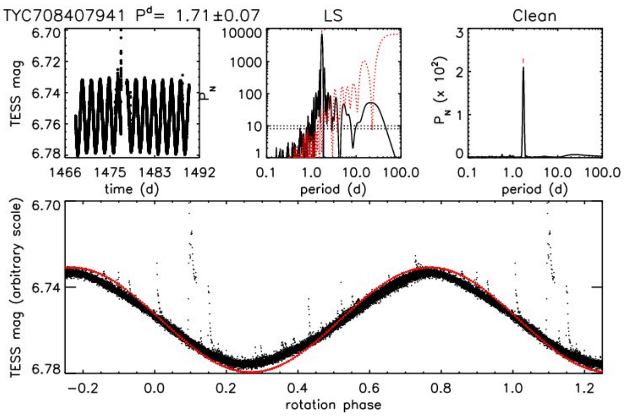

Fig. A.30: Photometric time sequence and periodogram for TYC 7084-0794-1

HIP 30030 = HD 43989 Originally classified as a member of Tuc-Hor; the updated analysis indicates membership in the Columba association. Using TESS photometric time series, we measured a rotation period P = 1.361±0.042 d with very high confidence (Fig. A.31), which supersedes the earlier determination of P = 1.16 d measured by Cutispoto et al. (1999).

HIP 30034 = HD 44627 = AB Pic Star with substellar companion close to the edge of the IRDIS field of view discovered by Chauvin et al. (2005b). The photometric rotation period first measured by Messina et al. (2010) is confirmed by our analysis of the TESS data (Fig. A.32).

HIP 30314 We measured for the first time the rotation period from the TESS photometric time series (Fig. A.33).

GSC 8894-0426 The photometric rotation period first measured by Kiraga (2012b) is confirmed by our analysis of the TESS data (Fig. A.34). Numerous flare events are detected in the TESS time series.

TYC 7617-0549-1 The photometric rotation period first measured by Messina et al. (2010) is confirmed by our analysis of the TESS data (Fig. A.35).

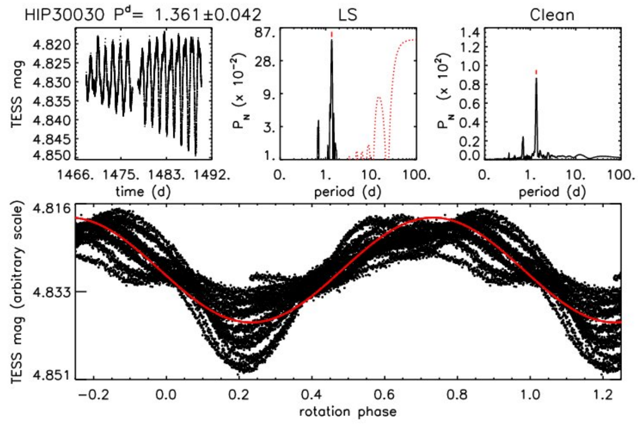

Fig. A.31: Photometric time sequence and periodogram for HIP 30030

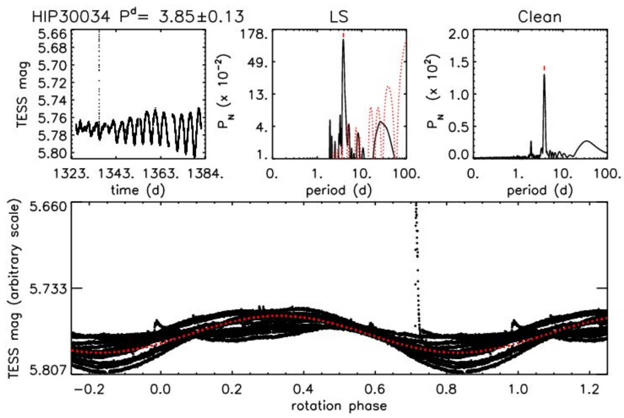

Fig. A.32: Photometric time sequence and periodogram for HIP 30034

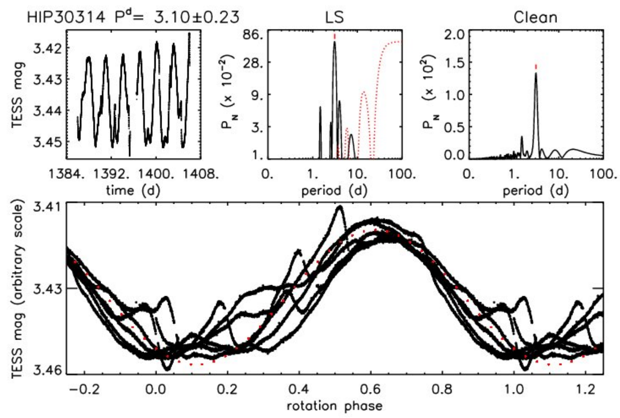

Fig. A.33: Photometric time sequence and periodogram for HIP 30314

HIP 31878 HIP 31711 at 18000 au is a probable wide companion. The discrepancy in the astrometric parameters in Gaia DR2 is likely linked to the binarity of HIP 31711. The photometric rotation period first measured by Messina et al. (2010) is confirmed by our analysis of the TESS data (Fig. A.36).

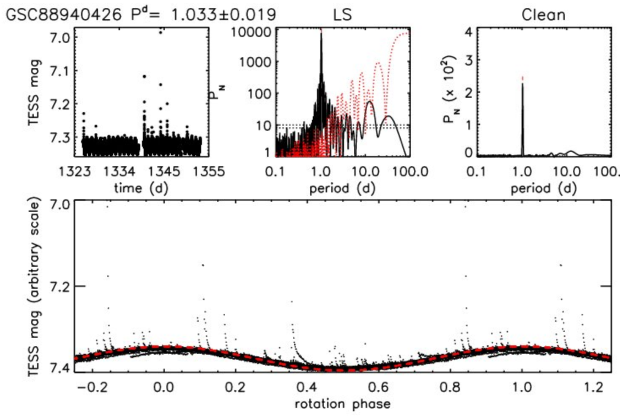

Fig. A.34: Photometric time sequence and periodogram for GSC 8894-0426

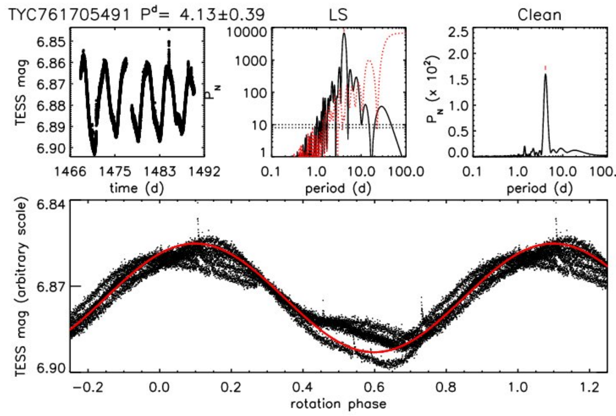

Fig. A.35: Photometric time sequence and periodogram for TYC 7617-0549-1

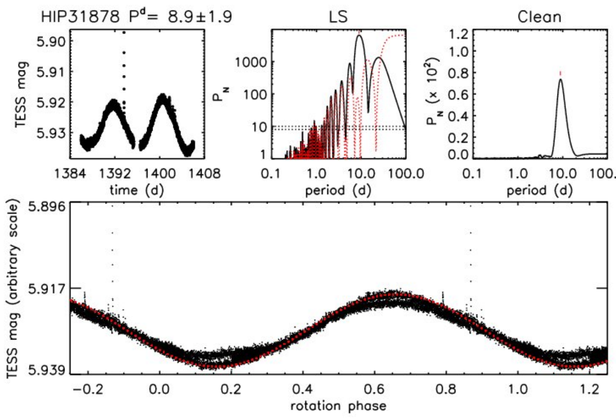

Fig. A.36: Photometric time sequence and periodogram for HIP 31878

HIP 32235 The photometric rotation period first measured by Messina et al. (2010) is confirmed by our analysis of the TESS data (Fig. A.37).

HD 51797 = TYC 8118-0871-1 The photometric rotation period first measured by Messina et al. (2010) is confirmed by our analysis of the TESS data (Fig. A.38).

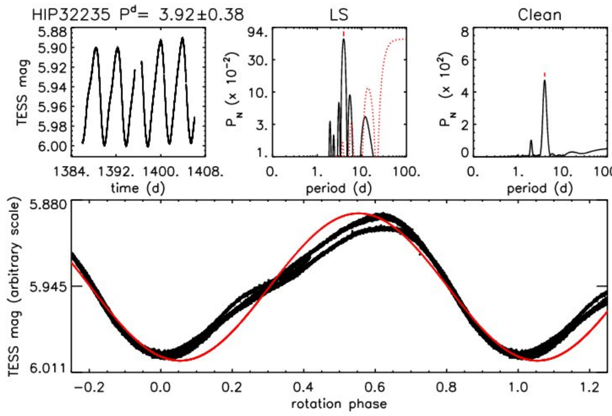

Fig. A.37: Photometric time sequence and periodogram for HIP 32235

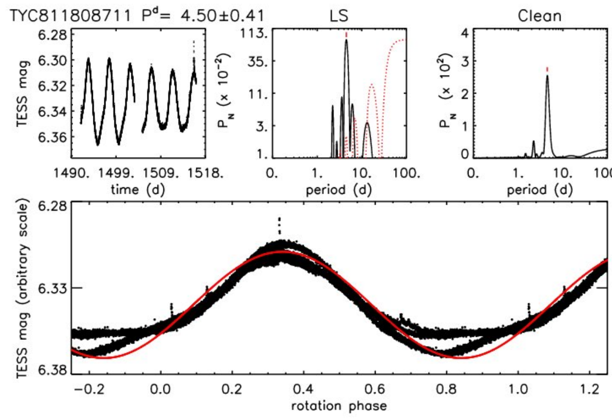

Fig. A.38: Photometric time sequence and periodogram for TYC 8118-0871-1

HIP 33737 = HD 55279 Originally classified as a member of Tuc-Hor, the updated analysis indicates membership in the Carina association. The photometric rotation period first measured by Messina et al. (2010) is confirmed by our analysis of the TESS data (Fig. A.39).

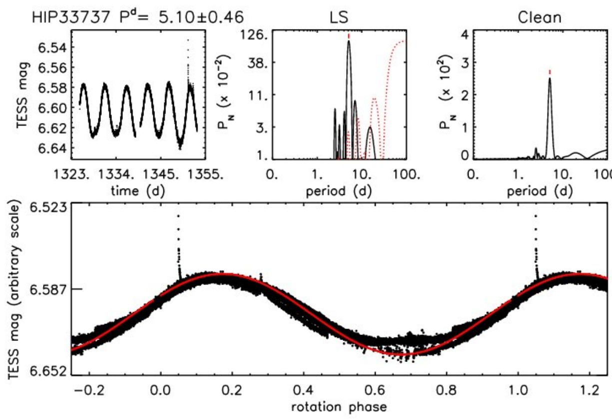

Fig. A.39: Photometric time sequence and periodogram for HIP 33737

2MASS 07065772-5353463 We measured for the first time the rotation period from the TESS photometric time series (Fig. A.40). Numerous flare events are detected in the TESS time series.

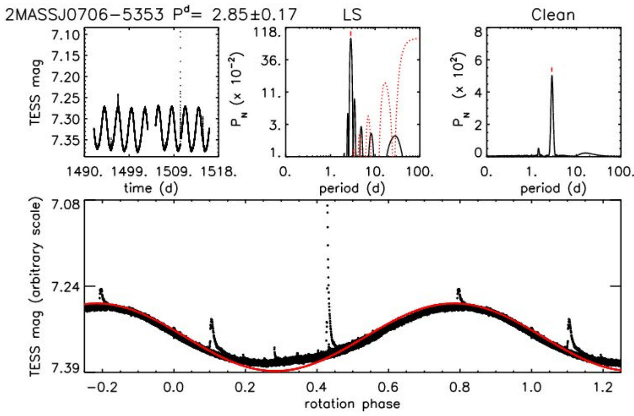

Fig. A.40: Photometric time sequence and periodogram for 2MASSJ0706-5353

BD+20 1790 = TYC 1355-214-1 = V429 Gem Member of AB Dor MG, with a very high activity level. The presence of a previously claimed hot Jupiter has been refuted by Carleo et al. (2018).

TYC 8128-1946-1 = CD-48 2972 Star with a wide companion HIP 36312 = HD 59659 (which is also in the SHINE sample but not observed within the date defining the targets of the present paper). It was originally identified as an Argus member by Torres et al. (2008), which has been confirmed in several works. Independently of the controversy over the existence of the Argus association, the very strong Li line confirms a young age. It is flagged as a possible SB in Desidera et al. (2015) based on the marginal RV difference between the two measurements. The recent RV determination by Zuckerman (2019), intermediate between the two previous measurements, does not support the presence of large RV variability. There is a marginal proper motion difference ($\sim 2\,\sigma$) between Gaia DR2 and Tycho2, while the Gaia DR1 and DR2 proper motions do not differ significantly. We kept the star in the sample, and we adopted the Argus membership and age.

HIP 36948 = HD 61005 Star with spatially resolved debris disk (e.g., Hines et al. 2007; Olofsson et al. 2016). The photometric rotation period first measured by Desidera et al. (2011) is confirmed by our analysis of the TESS data (Fig. A.41).

YZ CMi = HIP 37766 = GJ 285 The star is identified as a possible β Pic MG member in Montes et al. (2001), although it is not considered for membership in most of the studies on the group. The updated kinematic analysis using BANYAN Σ yields 0% membership probability. Considering it as a field object and taking the available results of age indicators into account, we adopted an age of 100 Myr with lower limit at 20 Myr and upper limit at 200 Myr. The photometric rotation period first measured by Chugainov (1974) is confirmed by our analysis of the TESS data (Fig. A.42). The TESS time series shows an uninterrupted flare activity.

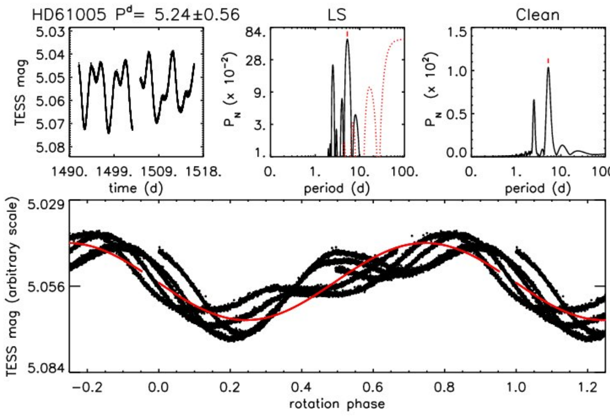

Fig. A.41: Photometric time sequence and periodogram for HIP36948 (HD 61005)

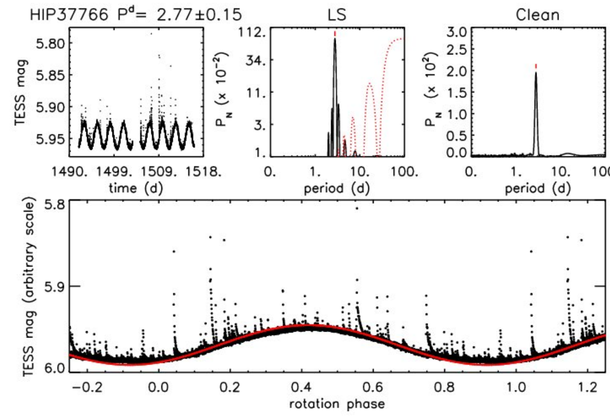

Fig. A.42: Photometric time sequence and periodogram for YZ CMi = HIP 37766

HIP 42808 We measured for the first time the rotation period from the TESS photometric time series (Fig. A.43). We note some residual instrumental effects around rotation phases $\phi = 0.3$–0.4.

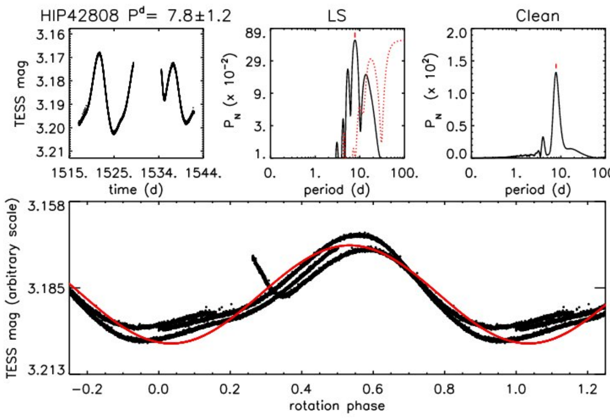

Fig. A.43: Photometric time sequence and periodogram for HIP 42808

η **Cha** Member of the η Cha open cluster (Mamajek et al. 1999). Nine comoving objects are found within 10 arcmin in Gaia DR2. We listed in Table 10 the closest one, EK Cha, at a projected separation of 19300 au.

HD 75505 = RECX13 Classified as a probable member of the η Cha open cluster (Mamajek et al. 1999). This is confirmed by kinematic analysis based on Gaia DR2 (Cantat-Gaudin & Anders 2020). It is also listed among the bona fide members by (Gagné et al. 2018b). On the other hand, the BANYAN Σ online tool yields a low membership probability (9%). Specific signatures of youth are elusive considering the spectral type of the star (A1V). We consider the star to be a member on the basis of the sky position, parallax, and proper motion, which are very similar to those of the other cluster members. Nine comoving objects are found within 10 arcmin in Gaia DR2. We listed in Table 10 the two with a projected separation of less than 20000 au, EH Cha and EI Cha, which are both confirmed members of the cluster.

V405 Hya = HIP 44526 = HD 77825 All age indicators are compatible with an age intermediate between Hyades and Pleiades. We adopted 300 Myr. The star was considered a member of Castor MG, whose existence is uncertain. Our adopted age is in any case close to the typical value for proposed Castor members. The M2.5 star UCAC4 371-053521, clearly comoving at a projected separation of 6000 au from Gaia DR2, was not previously recognized as a wide companion to V405 Hya. It was known as an active and X-ray emitter source. The photometric rotation period first measured by Kiraga (2012a) is confirmed by our analysis of the TESS data (Fig. A.44). The light curve is affected by residual instrumental effects.

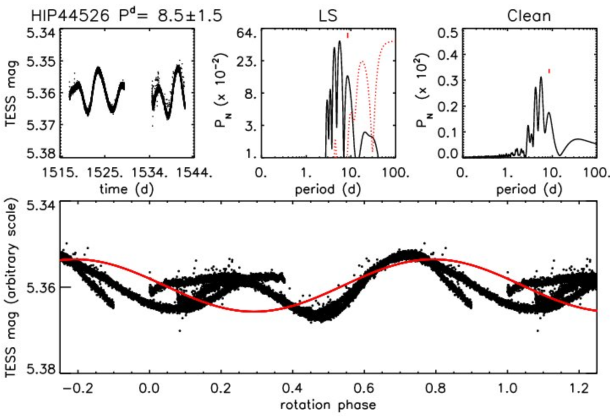

Fig. A.44: Photometric time sequence and periodogram for HIP 44526

HIP 47135 = HD 84075 G2 star classified as an Argus member in Torres et al. (2008), Zuckerman et al. (2011), Malo et al. (2013), Bell et al. (2015), and Zuckerman (2019). The age indicators are fully compatible with the proposed age for Argus. The star has an IR excess with two components (Zuckerman et al. 2011). We measured the photometric rotation period for the first time using photometric time series collected at the ROAD observatory. Our measurement was subsequently confirmed by our analysis of the TESS data (Fig. A.45-A.46).

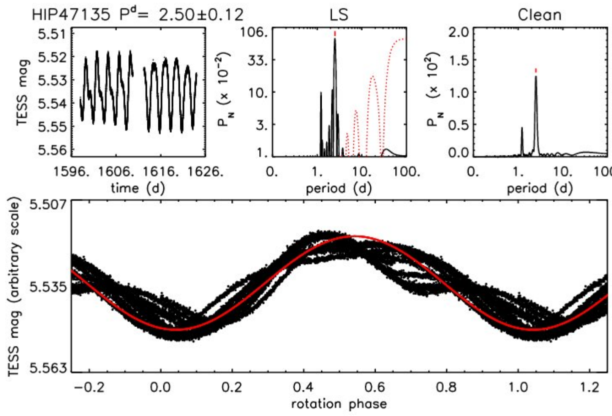

Fig. A.45: Photometric time sequence and periodogram for HIP 47135

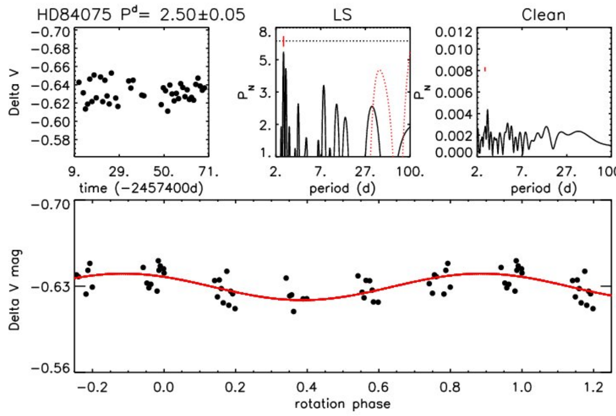

Fig. A.46: Photometric time sequence and periodogram for HIP 47135 (ROAD data)

HIP 50191 = HD 88955 = q Vel A2V star classified as an Argus member in Zuckerman et al. (2011), Bell et al. (2015), and Zuckerman (2019), and with Argus membership supported by BANYAN (probability 98%). Argus membership is also adopted in Nielsen et al. (2019). Actually, Zuckerman (2019) noted the slightly off-sequence position in B−V versus M_V CMD; instead the star is in a position similar to that of other Argus A-type stars in Gaia CMD. It should be noted that the Hipparcos parallaxes and proper motion have smaller errors than the Gaia values for such a bright star (V=3.85 mag). Furthermore, the star is classified as a primary standard for A2V spectral type by Pecaut & Mamajek (2013) [16]. Adopting their $T_{\rm eff}$ for this spectral type, (8840 K), the isochrone age results 458±182 Myr, similar to the age reported in the literature using this technique (Vican 2012; David & Hillenbrand 2015). The pre-MS age (6±1 Myr) is instead too young for Argus membership. We consider the post-ZAMS isochrone age reliable as the adopted data appears of high quality and there is no indication of binarity of the object, both at short separation from RV monitoring (Lagrange et al. 2009) and at larger separation from imaging. We adopted the isochronal age with an error bar extending

[16] http://www.pas.rochester.edu/~emamajek/spt/A2V.txt

down to 50 Myr to include the possibility of Argus membership. The star has a significant IR excess (Zuckerman et al. 2011).

TWA 6 = GSC7183-1477 = BX Ant Not member of TWA when using BANYAN Gaia DR2 paramaters. On the other hand, the TWA membership is supported by Lee & Song (2019). In any case, independently of any kinematic evaluation, the very strong lithium unambiguously shows the very young nature of the star. Isochrone fitting yields an age of 10±3 Myr, the same as the TWA group. The photometric rotation period first measured by Lawson & Crause (2005) is confirmed by our analysis of the TESS data (Fig. A.47).

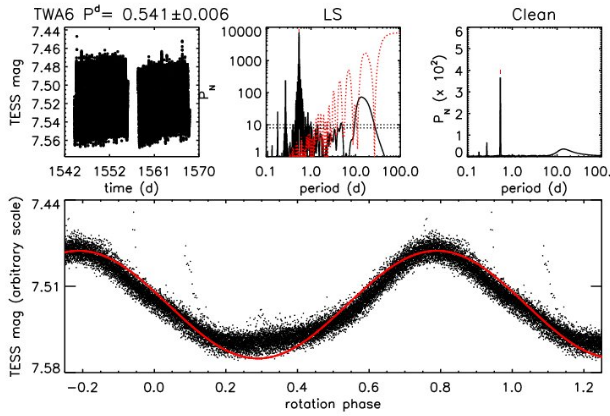

Fig. A.47: Photometric time sequence and periodogram for TWA6

HIP 51228 We measured for the first time the rotation period from the TESS photometric time series (Fig. A.48).

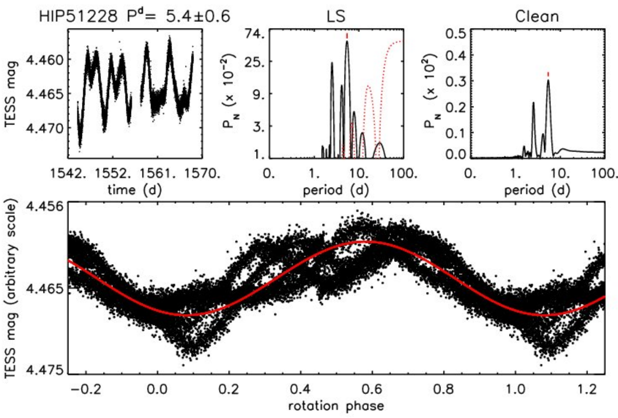

Fig. A.48: Photometric time sequence and periodogram for HIP 51228

HIP 51317 We measured for the first time the rotation period from the K2 Kepler photometric time series. (Fig. A.49)

HD 95086 Star with planetary companion first discovered by Rameau et al. (2013b). It is a Sco-Cen member according to de Zeeuw et al. (1999). BANYAN returns

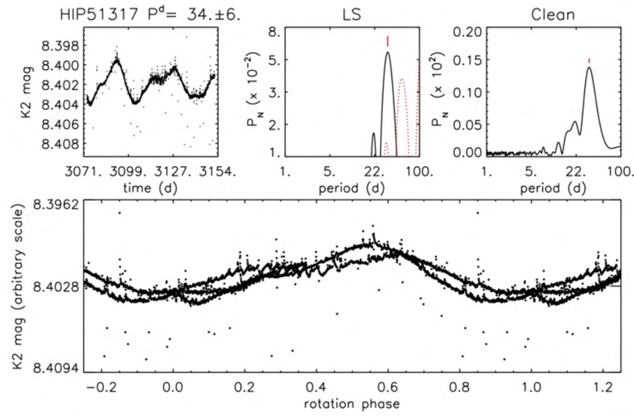

Fig. A.49: Photometric time sequence and periodogram for HIP 51317

a 48.5% probablity of membership in the Carina MG and 33.8% for LCC (without RV, the value listed in SIMBAD and several catalogs is the astrometric one by Madsen et al. 2002). The spatial position is in the outskirts of the Sco-Cen group. The age map by Pecaut & Mamajek (2016) yields an age of 26 Myr at the location of HD 95086, clearly older than the bulk of LCC. On the other hand, Schneider et al. (2019) recently proposed an age of 22 Myr for the Carina association. The isochrone age gives a lower limit of about 20 Myr for HD95086. Looking in Gaia DR2 for stars with similar position and kinematic parameters, we noticed the F2 star HIP 55334 (HD 98660) with a lower age limit of about 19 Myr (our analysis and Pecaut et al. (2012)), consistent with the Pecaut & Mamajek (2016) age map. Our tentative conclusion is that HD 95086 is part of a young population that is slightly older than the bulk of LCC and possibly connected to the Carina association, or part of it. We adopted the age from the Pecaut & Mamajek (2016) map, with lower and upper limits corresponding to the LCC and Carina.

HIP 54155 The wide companion HD 96064B has no astrometric solution in Gaia likely due to its close binarity (P=23 yr). The physical association of this triple system is nevertheless confirmed. The photometric rotation period first measured by Cutispoto et al. (1999) is confirmed by our analysis of the TESS data (Fig. A.50).

HIP 54231 Sco-Cen member according to de Zeeuw et al. (1999) and Rizzuto et al. (2011), but with low membership probability from BANYAN. We adopted the LCC age but with the upper limit derived by isochrone fitting (380 Myr). The literature spectral type is A0V, but the colors are more compatible with A1. The RV in SIMBAD is the expected value for membership (Madsen et al. 2002), not an observational measurement.

HIP 57632 = HD 102647 = β Leo BANYAN returns an 87.1% membership probability to Argus, 4.6% to Carina-Near, and 8.3% for field. Argus membership is also supported by Zuckerman et al. (2011). We adopted Argus membership. There are no Gaia astrometric data due to the very bright magnitude. The star has a two-belt debris disk.

HIP 58167 F-type star in Sco Cen. The star has a co-moving object (2MASS J11551267-5406215) with very

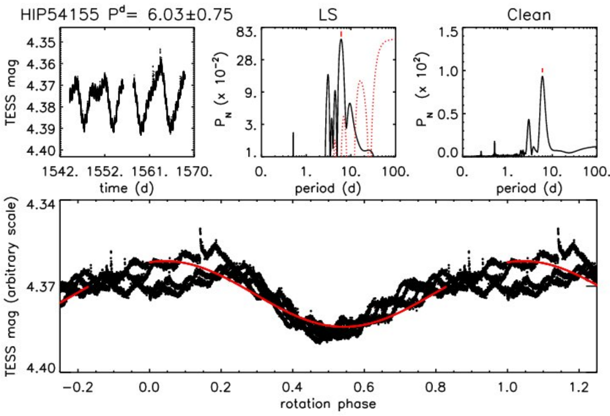

Fig. A.50: Photometric time sequence and periodogram for HIP 54155

similar astrometric parameters (proper motion difference of 1.6 and 1.2 mas yr^{-1}, parallax difference of 0.33 mas) in spite of the large projected separation (382″ corresponding to 41250 au). From the 2MASS magnitudes, a mass as low as 20 Mjup is derived for this object. In Gaia there is another possible comoving object, Gaia DR2 5344340167066548608 at 355" (with a different position angle with respect to 2MASS J11551267-5406215). Its magnitude is extremely faint (G=20.99) and it is not detected in 2MASS. The astrometric parameters are characterized by large errors (3.6 mas on parallax and more than 4 mas yr^{-1} on the components of proper motion). The object results comoving to HIP 58167 at about the 2 σ level. If confirmed, the magnitude fainter than 2MASS J11551267-5406215 (by 2.5 mag) would imply an extremely low-mass object. We measured for the first time the rotation period from the TESS photometric time series (Fig. A.51).

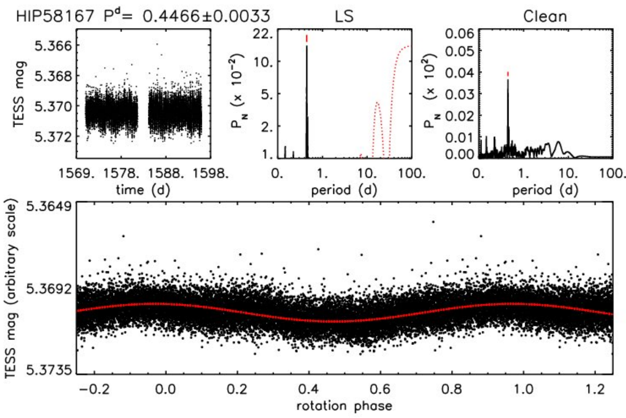

Fig. A.51: Photometric time sequence and periodogram for HIP 58167

HIP 60183 The star is flagged as a member of LCC by de Zeeuw et al. (1999) and as a member of one of the LCC sub-groups by Goldman et al. (2018); however it has however a low membership probability with Banyan. We adopted the LCC age, but with the upper limit derived from isochrone fitting.

HIP 60459 We measured for the first time the rotation period from the TESS photometric time series (Fig. A.52).

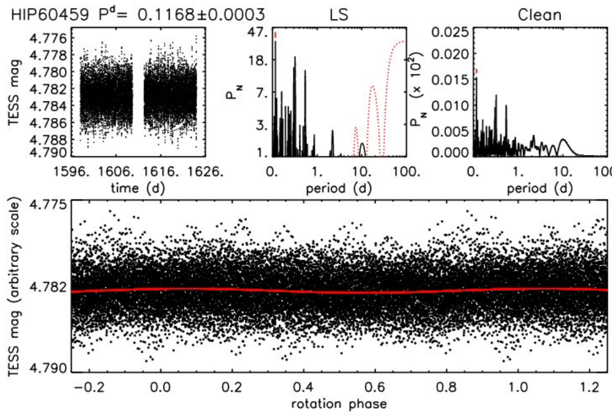

Fig. A.52: Photometric time sequence and periodogram for HIP 60459

HD 108767B Wide companion to the B-type star δ Crv = HD108767. We measured for the first time the rotation period from the TESS photometric time series (Fig. A.53).

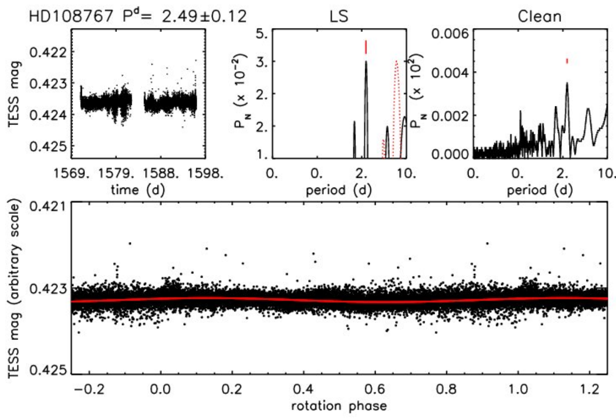

Fig. A.53: Photometric time sequence and periodogram for HD108767B

HIP 61468 The star has a secondary at 15″, clearly comoving from the Gaia DR2 astrometry. To our knowledge, the binarity has not been previously reported in the literature. The companion (2MASS J12354637-4101315) is expected to have a spectral type of M3.5 from photometric colors, and is a possible X-ray source from CHANDRA (Wang et al. 2016).

HIP 66252 We measured for the first time the rotation period from K2 photometric time series (Fig. A.54).

TYC 7286-0248-1 = CD-31 11053 K star with very strong lithium line identified by Torres et al. (2006). It is proposed as a possible member of UCL by Gagné et al. (2018b) on the basis of Gaia DR1 data, and inclusion of Gaia DR2 makes the case stronger (98% probability). Damiani et al. (2019) also support Sco-Cen membership. The RV difference between SACY and Gaia DR2

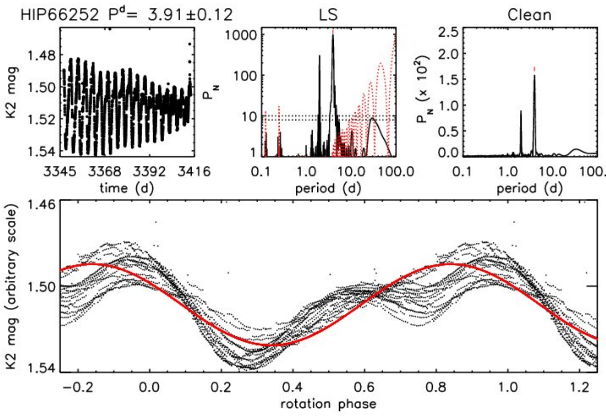

Fig. A.54: Photometric time sequence and periodogram for HIP 66252

(8.8 km s^{-1}) is not highly significant considering the large error of Gaia RV (4.1 km s^{-1}). The discrepancy between photometric colors and spectral type (K3Ve, Torres et al. 2006) indicates either a significant reddening (E(B−V) ∼ 0.1) or that the true spectral type is intermediate between K4 and K5. The lithium EW indicates an age at least as young as the β Pic MG. A very young age is also supported by the position on the CMD and the isochrone age, in spite of the ambiguity between effective temperature and reddening. These results are fully consistent with the UCL membership, which we then adopted.

HIP 69989 = HD 125451 = 18 Boo Mid-F star classified as a possible UMa member by Montes et al. (2001) and King et al. (2003). Instead, BANYAN analysis rejected the membership. We then considered the membership as unconfirmed. The age indicators are inconclusive considering the spectral type of the star. However, the chromospheric activity and X-ray emission are consistent with Hyades and UMa stars of similar temperature. The position on the CMD is close to ZAMS, with an upper limit of 1.9 Gyr. We adopted the UMa age with the upper limit from isochrone, as membership is uncertain. The star has RV monitoring by Borgniet et al. (2019) with SOPHIE. We used these data to provide a new value of absolute RV. The star also has an IR excess indicating a debris disk.

HIP 71724 A stellar companion (mass 146-217 Mjup) at 101 mas was claimed by Hinkley et al. (2015). It was not detected in our observations, although it is expected to lie beyond the coronagraphic mask.

HIP 71743 = HD 128987 = KU Lib G6V star whose age indicators (Li, Prot, X-rays, and RHK) nicely agree on an age close to that of the Hyades or slightly older. We adopted 700 ± 100 Myr. The star is classified as an extremely wide companion (separation of 1 pc) to the quadruple system α Lib (Caballero 2010). The membership to Castor MG is also proposed in that study.

HIP 73990 = HD 133803 The two brown dwarf companions at very small separations claimed by Hinkley et al. (2015) are not confirmed by SPHERE observations. See Paper II and Cantalloube et al. (in prep.) for further details. The star has a previously unrecognized wide companion (2MASS J15071795-2929501) at 5230 au projected separation.

HIP 74824 = HD 135379 = β Cir: A3V star with very wide brown dwarf companion (Smith et al. 2015) and IR excess. Analysis of kinematic parameters yields an 83% probability of being a member of β Pic MG when adopting the Gaia DR2 parameters. However, when adopting VL07 (which has smaller errors because of the very bright magnitude of the star), the membership probability drops to 19%. The star is slightly brighter than the ZAMS. Isochrone fitting yields ages of 450 ± 200 Myr and 8±3 Myr assuming post- and pre-MS phases, respectively. The pre-MS age is not compatible with β Pic MG. Furthermore, the BD companion β Cir B does not show signatures of youth or low gravity (Smith et al. 2015). We then adopted the post-MS solution, yielding an age of 450 Myr.

HIP 76063 = HD 138204 A7 star classified as a Sco-Cen member (UCL subgroup) in de Zeeuw et al. (1999) and Rizzuto et al. (2011) (probability 55%). BANYAN Σ yield a 26.5% membership probability on UCL. The distance is significantly closer than the vast majority of the Sco-Cen population, as previously noted by Wright & Mamajek (2018). This rules out membership in the core of the Sco-Cen association, but a link with a foreground population of young stars of similar age (see, e.g. the bona-fide young star NZ Lup at 60 pc Boccaletti et al. 2019) is possible. We then adopted the isochrone age (220 Myr), extending the lower limit to encompass the UCL age. Nielsen et al. (2019) adopted instead the UCL membership and age.

HIP 77457 Member of US group according to de Zeeuw et al. (1999), while membership is rejected by Pecaut et al. (2012). Our analysis with BANYAN also gives a low membership probability in US (11%). We adopted the isochrone age, with lower limit at the US age to take the possible membership into account.

HIP 77464 = HD 141378 A-type star, possibly chemically peculiar, with a dual-belt debris disk. The low-mass star 2MASS J15490081-0348147 is a previously unrecognized wide companion at 4240 au.

TYC 7846 1538 1 The photometric rotation period first measured by Marsden et al. (2011) is confirmed by our analysis of the TESS data (Fig. A.55).

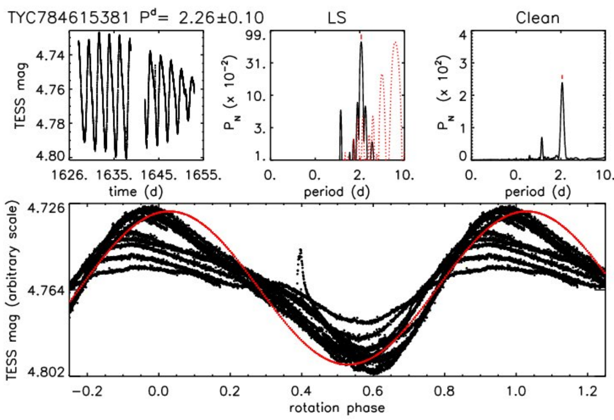

Fig. A.55: Photometric time sequence and periodogram for TYC 7846-1538-1

NZ Lup = HD 141943 See Boccaletti et al. (2019).

HIP 78099 The low-mass very wide companion 2MASS J15564019-2309291 was not previously associated with the primary, but was flagged as a bona fide Sco-Cen member (Damiani et al. 2019) and fast-rotating object (Stauffer et al. 2018).

HIP 78196 = HD 142851 A stellar companion (mass 98-152 Mjup) at 74 mas was claimed by Hinkley et al. (2015). It was not detected in our observations, although it is expected to lie beyond the coronagraphic mask.

HIP 78530 Late B-type object with a brown dwarf companion at very wide separation discovered by Lafrenière et al. (2011).

HIP 78541 = HD 143488 Originally considered to be member of UCL de Zeeuw et al. (1999), it is possibly a field object (85.6% probability from BANYAN). We adopted the UCL age with upper limit from our isochrone fitting.

HIP 80591 = HD 148055 Star member of UCL. 2MASS J16271281-3949144 at 21.9″ is a low-mass (0.16 $M_{\odot}$) companion, not previously mentioned in the literature as such.

HIP 81084 We measured for the first time the rotation period from photometric time series we collected at PEST observatory (Fig. A.56-A.57).

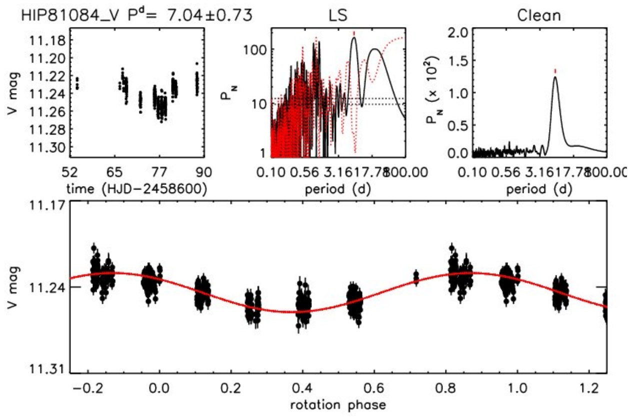

Fig. A.56: Photometric time sequence and periodogram for HIP81084 (V band)

TYC 7879-0980-1 = HD 326277 First identified as a young star in Torres et al. (2006) and more recently classified as a UCL member by Pecaut & Mamajek (2016). Gaia DR2 kinematics coupled to Banyan Σ confirms the UCL membership. The age indicators are fully compatible with this assignment. There is some discrepancy between the Torres et al. (2006) spectral type (K0IV) and the photometric colors, which would suggest instead a G7 star (from young stars Pecaut & Mamajek 2013, tables). The isochrone ages for the temperatures corresponding to K0 and G7 are 14-24 Myr respectively, further supporting the young age and bracketing the nominal UCL age. There is a significant (3.1 σ) proper motion difference between Tycho2 and Gaia DR2, but no other indication of binarity.

HIP 82388 We measured for the first time the rotation period from the photometric time series we collected at the YCO observatory (Fig. A.58).

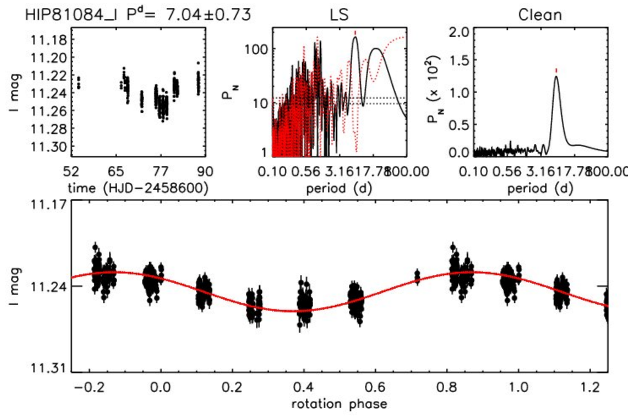

Fig. A.57: Photometric time sequence and periodogram for HIP 81084 (I band)

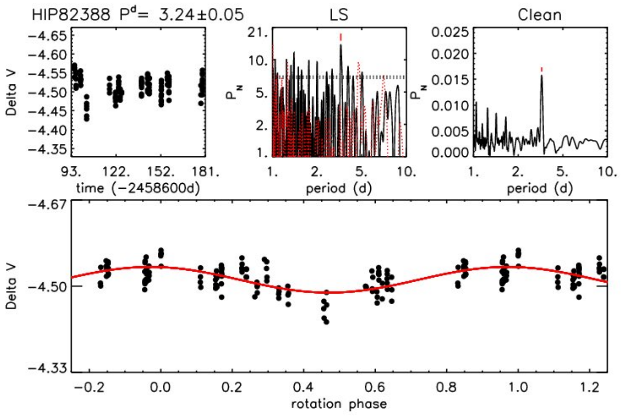

Fig. A.58: Photometric time sequence and periodogram for HIP 82388

TYC 7362-0724-1 = HD 156097 Young G5 star with strong lithium identified by Torres et al. (2006). The analysis based on the Gaia DR2 parameters yields a 46% membership probability to UCL and 13% to β Pic MG. Lithium and other indicators are fully compatible with a very young age (Desidera et al. 2015). Photometric colors are fully compatible with the G5 spectral classification by Torres et al. (2006). Adopting $T_{\rm eff}$ from the Pecaut & Mamajek (2013) tables, we infer an age of 11±3 Myr, consistent but more accurate than that obtained from indirect methods. We adopted the isochrone age, with UCL age as an upper limit due to the possible membership. We measured for the first time the rotation period from the photometric time series we collected at PEST, and subsequently confirmed by our analysis of the TESS data (Fig. A.59-A.60-A.61).

TYC 8728-2262-1 The photometric rotation period first measured by Messina et al. (2017) is confirmed by our analysis of the TESS data (Fig. A.62).

HIP 86598 = HD 160305 Star with debris disk spatially resolved from SHINE observations (Perrot et al. 2019) (see Fig. A.63 for the stellar rotation analysis).

HIP 88399 We measured for the first time the rotation period from the TESS photometric time series (Fig. A.64).

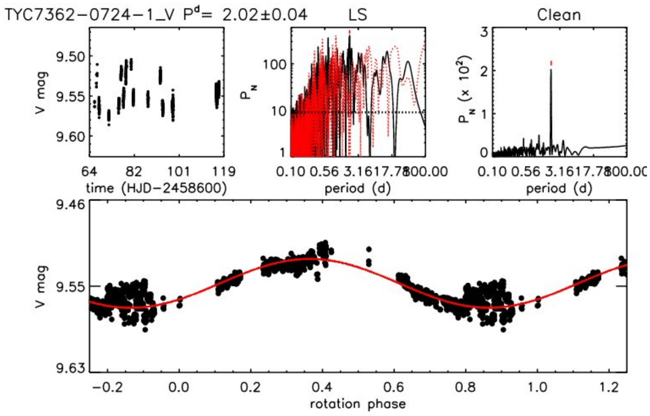

Fig. A.59: Photometric time sequence and periodogram for TYC 7362-0724-1 (V band; PEST data)

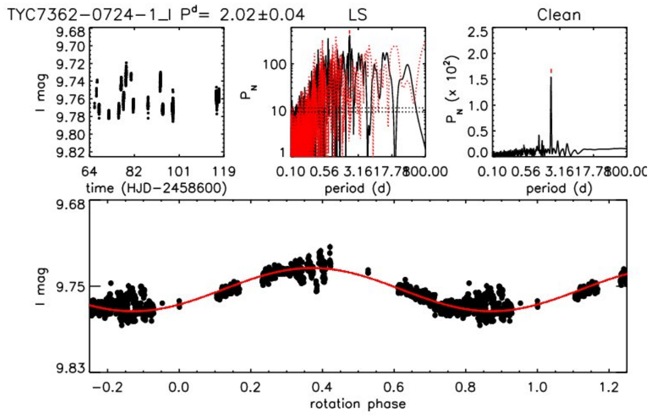

Fig. A.60: Photometric time sequence and periodogram for TYC 7362-0724-1 (I band; PEST data)

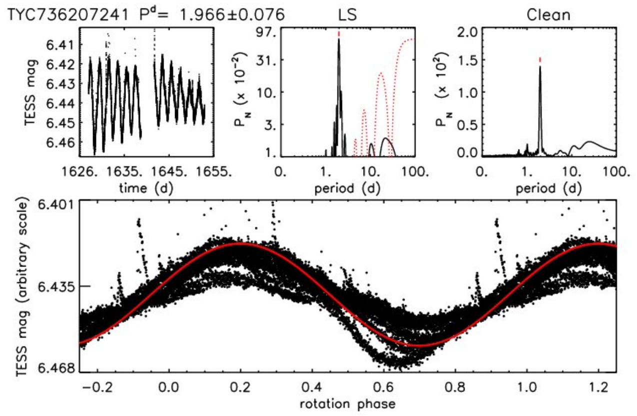

Fig. A.61: Photometric time sequence and periodogram for TYC 7362-0724-1

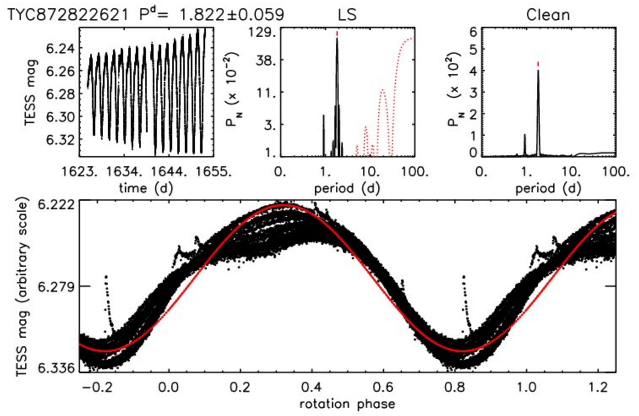

Fig. A.62: Photometric time sequence and periodogram for TYC 8728-2262-1

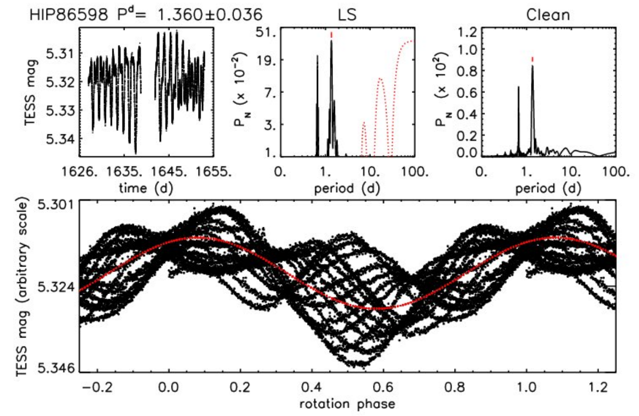

Fig. A.63: Photometric time sequence and periodogram for HIP 86598

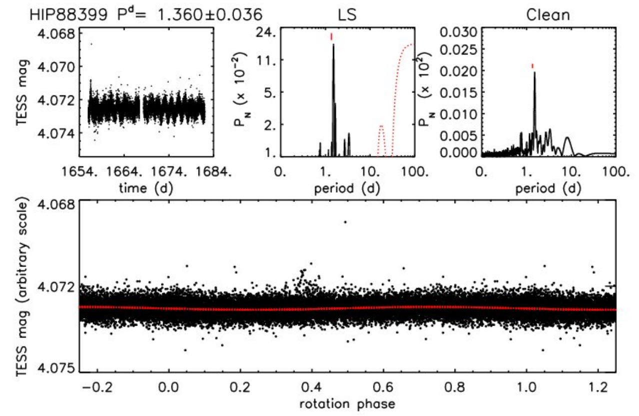

Fig. A.64: Photometric time sequence and periodogram for HIP 88399

TYC 9073-0762-1 The photometric rotation period first measured by Messina et al. (2010) is confirmed by our analysis of the TESS data. (Fig. A.65).

PZ Tel = HIP 92680 = HD 174429 Member of β Pic MG. It hosts a BD companion (PZ Tel B) discovered by Biller et al. (2010); Mugrauer et al. (2010) in a very eccentric orbit (Maire et al. 2016). The IR excess detected by Rebull et al. (2008) has been shown to be due to a background object (Biller et al. 2013).

HIP 92984 = HD 175726 The star shows moderate activity and fast rotation. The star has kinematic parameters somewhat similar to UMa although with some differences causing low membership probability in BANYAN Σ. It also has an IR excess suggesting the

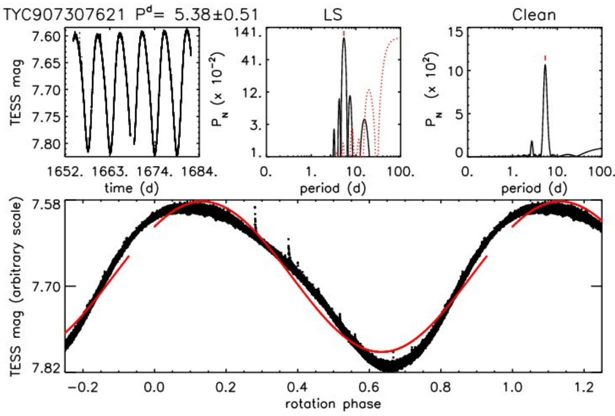

Fig. A.65: Photometric time sequence and periodogram for TYC 9073-0762-1

presence of a debris disk. The age indicators quite consistently indicate that it is intermediate between the Hyades and Pleiades, independently of UMa membership. We adopted an age of 400±200 Myr.

HIP 93375 As suspected in Desidera et al. (2015), Gaia DR2 astrometry shows conclusively that the star UCAC3 123-585870 at 11″ is not physically associated. We measured for the first time the rotation period from the ROAD photometric time series in the V and B bands. (Fig. A.66-Fig. A.67).

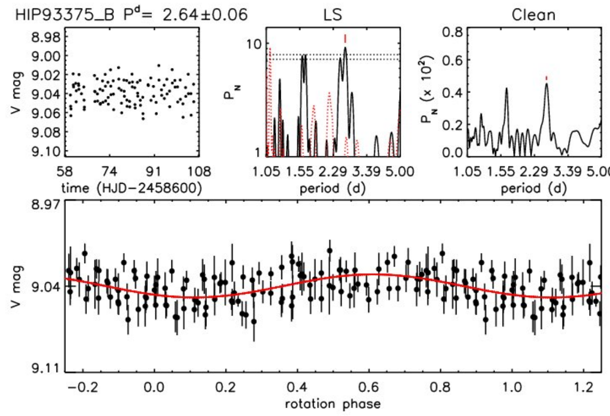

Fig. A.66: Photometric time sequence and periodogram for HIP 93375 (B band; ROAD data)

TYC 8760-1468-1 = CD-54 8168 Field K2Ve object with very fast rotation and high Li content, similar to the members of the Tuc-Hor association. The RV in RAVE DR5 (Kunder et al. 2017) differs by 22 km s^{-1} with respect to the SACY value, but the error is very large (6 km s^{-1}). We thus consider it a suspected SB. The photometric rotation period first measured by Kiraga (2012a) is confirmed by our analysis of the TESS data (Fig. A.68). The kinematic within the Zuckerman & Song (2004) "young box" is compatible with the young age estimated from lithium and rotation.

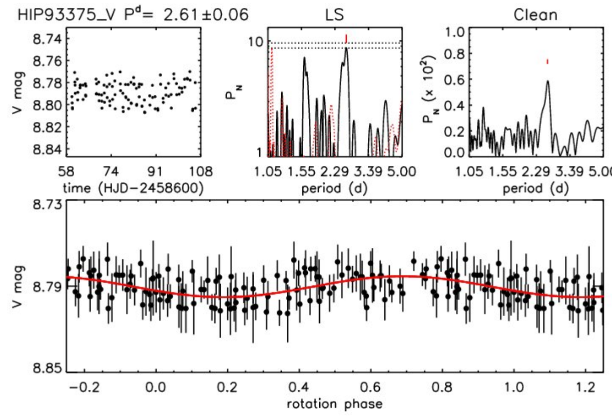

Fig. A.67: Photometric time sequence and periodogram for HIP 93375 (V band; ROAD data)

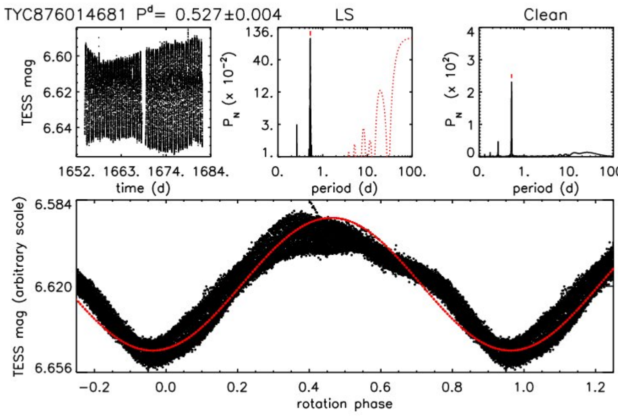

Fig. A.68: Photometric time sequence and periodogram for TYC 8760-1468-1

HIP 95270 We measured for the first time the rotation period from the TESS photometric time series (Fig. A.69).

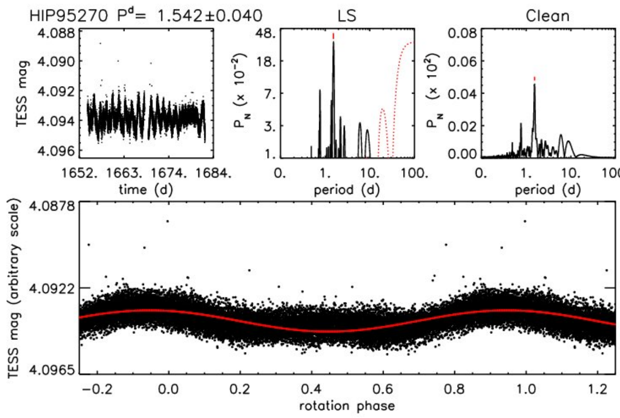

Fig. A.69: Photometric time sequence and periodogram for HIP 95270

η **Tel = HIP 95261** The star has a brown dwarf companion discovered by Lowrance et al. (2000) and confirmed by Guenther et al. (2001). It was not promoted as special object (P0) considering the already available characterization (e.g., Bonnefoy et al. 2014).

TYC 0486-4943-1 Member of AB Dor MG according to Torres et al. (2008) and Elliott et al. (2014). It has a low membership probability (19% for the adopted kinematic parameters) using BANYAN Σ. The lithium EW is very close to the median locus of AB Dor and Pleiades members, supporting a very similar age. The other age indicators are also compatible with this evaluation. Barenfeld et al. (2013) found some differences in the chemical composition with respect to AB Dor core members. We adopted an age very close to that of AB Dor MG with slightly increased error bars. From Gaia DR2 a wide companion (**2MASS J19330197+0345484**) with very similar parallax and proper motion is identified at 28″ (1968 au). The Gaia DR2 RV is also compatible with that of primary.

TYC 7443-1102-1 The Herschel IR source is actually identified with two separate sources at close separation from the star in ALMA observations (Tanner et al. 2020). This indicates they are likely background objects rather than associated with the star.

HD 189285 It is classified as a member of AB Dor in some studies (Torres et al. 2008), but BANYAN Σ returns a 0.0% membership probability. The discrepancy was already noticed in Desidera et al. (2015) using previous versions of the tool. On the other hand, all the age indicators (see Desidera et al. 2015, for details) are fully compatible with membership and Barenfeld et al. (2013) found that a chemical composition from several chemical elements is compatible with those of AB Dor core members. The kinematic discrepancy is unlikely to be due to unrecognized binarity as the RV from several sources (Desidera et al. 2015; Gaia Collaboration et al. 2018; Elliott et al. 2014; Frasca et al. 2018) is compatible within the errors, and the SPHERE images do not give any indication of stellar companions. In summary, independently of any membership assignment, we adopted an age close to that of AB Dor MG with slightly increased error bars. We measured the rotation period from the photometric time series we collected at the ROAD observatory, which superseded the measurement presented in Desidera et al. (2015) and therein flagged as uncertain (Fig. A.70-A.71).

HIP 98470 = HD 189245 A reanalysis of the Hipparcos data allowed us to detect a rotation period P = 0.8662±0.0003 d, which, differently from that presented in Desidera et al. (2015), is consistent with the stellar radius and projected rotational velocity (Fig. A.72).

TYC 8404-0354-1 = CD-52 9381 K6Ve star proposed as an Argus member by Torres et al. (2008). Considered as likely older than Argus by Zuckerman (2019) on the basis of CMD. Lithium is also lower than expected for a 50 Myr star, and similar to the mean values of Pleiades and AB Dor stars of similar color. The very fast rotation period (0.83 days) is also compatible with this age estimate. Our isochrone analysis confirms the position close to the ZAMS. We adopted 120 (50-200) Myr. The photometric rotation period first measured by Messina et al. (2011) is confirmed by our analysis of the TESS data (Fig. A.73). Numerous flare events are detected in the TESS time series.

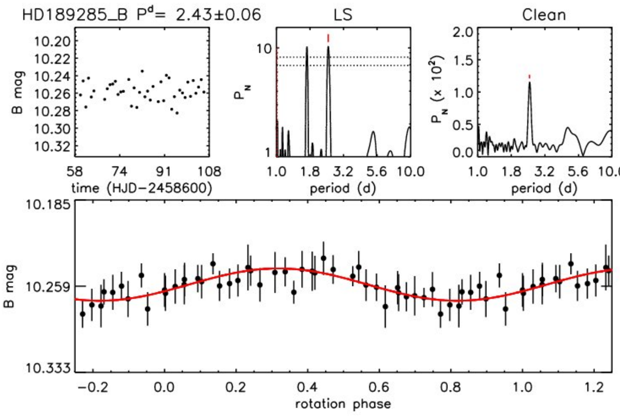

Fig. A.70: Photometric time sequence and periodogram for HD189285 (B band; ROAD data)

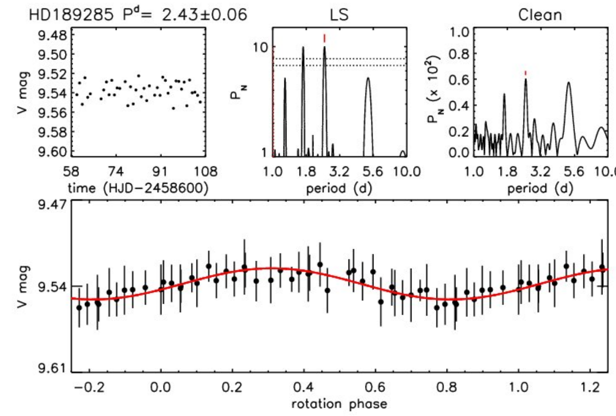

Fig. A.71: Photometric time sequence and periodogram for HD189285 (V band; ROAD data)

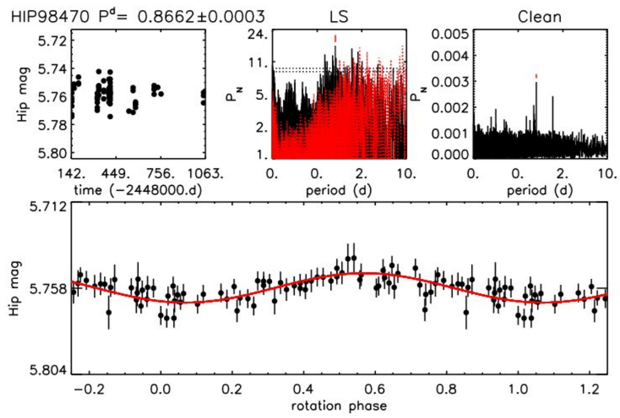

Fig. A.72: Photometric time sequence and periodogram for HIP 98470

AU Mic = HIP 102409 The star has a prominent debris disk seen close to edge-on first spatially resolved by Liu (2004). A transiting planet at short period has been discovered with TESS (Plavchan et al. 2020). The photometric rotation period measured by Messina et al. (2010) is confirmed by our analysis of the TESS data

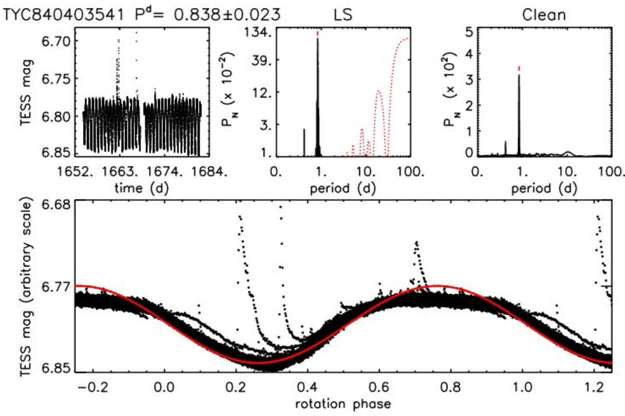

Fig. A.73: Photometric time sequence and periodogram for TYC 8404-0354-1

(Fig. A.74). Numerous flare events are detected in the TESS time series.

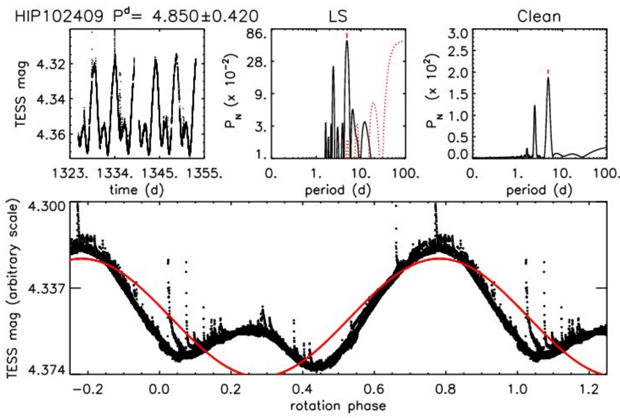

Fig. A.74: Photometric time sequence and periodogram for HIP 102409

HIP 102626 = HD 197890 = BO Mic Very fast-rotating star (P=0.380 d; $v \sin i$ 128 $\mathrm{km\,s^{-1}}$). This characteristic makes the determination of the spectral parameters difficult. Torres et al. (2006) determined a large Li EW, indicating a very young age. It was proposed by some studies (Kraus et al. 2014; Bell et al. 2015) to be a member of the Tuc-Hor association, but a very low probability is returned by the kinematic analysis including Gaia DR2. The controversial membership is linked to the wide dispersion of the astrometric parameters[17]. Gaia and Hipparcos parallaxes and even different Hipparcos reductions show large differences (up to 7.5 and 3.4 mas, respectively) while the proper motions derived from Gaia and Hipparcos differ by more than 20 mas $\mathrm{yr^{-1}}$. The original Hipparcos reduction includes an astrometric acceleration trend, while Gaia DR2 notes the presence of a large excess of astrometric noise. This suggests the presence of a fairly massive stellar companion that was not revealed in any in the various direct imaging surveys that targeted this object (Chauvin et al. 2010; Galicher et al. 2016), including SHINE-SPHERE (see Paper II). Radial velocities are hardly conclusive because of the extreme $v \sin i$ value. Barnes (2005) discussed the possible spectroscopic companions compatible with the observational constraints. The isochrone age results very young when adopting Gaia DR2 parallax (4 Myr for the $T_{\rm eff}$ corresponding to the K3 spectral type by Torres et al. (2006); 8 Myr for the $T_{\rm eff}$ corresponding to the K2 spectral type indicated by broadband colors), but we consider this highly uncertain as the errors on parallax are possibly underestimated. The minimum radius from the observed rotation period and $v \sin i$ is 0.99 $R_\odot$. The inclination value of 70 deg proposed by Barnes (2005) through the Doppler imaging technique implies R=1.05 $R_\odot$, compatible with a pre-main sequence star of early K spectral type. We conclude that membership in Tuc-Hor cannot be ruled out until the spread in the astrometric values and the possibility of binarity are better understood. The very strong lithium line in any case indicates an age younger than 100 Myr. We thus adopted the Tuc-Hor age, with min–max values of 5–100 Myr considering the various indicators.
The photometric rotation period measured by Kiraga (2012a) is confirmed by our analysis of the TESS data (Fig. A.75).

[17] When using the Tycho2 long-term proper motion coupled with the Hipparcos parallax, BANYAN returns a membership probability of 82.4% in Tuc-Hor

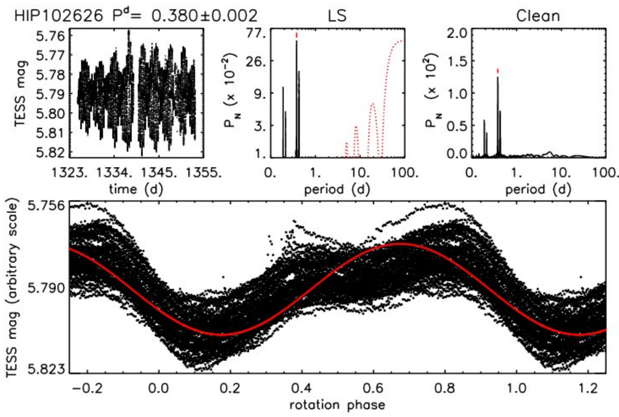

Fig. A.75: Photometric time sequence and periodogram for HIP 102626

TYC 1090-0543-1 Star with a low membership probability on AB Dor MG (8.8%) in spite of the previous kinematic assignment (Torres et al. 2008). It is a wide companion of **HD199058**, which is itself a tight visual binary (Chauvin et al. 2015), making the system triple. Barenfeld et al. (2013) found the HD 199058 chemical pattern to be compatible with that of AB Dor core members. Lithium and the activity and rotation indicators of both components are compatible with those of AB Dor and Pleiades of similar spectral type.

HIP 104365 = HD 201184 = χ Cap A0V star, flagged as a possible member of Tuc-Hor by Zuckerman & Song (2012). BANYAN Σ yields a 20% membership probability (80% field). We adopted the age from isochrone fitting, with the minimum value set at the minimum age of Tuc-Hor. This is in any case close to the lower limit allowed by stellar models. This is a triple system, as there is a close pair of comoving objects (Vigan et al. 2012) at 9″ labeled WDS 21086-2112E and WDS 21086-2112F. There is one corresponding entry in Gaia DR2, Gaia DR2 6832248844207846144, without astrometric parameters, likely because of the multiplicity.

HIP 105388 The photometric rotation period first measured by Messina et al. (2010) is confirmed by our analysis of the TESS data (Fig. A.76).

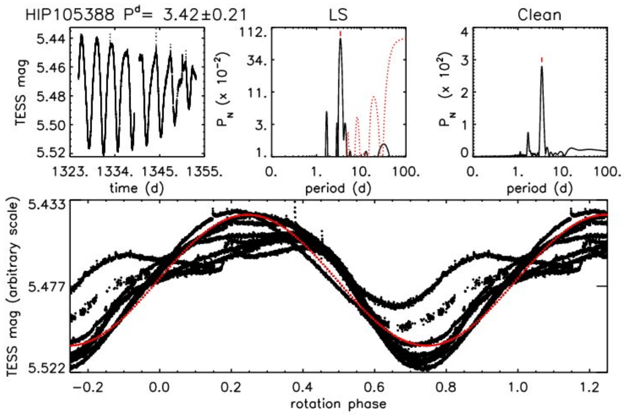

Fig. A.76: Photometric time sequence and periodogram for HIP 105388

TYC 9482-121-1 We measured for the first time the rotation period from the TESS photometric time series (Fig. A.77).

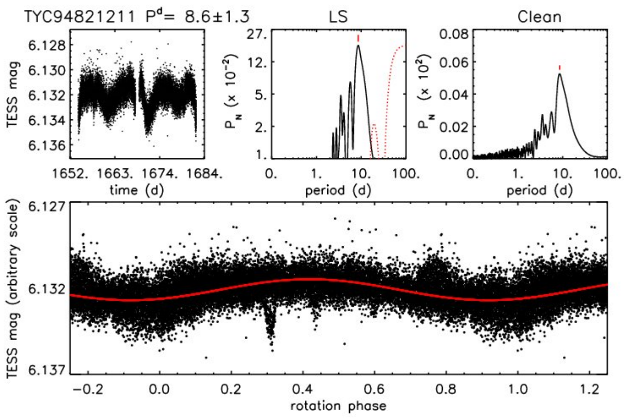

Fig. A.77: Photometric time sequence and periodogram for TYC 94821211

HIP 107345 The photometric rotation period first measured by Messina et al. (2010) is confirmed by our analysis of the TESS data (Fig. A.78). A large amplitude flare is detected in the TESS time series.

HIP 107350 = HD 206860 = HN Peg The star has a low-mass brown dwarf companion at wide separation.

HIP 107412 = HD 206893 Star with a debris disk and with a substellar companion detected by Milli et al. (2017) and characterized by Delorme et al. (2017) and

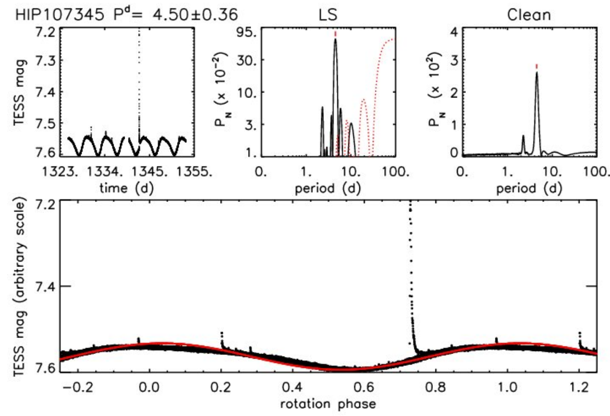

Fig. A.78: Photometric time sequence and periodogram for HIP 107345

Grandjean et al. (2019) (see Delorme et al. (2017) for further details on stellar parameters).

2MASS J22021616-4210329 The photometric rotation period first measured by Kiraga (2012b) is confirmed by our analysis of the TESS data (Fig. A.79). Numerous flare events are detected in the TESS time series.

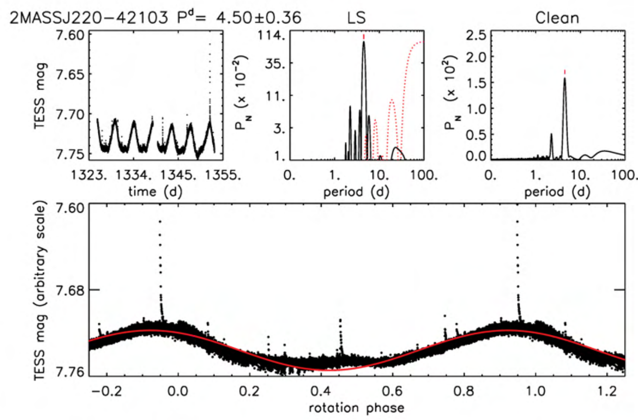

Fig. A.79: Photometric time sequence and periodogram for 2MASSJ220-42103

TYC 9340-0437-1 Star with debris disk spatially resolved by Herschel observations (Tanner et al. 2020). The photometric rotation period first measured by Messina et al. (2010) is confirmed by our analysis of the TESS data (Fig. A.80). Numerous flare events are detected in the TESS time series.

HIP 113283 = TW PsA = Fomalhaut B IR excess at 160 micron detected by Montesinos et al. (2016), but not seen at shorter wavelengths, indicating very cold dust. The star has a significant Gaia–Hipparcos proper motion difference. A dedicated search using imaging and radial velocities did not detect companions responsible for the astrometric signature De Rosa et al. (2019). Our even deeper imaging observations confirm this result. The age of the system is from Mamajek (2012). The photometric rotation period first measured by Busko & Torres (1978) is confirmed by our analysis of the TESS data (Fig. A.81).

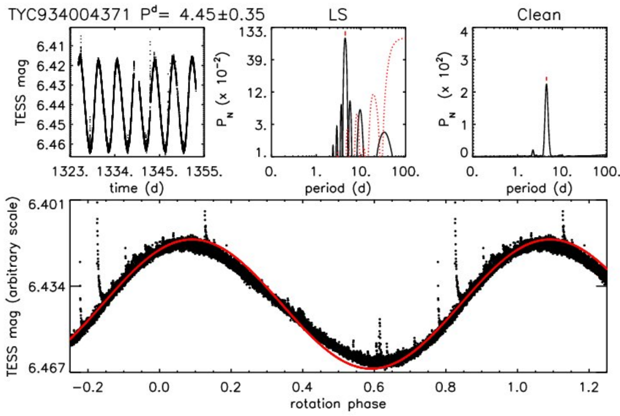

Fig. A.80: Photometric time sequence and periodogram for TYC 9340-0437-1

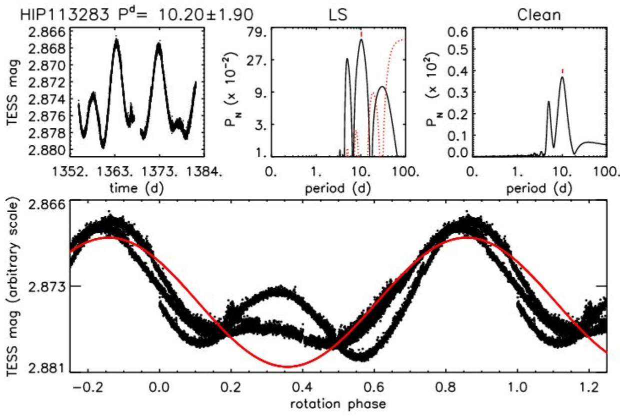

Fig. A.81: Photometric time sequence and periodogram for HIP 113283

Fomalhaut = HIP 113368 The age of the system is from Mamajek (2012). The controversial planet candidate Fomalhaut b Kalas et al. (2008); Janson et al. (2012); Lawler et al. (2015) is well outside the field of view of SPHERE.

HIP 114189 = HD 218396 = HR 8799 Star with the first multi-planetary system detected through imaging (Marois et al. 2008, 2010). It was proposed as a member of the Columba association by Marois et al. (2010). BANYAN returns a moderate membership probability (49%) to this group. Very recently, Lee & Song (2019) proposed it as a probable member of β Pic MG. A younger age would imply lower masses for the four planets orbiting the star. This would expand the extremely narrow space of parameters that fit the astrometric data ensuring at the same time dynamical stability (Esposito et al. 2013; Wang et al. 2018). We adopted the Columba age with a lower limit extending to β Pic MG age.

HIP 114530 The photometric rotation period first measured by Messina et al. (2010) is confirmed by our analysis of the TESS data (Fig. A.82). It is interesting to note that the light curve clearly shows evidence of a secondary small-amplitude periodicity superimposed on the P = 5.10 d rotation period. In Fig. A.83 we show that a period P = 0.3493±0.0022 d is detected by both Lomb–Scargle and Clean with a rotational modulation amplitude of about 0.02 mag. Considering the stability of the light curve phased with this short period, compared to the short timescale evolution of that phased with the longer period, we suspect that such a short periodicity does not arise from magnetic activity rather than the ellipsoidal effect of a likely close binary star observed within the TESS aperture radius.

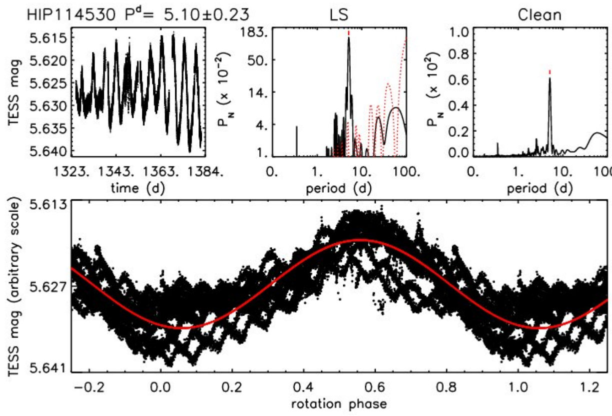

Fig. A.82: Photometric time sequence and periodogram for HIP 114530

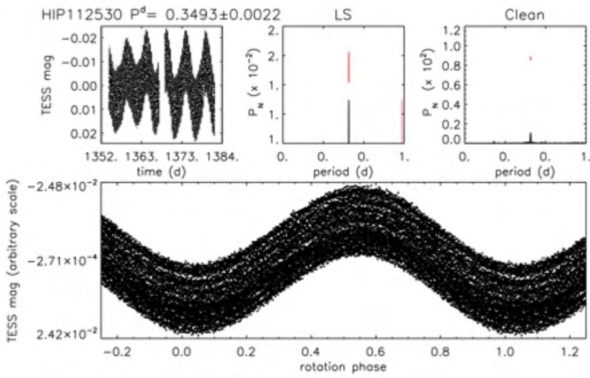

Fig. A.83: Photometric time sequence and periodogram for HIP 114530 after filtering out the P = 5.10 d rotational modulation.

HIP 114948 We measured for the first time the rotation period from the TESS photometric time series (Fig. A.84).

HIP 118008 We measured for the first time the rotation period from the TESS photometric time series (Fig. A.85).

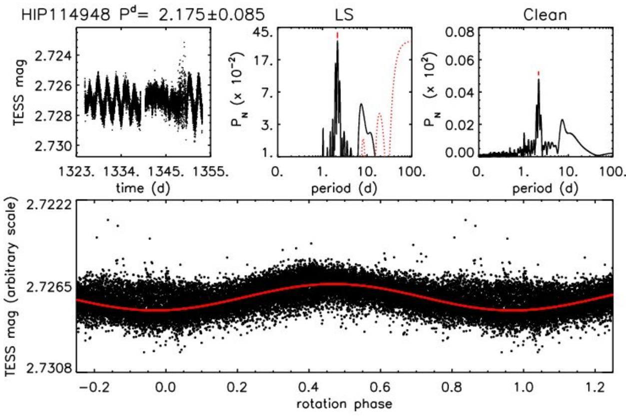

Fig. A.84: Photometric time sequence and periodogram for HIP 114948

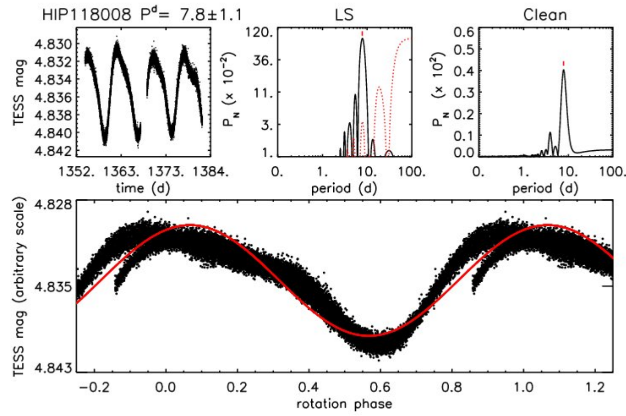

Fig. A.85: Photometric time sequence and periodogram for HIP 118008

Table 5. Summary of target parameters: names, coordinates, and photometry (V, J, H and K magnitude, B-V and V-I colors),

#	Name	other-ID	other-ID	RA(2000)	Dec(2000)	G (mag)	BPRP (mag)	V (mag)	B-V (mag)	V-I (mag)	J (mag)	H (mag)	K (mag)
1	HIP 490	HD 105		0 5 52.50	-41 45 11.00	7.383	0.761	7.53	0.590	0.64	6.464	6.189	6.117
2	HIP 682	HD 377		0 8 25.75	6 37 0.50	7.435	0.792	7.59	0.626	0.69	6.422	6.149	6.116
3	HIP 1113	HD 987		0 13 53.00	-74 41 18.00	8.623	0.954	8.78	0.740	0.82	7.406	7.087	6.962
4	2M J0017-6645	SCR 0017-6645		0 17 23.54	-66 45 12.50	11.338	2.487	12.45		2.45	8.560	7.930	7.700
5	HIP 1481	HD 1466		0 18 26.10	-63 28 39.00	7.326	0.706	7.46	0.540	0.61	6.462	6.248	6.149
6	HIP 1993	GSC8841-1145	CT Tuc	0 25 14.70	-61 30 48.00	10.680	1.830	11.47	1.350	1.81	8.615	7.943	7.749
7	HIP 2578	HD 3003		0 32 43.80	-63 1 53.00	5.035	0.040	5.07	0.040	0.05	5.061	5.156	4.985
8	HIP 6276	BD-12 243		1 20 32.27	-11 28 3.74	8.225	0.969	8.43	0.791	0.83	7.026	6.654	6.549
9	HIP 6485	HD 8558		1 23 21.30	-57 28 51.00	8.376	0.890	8.51	0.680	0.77	7.241	6.946	6.847
10	HIP 6856	HD 9054	CC Phe	1 28 8.70	-52 38 19.00	8.971	1.196	9.07	0.910	1.01	7.405	6.944	6.834
11	TYC 8047 0232 1	CD-52 381		1 52 14.60	-52 19 33.00	10.610	1.227	10.89	0.950	1.08	9.057	8.525	8.405
12	HIP 10602	HD 14228		2 16 30.60	-51 30 44.00	3.470	3.165	3.56	-0.120	-0.11	4.026	3.951	4.127
13	HIP 11360	HD 15115		2 26 16.20	6 17 33.00	6.678	0.540	6.79	0.399	0.46	6.028	5.863	5.822
14	ϵ Hyi	HIP 12394	HD 16978	2 39 35.20	-68 16 1.00	4.037	-0.072	4.12	-0.060	-0.07	4.443	4.433	4.254
15	HIP 13402	HD 17925	EP Eri	2 52 32.13	-12 46 10.97	5.797	1.029	6.05	0.862	0.91	4.830	4.230	4.167
16	HIP 14551	HD 19545	HR 943	3 7 50.85	-27 49 52.14	6.139	0.219	6.18	0.166	0.18	5.891	5.851	5.772
17	TYC 7026 0325 1	CD-35 1167		3 19 8.70	-35 7 0.00	10.430	1.658	11.12	1.150		8.576	7.919	7.723
18	κ Cet	HIP 15457	HD 20630	3 19 21.70	3 22 12.71	4.599	0.840	4.84	0.681	0.73	3.407	3.039	2.957
19	TYC 8060 1673 1	CD-46 1064		3 30 49.10	-45 55 57.00	9.380	1.271	9.55	1.110		7.772	7.251	7.103
20	HIP 17764	HD 24636		3 48 11.47	-74 41 38.81	7.022	0.538	7.13	0.400	0.46	6.367	6.224	6.136
21	HD 25284B	TYC 6461 1120 2		4 0 3.96	-29 2 27.85	9.996	1.403	10.40	1.110		8.280	7.694	7.523
22	TYC 5882 1169 1	BD-15 705	PPM 213757	4 2 16.50	-15 21 30.00	9.753	1.228	10.17	1.010		8.228	7.703	7.573
23	51 Eri	HIP 21547	HD 29391	4 37 36.10	-2 28 25.00	5.122	0.389	5.22	0.280	0.33	4.744	4.770	4.537
24	HIP 22226	HD 30447		4 46 49.50	-26 18 0.00	7.754	0.534	7.85	0.393	0.46	7.099	6.951	6.894
25	HIP 22295	HD 32195		4 48 5.18	-80 46 45.30	8.006	0.698	8.14	0.540	0.61	7.170	6.991	6.868
26	TYC 5899 0026 1	NLTT 14116	LP 776-25	4 52 24.40	-16 49 22.00	10.433	2.533	11.61			7.740	7.146	6.891
27	HIP 23200	V1005 Ori	GJ 182	4 59 34.83	1 47 0.68	9.319	1.913	10.05	1.394	1.84	7.117	6.450	6.261
28	HIP 23309	CD-57 1054		5 0 47.10	-57 15 25.00	9.353	1.919	10.00	1.400	1.79	7.095	6.429	6.244
29	HIP 24947	HD 35114	AS Col	5 20 38.00	-39 45 18.00	7.246	0.665	7.34	0.490	0.56	6.416	6.218	6.144
30	HIP 25283	HD 35650		5 24 30.17	-38 58 10.76	8.526	1.572	9.08	1.248	1.21	6.702	6.105	5.921
31	HIP 25544	HD 36435	GJ 9180	5 27 39.35	-60 24 57.58	6.789	0.945	6.99	0.755	0.79	5.704	5.342	5.200
32	HIP 27288	HD 38678	zeta Lep	5 46 57.34	-14 49 19.00	3.454	0.255	3.55	0.104	0.11	3.390	3.314	3.286
33	β Pic	HIP 27321	HD 39060	5 47 17.10	-51 3 59.00	3.725	0.275	3.85	0.170	0.18	3.669	3.544	3.526
34	TYC 7084 0794 1	CD-35 2722		6 9 19.20	-35 49 31.00	10.218	2.049	10.98	1.690		7.920	7.283	7.046
35	HIP 30030	HD 43989	V1358 Ori	6 19 8.10	-3 26 20.00	7.702	0.736	7.95	0.590	0.66	6.848	6.591	6.552
36	AB Pic	HIP 30034	HD 44627	6 19 12.90	-58 3 16.00	8.838	1.094	9.13	0.860	0.90	7.576	7.088	6.981
37	HIP 30314	HD 45270		6 22 30.94	-60 13 7.15	6.349	0.785	6.53	0.614	0.66	5.433	5.156	5.045
38	GSC 8894-0426	2RE J0625-600		6 25 55.39	-60 3 29.20	11.026	2.785	12.32		2.76	8.094	7.470	7.206
39	TYC 7617 0549 1	CD-40 2458		6 26 6.90	-41 2 54.00	9.856	1.041	10.00	0.800		8.534	8.157	8.020
40	HIP 31878	CD-61 1439		6 39 50.02	-61 28 41.52	9.252	1.643	9.71	1.257	1.53	7.301	6.643	6.500
41	HIP 32235	HD 49855		6 43 46.20	-71 58 35.00	8.980	0.944	8.94	0.699	0.76	7.693	7.380	7.278
42	HD 51797	TYC 8118 0871 1		6 56 23.50	-46 46 55.00	9.418	0.993	9.84	0.780		8.390	7.893	7.803

Table 5. (continued)

#	Name	other-ID	other-ID	RA(2000)	Dec(2000)	G (mag)	BPRP (mag)	V (mag)	B-V (mag)	V-I (mag)	J (mag)	H (mag)	K (mag)
43	HIP 33737	HD 55279		7 0 30.50	-79 41 46.00	9.779	1.199	10.11	0.910	0.95	8.265	7.831	7.652
44	2M J0706-5353			7 6 57.72	-53 53 46.30	10.708	1.870	11.42			8.542	7.897	7.666
45	HIP 34899	HD 56022	OU Pup	7 13 13.35	-45 10 57.86	4.840	-0.014	4.87	-0.003	0.02	5.020	4.949	4.874
46	TYC 1355 214 1	BD+20 1790	V429 Gem	7 23 43.60	20 24 59.00	9.507	1.530	9.93	1.150		7.643	7.032	6.879
47	TYC 8128 1946 1	CD-48 2972		7 28 22.00	-49 8 38.00	9.628	0.900	9.84	0.800		8.505	8.132	8.058
48	HIP 36948	HD 61005		7 35 47.46	-32 12 14.04	8.003	0.917	8.23	0.751	0.80	6.905	6.578	6.458
49	HIP 37766	YZ CMi	GJ 285	7 44 40.17	3 33 8.83	9.681	3.003	11.19	1.600	2.95	6.581	6.005	5.698
50	HIP 41307	HD 71155	30 Mon	8 25 39.63	-3 54 23.13	3.815	0.012	3.91	-0.012	-0.02	4.117	4.090	4.079
51	η Cha	HIP 42637	RECX2	8 41 19.51	-78 57 48.10	5.431	-0.129	5.46	-0.101	-0.08	5.688	5.721	5.718
52	HD 75505	RECX13		8 41 44.80	-79 2 53.00	7.356	0.229	6.87	9.869	-0.06	6.945	6.916	6.883
53	HIP 42808	HD 74576		8 43 18.00	-38 52 57.00	6.270	1.119	6.58	0.920	0.97	4.937	4.441	4.358
54	HIP 44526	HD 77825	V405 Hya	9 4 20.69	-15 54 51.40	8.452	1.197	8.77	0.960	1.01	7.005	6.542	6.388
55	HIP 47135	HD 84075		9 36 17.82	-78 20 41.59	8.433	0.764	8.59	0.588	0.66	7.475	7.241	7.160
56	HIP 50191	HD 88955	q Vel	10 14 44.15	-42 7 18.99	3.755	0.081	3.85	0.051	0.03	3.858	3.713	3.775
57	TWA 6	GSC7183-1477	BX Ant	10 18 28.70	-31 50 3.00	10.847	1.712	11.62	1.310	1.68	8.869	8.180	8.042
58	HIP 51228	HD 90712		10 27 47.78	-34 23 58.14	7.361	0.771	7.52	0.585	0.66	6.408	6.147	6.042
59	HIP 51317	GJ 393	BD+01 2447	10 28 55.55	0 50 27.58	8.674	2.304	9.65	1.507	2.26	6.176	5.605	5.311
60	TWA 7	GSC7190-2111	CE Ant	10 42 30.10	-33 40 17.00	10.619	2.519	11.65	1.460	2.44	7.792	7.125	6.899
61	HIP 53524	HD 95086		10 57 3.02	-68 40 2.45	7.309	0.325	7.36	0.230	0.26	6.906	6.867	6.789
62	HIP 54155	HD 96064	HH Leo	11 4 41.47	-4 13 15.92	7.401	0.947	7.64	0.770	0.81	6.302	5.903	5.801
63	HIP 54231	HD 96338		11 5 45.74	-47 26 32.27	6.802	0.041	6.82	0.043	0.06	6.778	6.762	6.769
64	β Leo	HIP 57632	HD 102647	11 49 3.58	14 34 19.42			2.14	0.090	0.10	1.854	1.925	1.930
65	HIP 58167	HD 103599		11 55 43.55	-54 10 50.48	8.178	0.568	8.21	0.375	0.42	7.448	7.345	7.274
66	HIP 58465	HD 104125		11 59 23.74	-57 10 4.74	6.731	0.243	6.77	0.173	0.19	6.404	6.344	6.293
67	HIP 59505	HD 106048		12 12 12.01	-54 13 49.64	8.519	0.462	8.60	0.332	0.39	7.917	7.738	7.701
68	HIP 60183	HD 107301	HR 4692	12 20 28.22	-65 50 33.56	6.181	-0.055	6.20	-0.041	-0.02	6.253	6.277	6.270
69	HIP 60459	HD 107821		12 23 42.19	-63 52 12.29	7.375	0.211	7.41	0.146	0.16	7.082	7.051	7.015
70	HD 108767B		δ CrvB	12 29 50.91	-16 31 14.99	8.167	1.122	8.51	0.950		6.793	6.370	6.235
71	HIP 61468	HD 109536		12 35 45.53	-41 1 19.00	5.039	0.313	5.12	0.224	0.26	4.737	4.708	4.571
72	TWA 11	HIP 61498	HD 109573	12 36 1.03	-39 52 10.20	5.771	-0.002	5.78	0.000	-0.02	5.784	5.794	5.769
73	ρ Vir	HIP 61960	HD 110411	12 41 53.06	10 14 8.25	4.817	0.104	4.88	0.076	0.08	4.986	4.761	4.678
74	HIP 63839	HD 113457		13 5 2.04	-64 26 29.71	6.618	-0.005	6.64	0.006	0.03	6.608	6.647	6.640
75	HIP 64892	HD 115470		13 18 5.10	-44 3 19.37	6.784	-0.028	6.80	-0.018	0.00	6.809	6.879	6.832
76	HIP 64995	HD 115600		13 19 19.54	-59 28 20.44	8.137	0.505	8.23	0.398	0.46	7.504	7.385	7.337
77	HIP 65426	HD 116434		13 24 36.10	-51 30 16.05	6.983	0.117	6.98	0.083	0.09	6.817	6.848	6.768
78	HIP 66252	HD 118100	EQ Vir	13 34 43.21	-8 20 31.33	8.710	1.496	9.24	1.210	1.41	6.876	6.312	6.116
79	HIP 66566	HD 118588		13 38 42.88	-44 30 58.63	7.519	0.101	7.53	0.101	0.11	7.371	7.392	7.336
80	HIP 66651	HD 118697		13 39 45.73	-54 8 53.31	7.321	-0.013	7.34	-0.003	0.02	7.334	7.372	7.334
81	HIP 68781	HD 122705		14 4 42.15	-50 4 17.06	7.619	0.154	7.64	0.125	0.14	7.406	7.425	7.341
82	TYC 7286 0248 1	CD-31 11053		14 17 20.10	-32 30 47.00	10.383	1.501	10.59	1.065	1.27	8.396	7.801	7.676
83	HIP 69989	HD 125451	18 Boo	14 19 16.28	13 0 15.48	5.265	0.551	5.41	0.385	0.41	4.739	4.538	4.394
84	HIP 71724	HD 128819		14 40 17.65	-40 50 30.11	6.626	-0.068	6.65	-0.069	-0.05	6.729	6.832	6.775
85	HIP 71743	HD 128987	KU Lib	14 40 31.11	-16 12 33.44	7.044	0.900	7.24	0.710	0.76	5.947	5.629	5.531

Table 5. (continued)

#	Name	other-ID	other-ID	RA(2000)	Dec(2000)	G (mag)	BPRP (mag)	V (mag)	B-V (mag)	V-I (mag)	J (mag)	H (mag)	K (mag)
86	HIP 73145	HD 131835		14 56 54.47	-35 41 43.65	7.869	0.202	7.88	0.192	0.21	7.604	7.564	7.524
87	HIP 73990	HD 133803		15 7 14.94	-29 30 16.12	8.068	0.459	8.14	0.362	0.42	7.499	7.362	7.321
88	β Cir	HIP 74824	HD 135379	15 17 30.85	-58 48 4.35	3.973	0.130	4.07	0.088	0.08	3.928	3.806	3.875
89	HIP 76063	HD 138204		15 32 4.19	-38 37 21.15	6.178	0.287	6.23	0.212	0.23	5.832	5.769	5.715
90	HIP 77317	HD 140840		15 47 6.17	-35 31 4.94	7.334	-0.003	7.34	0.005	0.03	7.345	7.406	7.361
91	HIP 77457	HD 141190		15 48 52.13	-29 29 0.40	7.898	0.364	7.96	0.259	0.29	7.409	7.367	7.276
92	HIP 77464	HD 141378		15 48 56.80	-3 49 6.65	5.497	0.145	5.53	0.120	0.09	5.328	5.267	5.256
93	HD 141943	TYC 7846 1538 1	NZ Lup	15 53 27.30	-42 16 1.00	7.779	0.842	7.92	0.650	0.71	6.738	6.413	6.342
94	HIP 78099	HD 142705		15 56 47.85	-23 11 2.68	7.692	0.292	7.74	0.198	0.22	7.253	7.278	7.183
95	HIP 78196	HD 142851		15 57 59.35	-31 43 44.15	7.008	-0.027	7.03	-0.011	0.01	7.005	7.120	7.032
96	HIP 78530	HD 143567		16 1 55.46	-21 58 49.40	7.147	0.149	7.19	0.089	0.10	6.928	6.946	6.903
97	HIP 78541	HD 143488		16 2 4.84	-36 44 38.09	6.970	0.011	6.99	0.006	0.03	6.945	7.009	6.967
98	HIP 80324	HD 147553		16 23 56.72	-33 11 57.83	6.981	-0.016	6.45	0.013	0.03	6.963	7.008	6.987
99	HIP 80591	HD 148055		16 27 14.58	-39 49 21.97	8.286	0.284	8.33	0.206	0.23	7.930	7.856	7.831
100	HIP 81084	LP 745-70		16 33 41.61	-9 33 11.95	10.525	1.867	11.30	1.439	1.77	8.377	7.779	7.547
101	HD 326277	TYC 7879 0980 1		16 49 13.30	-43 55 28.00	9.938	0.991	10.10	0.770	0.85	8.750	8.298	8.242
102	HIP 82388	HD 151798		16 50 5.16	-12 23 14.85	7.770	0.788	7.95	0.627	0.69	6.816	6.599	6.480
103	HIP 82430	HD 151726		16 50 45.52	-38 15 23.11	7.209	-0.021	7.24	-0.038	-0.02	7.218	7.261	7.261
104	HD 156097	TYC 7362 0724 1		17 16 58.00	-31 9 4.00	9.347	0.891	9.51	0.690	0.76	8.218	7.843	7.799
105	TYC 8728 2262 1	CD-54 7336		17 29 55.10	-54 15 49.00	9.327	1.079	9.55	0.850	0.95	7.941	7.462	7.364
106	HD 159911	BD-13 4687		17 37 46.47	-13 14 46.64	9.555	1.557	10.10	1.070	1.43	7.626	7.017	6.835
107	π Ara	HIP 86305	HD 159492	17 38 5.52	-54 30 1.56	5.184	0.252	5.25	0.195	0.20	4.920	4.866	4.780
108	HIP 86598	HD 160305		17 41 49.04	-50 43 28.05	8.181	0.734	8.33	0.574	0.65	7.345	7.092	6.992
109	HIP 88399	HD 164249A		18 3 3.40	-51 38 56.00	6.896	0.583	7.01	0.460	0.53	6.159	6.022	5.913
110	HIP 89829	HD 168210		18 19 52.20	-29 16 33.00	8.664	0.922	8.89	0.690	0.78	7.526	7.198	7.053
111	HIP 92024	HD 172555	HR 7012	18 45 26.90	-64 52 16.00	4.693	0.268	4.78	0.200	0.21	4.382	4.251	4.298
112	TYC 9073 0762 1	AC 4357199		18 46 52.60	-62 10 36.00	11.103	2.051	12.08	1.460	2.09	8.746	8.047	7.854
113	TYC 7408 0054 1	CD-31 16041		18 50 44.50	-31 47 47.00	10.495	1.828	11.20	1.350	1.76	8.314	7.667	7.462
114	PZ Tel	HIP 92680	HD 174429	18 53 5.90	-50 10 50.00	8.099	0.972	8.29	0.770	0.85	6.856	6.486	6.366
115	HIP 92984	HD 175726		18 56 37.17	4 15 54.46	6.563	0.741	6.71	0.583	0.65	5.703	5.418	5.346
116	HIP 93375	HD 176367		19 1 6.00	-28 42 50.00	8.360	0.735	8.48	0.560	0.62	7.463	7.278	7.151
117	ζ Aql	HIP 93747		19 5 24.61	13 51 48.52	2.855	0.290	2.99	0.014	-0.01	3.084	3.048	2.876
118	TYC 8760 1468 1	CD-54 8168		19 9 21.50	-54 17 7.00	9.713	1.156	10.19	0.970	1.09	8.328	7.850	7.699
119	α CrA	HIP 94114	HD 178253	19 9 28.34	-37 54 16.11	4.078	0.097	4.11	0.042	0.03	4.094	3.915	4.049
120	HIP 95270	HD 181327		19 22 58.90	-54 32 17.00	6.920	0.617	7.03	0.480	0.53	6.200	5.980	5.910
121	η Tel	HIP 95261	HD 181296	19 22 51.20	-54 25 24.00	4.998	0.001	5.03	0.020	0.04	5.096	5.148	5.008
122	α Sgr	HIP 95347	HD 181869	19 23 53.18	-40 36 57.38	3.916	-0.102	3.96	-0.105	-0.10	4.173	4.195	4.195
123	TYC 0486 4943 1			19 33 3.80	3 45 40.00	10.802	1.274	11.28	1.023	1.21	9.301	8.779	8.656
124	TYC 7443 1102 1			19 56 4.37	-32 7 37.71	10.824	1.860	11.80			8.710	8.027	7.846
125	HD 189285	BD-04 4987		19 59 24.10	-4 32 6.00	9.306	0.885	9.46	0.710		8.259	7.963	7.841
126	HIP 98470	HD 189245		20 0 20.25	-33 42 12.43	5.508	0.655	5.65	0.498	0.57	4.513	4.641	4.476
127	ϵ Pav	HIP 98495	HD 188228	20 0 35.55	-72 54 37.81	3.864	-0.021	3.97	-0.032	-0.04	3.798	3.762	3.800
128	2M J2001-3313			20 1 37.18	-33 13 14.00	11.460	2.072	12.25			9.155	8.461	8.244

Table 5. (continued)

#	Name	other-ID	other-ID	RA(2000)	Dec(2000)	G (mag)	BPRP (mag)	V (mag)	B-V (mag)	V-I (mag)	J (mag)	H (mag)	K (mag)
129	TYC 8404 0354 1	CD-52 9381		20 7 23.80	-51 47 27.00	10.045	1.597	10.59	1.240	1.52	8.158	7.565	7.388
130	ρ Aql	HIP 99742	HD 192425	20 14 16.62	15 11 51.39	4.896	0.087	4.94	0.072	0.09	4.865	4.801	4.767
131	AU Mic	HIP 102409	HD 197481	20 45 9.50	-31 20 27.00	7.840	2.124	8.73	1.490	2.09	5.436	4.831	4.529
132	BO Mic	HIP 102626	HD 197890	20 47 45.02	-36 35 40.83	8.930	1.209	9.44	0.939	0.93	7.513	6.930	6.794
133	TYC 1090 0543 1	QV Del		20 54 28.00	9 6 7.00	11.254	1.397	11.73	1.070		9.486	8.905	8.823
134	HIP 104365	HD 201184	χ Cap	21 8 33.62	-21 11 37.21	5.286	-0.001	5.30	0.000	0.02	5.313	5.334	5.305
135	HD 201919	TYC 6351 0286 1		21 13 5.30	-17 29 13.00	10.183	1.537	10.64	1.210	1.42	8.348	7.745	7.583
136	HIP 105388	HD 202917		21 20 50.00	-53 2 3.00	8.488	0.915	8.69	0.720	0.80	7.386	7.026	6.908
137	TYC 9482 121 1	CD-81 812		21 44 14.30	-80 31 32.61	9.486	1.769	10.18	1.260		7.450	6.824	6.652
138	HIP 107345	GSC9116-1363	BPM14269	21 44 30.10	-60 58 39.00	10.939	1.906	11.61	1.410	1.83	8.751	8.087	7.874
139	HIP 107350	HD 206860	HN Peg	21 44 31.33	14 46 18.98	5.811	0.767	5.96	0.587	0.66	4.793	4.598	4.559
140	HIP 107412	HD 206893		21 45 21.91	-12 47 0.07	6.568	0.589	6.69	0.439	0.51	5.869	5.687	5.593
141	2M J2202-4210			22 2 16.26	-42 10 32.90	11.226	2.092	12.15			8.925	8.225	7.993
142	TYC 9340 0437 1	CP-72 2713		22 42 48.90	-71 42 21.00	9.828	1.760	10.60	1.350	1.73	7.791	7.123	6.894
143	HIP 112312	GJ 871.1A		22 44 58.00	-33 15 2.00	10.736	2.785	12.07	1.480	2.80	7.786	7.154	6.932
144	HIP 113283	HD 216803	TW PsA	22 56 24.05	-31 33 56.00	6.069	1.326	6.48	1.090	1.20	4.533	3.804	3.805
145	Fomalhaut	HIP 113368	HD 216956	22 57 39.05	-29 37 20.05			1.17	0.145	0.16	1.037	0.937	0.945
146	HR 8799	HIP 114189	HD 218396	23 7 28.72	21 08 03.30	5.898	0.394	5.97	0.259	0.29	5.383	5.280	5.240
147	HIP 114530	HD 218860A		23 11 52.05	-45 08 10.63	8.604	0.931	8.75	0.750	0.79	7.467	7.109	7.032
148	HIP 114948	HD 219482	GJ 1282	23 16 57.69	-62 00 04.31	5.502	0.666	5.64	0.521	0.59	5.100	4.606	4.437
149	κ Psc	HIP 115738	HD 220825	23 26 55.96	01 15 20.19	4.871	0.032	4.95	0.036	0.01	5.317	4.984	4.902
150	HIP 118008	HD 224228		23 56 10.67	-39 03 08.40	7.930	1.184	8.22	0.973	1.02	6.510	6.007	5.907

Table 6. Summary of target parameters: name, trigonometric parallax π, proper motion, radial velocity, U, V, W space velocities, moving group membership.,

#	Name	other-ID	π (mas)	ref ref	μ_α (mas/yr)	μ_δ (mas/yr)	ref ref	RV (km/s)	ref	U (km/s)	V (km/s)	W (km/s)	MG
1	HIP 490	HD 105	25.74±0.06	Gaia2	97.75±0.05	-76.42±0.05	Gaia2	2.2± 0.2	Des20	-9.2	-21.0	-1.7	TUC
2	HIP 682	HD 377	25.96±0.06	Gaia2	87.38±0.13	-1.74±0.09	Gaia2	1.2± 0.2	Nid02	-13.9	-7.0	-3.7	
3	HIP 1113	HD 987	21.81±0.02	Gaia2	82.81±0.05	-49.08±0.04	Gaia2	9.5± 0.2	Des20	-8.9	-21.1	-1.1	TUC
4	2M J0017-6645	SCR 0017-6645	27.17±0.03	Gaia2	103.04±0.05	-16.87±0.05	Gaia2	10.8± 0.2	Mal14	-10.4	-16.3	-8.7	BPIC
5	HIP 1481	HD 1466	23.27±0.03	Gaia2	90.07±0.05	-59.18±0.05	Gaia2	6.8± 0.2	Des20	-9.2	-21.0	-0.7	TUC
6	HIP 1993	GSC8841-1145	22.64±0.03	Gaia2	87.93±0.04	-56.17±0.04	Gaia2	6.5± 0.2	Des20	-9.2	-20.8	-0.5	TUC
7	HIP 2578	HD 3003	21.79±0.13	Gaia2	86.42±0.21	-50.35±0.21	Gaia2	5.0±2.0	Duf95	-10.1	-19.9	1.1	TUC
8	HIP 6276	BD-12 243	28.30±0.05	Gaia2	111.44±0.09	-136.88±0.07	Gaia2	10.6± 0.2	Des20	-5.1	-27.6	-14.2	ABDO
9	HIP 6485	HD 8558	22.07±0.03	Gaia2	92.79±0.05	-36.08±0.04	Gaia2	9.2± 0.5	SACY	-9.4	-21.2	-1.4	TUC
10	HIP 6856	HD 9054	25.10±0.03	Gaia2	106.14±0.05	-42.98±0.04	Gaia2	8.2± 0.2	Des20	-9.6	-21.0	-1.0	TUC
11	TYC 8047 0232 1	CD-52 381	11.59±0.04	Gaia2	49.94±0.05	-10.43±0.05	Gaia2	14.4±	SACY	-10.9	-22.1	-6.1	COL
12	HIP 10602	HD 14228	21.22±0.12	VL07	91.03±0.12	-22.23±0.12	VL07	10.4± 1.3	Duf95	-9.9	-21.2	-0.6	TUC
13	HIP 11360	HD 15115	20.41±0.04	Gaia2	88.03±0.08	-50.51±0.07	Gaia2	1.7± 1.0	Des15	-9.7	-21.6	-0.2	TUC
14	HIP 12394	HD 16978	21.48±0.09	VL07	87.30±0.09	0.09±0.10	VL07	13.6± 0.9	XHIP	-9.1	-21.7	-1.8	TUC
15	HIP 13402	HD 17925	96.54±0.04	Gaia2	397.35±0.08	-189.11±0.08	Gaia2	18.2± 0.2	Des20	-15.4	-21.9	-9.1	
16	HIP 14551	HD 19545	18.44±0.12	Gaia2	65.22±0.13	-18.38±0.16	Gaia2	13.8± 0.8	Zuk11	-10.9	-19.0	-3.7	TUC
17	TYC 7026 0325 1	CD-35 1167	21.95±0.04	Gaia2	88.01±0.07	-19.54±0.08	Gaia2	13.5± 0.5	SACY	-10.4	-21.3	-0.9	TUC
18	HIP 15457	HD 20630	109.41±0.27	VL07	269.30±0.24	93.75±0.22	VL07	19.0± 0.2	Nid02	-21.8	-4.4	-4.5	
19	TYC 8060 1673 1	CD-46 1064	22.77±0.02	Gaia2	88.55±0.04	-4.95±0.05	Gaia2	14.9± 0.7	Des15	-10.3	-21.3	-1.1	TUC
20	HIP 17764	HD 24636	17.53±0.02	Gaia2	63.49±0.04	24.33±0.05	Gaia2	15.5± 1.3	Zuk11	-8.8	-22.3	-1.9	TUC
21	HD 25284B	TYC 6461 1120 2	20.48±0.03	Gaia2	74.55±0.05	-17.85±0.05	Gaia2	15.2± 0.6	Gaia2	-10.1	-21.1	-0.5	TUC?
22	TYC 5882 1169 1	BD-15 705	18.23±0.03	Gaia2	66.08±0.04	-26.84±0.03	Gaia2	15.6± 0.2	Des20	-11.6	-21.2	-1.4	COL
23	HIP 21547	HD 29391	33.58±0.14	Gaia2	44.35±0.23	-63.83±0.18	Gaia2	21.0± 2.0	Duf95	-14.0	-16.4	-9.8	BPIC
24	HIP 22226	HD 30447	12.42±0.04	Gaia2	33.61±0.06	-5.14±0.08	Gaia2	24.6± 0.6	Gaia2	-14.6	-23.1	-5.6	COL
25	HIP 22295	HD 32195	15.93±0.03	Gaia2	47.75±0.05	40.18±0.06	Gaia2	11.5± 2.0	Nor04	-10.0	-19.4	0.5	TUC
26	TYC 5899 0026 1	NLTT 14116	63.16±0.05	Gaia2	122.14±0.06	-210.57±0.06	Gaia2	26.5± 0.3	Des20	-8.5	-28.5	-12.4	ABDO
27	HIP 23200	V1005 Ori	40.98±0.03	Gaia2	39.23±0.06	-95.05±0.04	Gaia2	19.9± 0.4	Des20	-13.1	-16.6	-9.4	BPIC
28	HIP 23309	CD-57 1054	37.17±0.03	Gaia2	35.20±0.05	74.14±0.05	Gaia2	19.3± 0.2	Des20	-11.2	-16.7	-9.0	BPIC
29	HIP 24947	HD 35114	20.98±0.03	Gaia2	38.67±0.06	12.90±0.07	Gaia2	23.0± 0.5	SACY	-11.7	-21.2	-5.1	COL
30	HIP 25283	HD 35650	57.21±0.03	Gaia2	43.03±0.05	-57.34±0.05	Gaia2	32.4± 0.2	Des20	-8.0	-28.1	-15.2	ABDO
31	HIP 25544	HD 36435	51.34±0.03	Gaia2	-148.44±0.06	-93.33±0.06	Gaia2	13.7± 0.5	SACY	9.2	-4.2	-18.6	
32	HIP 27288	HD 38678	46.28±0.16	VL07	-14.54±0.13	-1.07±0.10	VL07	24.7± 1.0	XHIP	-17.8	-14.1	-9.9	CAS?
33	HIP 27321	HD 39060	51.44±0.12	VL07	4.65±0.11	83.10±0.15	VL07	20.2± 0.4	Zuk01	-11.0	-16.2	-9.1	BPIC
34	TYC 7084 0794 1	CD-35 2722	44.63±0.03	Gaia2	-3.72±0.04	-56.27±0.05	Gaia2	31.4± 0.5	SACY	-7.9	-27.4	-14.4	ABDO
35	HIP 30030	HD 43989	19.23±0.05	Gaia2	10.71±0.08	-42.30±0.09	Gaia2	19.4± 1.0	Mon01	-10.2	-19.0	-5.2	TUC
36	HIP 30034	HD 44627	19.95±0.03	Gaia2	14.34±0.06	45.07±0.06	Gaia2	22.7± 0.2	Des20	-11.2	-22.0	-5.7	CAR
37	HIP 30314	HD 45270	41.86±0.03	Gaia2	-11.60±0.06	64.43±0.05	Gaia2	31.8± 0.2	Des20	-7.7	-28.3	-14.5	ABDO
38	GSC 8894-0426	2RE J0625-600	74.37±0.04	Gaia2	-25.39±0.09	110.75±0.09	Gaia2	32.0± 0.5	Des20	-7.6	-28.4	-14.5	ABDO
39	TYC 7617 0549 1	CD-40 2458	10.08±0.02	Gaia2	4.24±0.04	12.56±0.04	Gaia2	25.0± 0.5	SACY	-13.4	-21.2	-5.8	COL
40	HIP 31878	CD-61 1439	44.96±0.03	Gaia2	-27.31±0.06	75.00±0.06	Gaia2	31.8± 0.2	Des20	-7.7	-28.5	-14.4	ABDO
41	HIP 32235	HD 49855	17.99±0.03	Gaia2	7.37±0.05	60.60±0.08	Gaia2	20.7± 0.2	Des20	-10.6	-23.3	-5.5	CAR

Table 6. (continued)

#	Name	other-ID	π (mas)	ref ref	μ_α (mas/yr)	μ_δ (mas/yr)	ref ref	RV (km/s)	ref	U (km/s)	V (km/s)	W (km/s)	MG
42	TYC 8118 0871 1	HD 51797	10.45±0.03	Gaia2	-2.86±0.05	19.31±0.05	Gaia2	25.2± 0.5	SACY	-14.0	-21.9	-6.2	COL
43	HIP 33737	HD 55279	15.67±0.02	Gaia2	2.17±0.04	60.08±0.04	Gaia2	17.6± 0.5	SACY	-10.4	-22.6	-5.0	TUC
44	2MASS J0706-5353		21.43±0.02	Gaia2	-7.41±0.04	38.88±0.04	Gaia2	22.4± 0.6	Mal14	-10.7	-20.7	-6.0	CAR
45	HIP 34899	HD 56022	17.45±0.13	Gaia2	-25.19±0.24	-87.24±0.24	Gaia2	4.3± 2.8	Gon06	18.4	-4.5	-16.4	
46	TYC 1355 214 1	BD+20 1790	35.98±0.07	Gaia2	-65.58±0.09	-230.95±0.07	Gaia2	7.9± 0.3	Car18	-5.1	-27.4	-17.0	ABDO
47	TYC 8128 1946 1	CD-48 2972	11.42±0.02	Gaia2	-24.25±0.04	45.12±0.04	Gaia2	19.0± 2.1	Des15	-23.7	-14.7	-5.7	ARG
48	HIP 36948	HD 61005	27.41±0.03	Gaia2	-55.11±0.05	74.15±0.06	Gaia2	22.6± 0.2	Des20	-23.4	-14.2	-4.2	ARG?
49	HIP 37766	YZ CMi	167.02±0.06	Gaia2	-348.10±0.11	-445.88±0.06	Gaia2	26.5± 0.3	Nid02	-19.6	-22.7	-7.7	BPIC?
50	HIP 41307	HD 71155	26.66±0.19	VL07	-66.43±0.17	-23.41±0.16	VL07	10.0± 2.0	Duf95	-10.8	-8.4	-8.3	
51	HIP 42637	RECX2	10.04±0.09	Gaia2	-29.78±0.22	26.60±0.25	Gaia2	14.0±10.0	Eva67	-12.5	-17.2	-10.0	ETAC
52	HD 75505	RECX13	10.00±0.03	Gaia2	-30.75±0.06	27.04±0.08	Gaia2						ETAC
53	HIP 42808	HD 74576	89.40±0.03	Gaia2	-301.15±0.04	340.12±0.04	Gaia2	12.9± 0.5	SACY	-26.0	-8.5	-0.6	
54	HIP 44526	HD 77825	36.52±0.05	Gaia2	-107.83±0.08	-30.94±0.08	Gaia2	4.8± 0.3	Des20	-8.9	-6.0	-11.0	CAS?
55	HIP 47135	HD 84075	15.60±0.02	Gaia2	-73.32±0.04	49.37±0.04	Gaia2	5.3± 0.2	Des20	-22.8	-13.8	-6.4	ARG
56	HIP 50191	HD 88955	32.18±0.15	VL07	-150.09±0.10	49.44±0.11	VL07	7.4± 2.7	Gon06	-21.6	-10.4	-4.8	ARG?
57	TWA 6	GSC7183-1477	15.23±0.03	Gaia2	-56.61±0.05	-18.46±0.05	Gaia2	20.7± 1.5	SACY	-11.3	-24.5	-6.6	TWA?
58	HIP 51228	HD 90712	26.39±0.05	Gaia2	-120.76±0.07	-39.15±0.07	Gaia2	20.0± 0.3	Des20	-13.2	-25.4	-9.9	
59	HIP 51317	GJ 393	142.19±0.05	Gaia2	-603.00±0.08	-732.08±0.07	Gaia2	8.5± 0.3	Des20	-7.4	-28.2	-15.0	ABDO
60	TWA 7	GSC7190-2111	29.39±0.07	Gaia2	-118.93±0.11	-19.85±0.11	Gaia2	11.9± 0.3	Des20	-13.6	-16.9	-7.0	TWA
61	HIP 53524	HD 95086	11.57±0.03	Gaia2	-41.14±0.05	12.70±0.05	Gaia2						LCC?
62	HIP 54155	HD 96064	38.11±0.06	Gaia2	-179.93±0.08	-104.34±0.07	Gaia2	18.8± 0.2	Des20	-15.0	-28.3	-1.1	HELY?
63	HIP 54231	HD 96338	8.59±0.04	Gaia2	-31.69±0.07	-3.12±0.06	Gaia2						LCC
64	HIP 57632	HD 102647	90.91±0.52	VL07	-497.68±0.87	-114.67±0.44	VL07	-0.2± 1.0	Duf95	-19.9	-16.1	-7.5	ARG
65	HIP 58167	HD 103599	9.26±0.04	Gaia2	-36.16±0.06	-9.40±0.05	Gaia2	21.3± 2.0	Che11	-6.0	-27.4	-5.6	LCC
66	HIP 58465	HD 104125	10.09±0.14	Gaia2	-38.71±0.19	-9.24±0.15	Gaia2						LCC
67	HIP 59505	HD 106048	8.69±0.14	Gaia2	-30.22±0.18	-5.93±0.16	Gaia2						LCC
68	HIP 60183	HD 107301	10.27±0.06	Gaia2	-41.43±0.10	-11.32±0.08	Gaia2	-8.3± 2.0	Duf95	-20.3	-1.7	-6.8	LCC
69	HIP 60459	HD 107821	9.24±0.06	Gaia2	-39.04±0.10	-10.20±0.08	Gaia2						LCC
70	HD 108767B		37.45±0.06	Gaia2	-211.05±0.09	-136.37±0.07	Gaia2	7.0± 1.0	Mon01	-13.6	-28.2	-8.9	
71	HIP 61468	HD 109536	28.66±0.15	Gaia2	-107.61±0.25	1.07±0.23	Gaia2	-11.0± 4.2	Gon06	-22.8	3.8	-6.7	
72	TWA 11	HIP 61498	13.91±0.13	Gaia2	-55.65±0.18	-23.74±0.23	Gaia2	9.4± 2.3	Fer08	-9.8	-19.9	-4.8	TWA
73	HIP 61960	HD 110411	26.20±0.21	Gaia2	82.11±0.44	-88.85±0.29	Gaia2	-0.7± 2.4	Gon06	20.8	-4.8	-5.0	
74	HIP 63839	HD 113457	9.45±0.05	Gaia2	-36.63±0.08	-16.73±0.08	Gaia2	15.0± 7.4	Duf95	-7.1	-22.9	-7.7	LCC
75	HIP 64892	HD 115470	7.99±0.09	Gaia2	-30.67±0.12	-20.27±0.11	Gaia2	14.9± 1.0	Che18	-4.5	-25.6	-4.6	LCC
76	HIP 64995	HD 115600	9.12±0.04	Gaia2	-32.63±0.05	-18.32±0.05	Gaia2	12.3± 0.3	Che11	-6.8	-20.9	-6.8	LCC
77	HIP 65426	HD 116434	9.16±0.06	Gaia2	-34.25±0.10	-18.81±0.09	Gaia2	5.2± 1.3	Cha17	-17.1	-8.9	-8.0	LCC
78	HIP 66252	HD 118100	48.73±0.06	Gaia2	-286.58±0.11	-91.87±0.08	Gaia2	-22.2± 0.2	Des20	-28.4	-14.9	-17.9	
79	HIP 66566	HD 118588	7.35±0.13	Gaia2	-26.48±0.18	-19.19±0.19	Gaia2						LCC
80	HIP 66651	HD 118697	7.35±0.06	Gaia2	-25.22±0.11	-18.66±0.10	Gaia2						LCC
81	HIP 68781	HD 122705	8.16±0.06	Gaia2	-26.89±0.09	-21.64±0.10	Gaia2						UCL
82	TYC 7286 0248 1	CD-31 11053	11.07±0.08	Gaia2	-34.21±0.17	-30.38±0.14	Gaia2	5.2± 0.5	SACY	-4.8	-19.4	-3.6	UCL
83	HIP 69989	HD 125451	38.13±0.13	Gaia2	105.27±0.27	-31.39±0.26	Gaia2	-1.4± 0.3	Des20	11.8	5.6	-4.2	UMA?
84	HIP 71724	HD 128819	6.05±0.17	Gaia2	-19.23±0.25	-21.71±0.26	Gaia2	2.0± 1.1	Gon06	-8.4	-19.7	-7.8	UCL

Table 6. (continued)

#	Name	other-ID	π (mas)	ref ref	μ_α (mas/yr)	μ_δ (mas/yr)	ref ref	RV (km/s)	ref	U (km/s)	V (km/s)	W (km/s)	MG
85	HIP 71743	HD 128987	42.09±0.04	Gaia2	-111.69±0.08	-65.99±0.08	Gaia2	-23.3± 0.2	Nor04	-22.6	-6.7	-14.3	
86	HIP 73145	HD 131835	7.48±0.20	Gaia2	-23.35±0.26	-24.94±0.30	Gaia2						UCL
87	HIP 73990	HD 133803	9.03±0.06	Gaia2	-27.43±0.11	-29.03±0.09	Gaia2						UCL
88	HIP 74824	HD 135379	32.73±0.19	VL07	-97.74±0.28	-134.15±0.22	VL07	9.6± 2.7	Gon06	-6.7	-23.3	-9.1	
89	HIP 76063	HD 138204	18.08±0.05	Gaia2	-51.45±0.10	-69.56±0.08	Gaia2	-1.2± 4.3		-8.9	-19.8	-6.7	
90	HIP 77317	HD 140840	6.75±0.05	Gaia2	-18.87±0.10	-25.00±0.07	Gaia2						UCL
91	HIP 77457	HD 141190	7.94±0.06	Gaia2	-7.43±0.11	-18.97±0.06	Gaia2						US
92	HIP 77464	HD 141378	18.68±0.12	Gaia2	-29.91±0.21	7.39±0.17	Gaia2	-16.4± 2.9		-17.1	-4.6	-4.1	
93	TYC 7846 1538 1	HD 141943	16.57±0.05	Gaia2	-43.08±0.09	-65.52±0.07	Gaia2	-1.7± 0.5	SACY	-9.6	-19.3	-6.5	UCL?
94	HIP 78099	HD 142705	6.93±0.08	Gaia2	-12.52±0.14	-24.19±0.12	Gaia2	-6.5± 2.9	Gon06	-7.0	-16.7	-7.8	US
95	HIP 78196	HD 142851	6.94±0.06	Gaia2	-13.79±0.14	-26.10±0.08	Gaia2						US
96	HIP 78530	HD 143567	7.28±0.08	Gaia2	-12.01±0.12	-24.11±0.07	Gaia2	-9.0± 4.4	Gon06	-8.8	-15.5	-8.4	US
97	HIP 78541	HD 143488	7.28±0.05	Gaia2	-23.30±0.12	-20.58±0.07	Gaia2						UCL
98	HIP 80324	HD 147553	7.24±0.07	Gaia2	-15.04±0.14	-27.47±0.10	Gaia2	-2.1± 1.5	Gon06	-5.7	-19.0	-5.4	US
99	HIP 80591	HD 148055	6.82±0.05	Gaia2	-13.09±0.11	-28.65±0.10	Gaia2						UCL
100	HIP 81084	LP 745-70	32.17±0.04	Gaia2	-64.90±0.08	-177.87±0.03	Gaia2	-13.4± 0.3	Des20	-5.8	-27.7	-12.5	ABDO
101	TYC 7879 0980 1	HD 326277	10.45±0.05	Gaia2	-17.77±0.08	-45.63±0.07	Gaia2	-0.6± 1.0	SACY	-7.2	-19.8	-7.0	
102	HIP 82388	HD 151798	23.32±0.05	Gaia2	-72.86±0.09	-105.64±0.05	Gaia2	-16.5± 2.2	Whi07	-12.1	-27.8	-5.7	
103	HIP 82430	HD 151726	5.85±0.06	Gaia2	-12.03±0.11	-22.57±0.07	Gaia2						UCL
104	TYC 7362 0724 1	HD 156097	8.57±0.07	Gaia2	-4.99±0.10	-32.92±0.07	Gaia2	-3.1± 0.5	SACY	-4.0	-16.2	-8.4	
105	TYC 8728 2262 1	CD-54 7336	14.76±0.04	Gaia2	-5.41±0.07	-63.55±0.06	Gaia2	1.6± 0.7	SACY	-7.4	-16.8	-9.3	BPIC
106	BD-13 4687	HD 159911	30.10±0.05	Gaia2	-17.48±0.08	-126.07±0.07	Gaia2						ABDO
107	HIP 86305	HD 159492	24.19±0.16	Gaia2	-50.89±0.32	-149.19±0.38	Gaia2	-3.3± 3.1	Gon06	-15.8	-26.3	-5.1	
108	HIP 86598	HD 160305	15.21±0.05	Gaia2	-2.02±0.07	-65.86±0.06	Gaia2	2.4± 1.1	Kis11	-5.4	-17.3	-10.0	BPIC
109	HIP 88399	HD 164249A	20.16±0.05	Gaia2	2.34±0.07	-86.10±0.08	Gaia2	0.5± 0.5	SACY	-7.4	-16.5	-9.2	BPIC
110	HIP 89829	HD 168210	12.60±0.05	Gaia2	4.38±0.10	-46.20±0.08	Gaia2	-7.0± 2.0	SACY	-7.2	-15.2	-8.5	BPIC
111	HIP 92024	HD 172555	35.03±0.19	VL07	32.40±0.17	-149.48±0.17	VL07	2.0± 4.2	Gon06	-10.7	-15.4	-8.9	BPIC
112	TYC 9073 0762 1	AC 4357199	19.78±0.05	Gaia2	13.37±0.06	-80.14±0.06	Gaia2	2.4± 0.5	SACY	-8.8	-15.6	-8.1	BPIC
113	TYC 7408 0054 1	CD-31 16041	20.16±0.03	Gaia2	17.38±0.07	-72.28±0.06	Gaia2	-6.0± 0.5	SACY	-7.4	-14.5	-8.7	BPIC
114	HIP 92680	HD 174429	21.22±0.06	Gaia2	16.35±0.08	-85.25±0.08	Gaia2	-3.4± 1.0	SACY	-10.4	-15.0	-7.4	BPIC
115	HIP 92984	HD 175726	37.56±0.05	Gaia2	-2.24±0.09	-84.71±0.07	Gaia2	10.3±	Nid02	14.0	-1.3	-4.6	UMA?
116	HIP 93375	HD 176367	15.27±0.04	Gaia2	5.33±0.08	-95.09±0.08	Gaia2	-5.7± 0.5	SACY	-5.1	-27.5	-11.2	ABDO
117	HIP 93747	HD 177724	39.28±0.16	VL07	-7.25±0.15	-95.56±0.12	VL07	-25.0± 4.0	XHIP	-9.0	-25.4	-5.8	
118	TYC 8760 1468 1	CD-54 8168	19.06±0.04	Gaia2	-26.86±0.06	-95.35±0.05	Gaia2	4.8± 1.0	SACY	-2.6	-24.9	-1.0	
119	HIP 94114	HD 178253	26.02±0.25	VL07	84.87±0.39	-95.99±0.20	VL07	-18.4± 1.8	XHIP	-24.3	-11.2	-12.8	
120	HIP 95270	HD 181327	20.74±0.06	Gaia2	24.56±0.08	-81.91±0.05	Gaia2	-0.1± 0.2	Des20	-9.0	-15.5	-7.9	BPIC
121	HIP 95261	HD 181296	21.11±0.19	Gaia2	25.62±0.27	-82.54±0.23	Gaia2	13.0± 4.2	Gon06	2.2	-18.6	-13.9	BPIC
122	HIP 95347	HD 181869	17.94±0.22	VL07	30.49±0.35	-119.21±0.18	VL07	-0.7± 4.1	Zuk11	-8.3	-27.6	-15.0	ABDO
123	TYC 0486 4943 1		14.24±0.03	Gaia2	15.79±0.06	-65.51±0.04	Gaia2	-20.7± 0.9	Ell14	-5.9	-27.5	-12.0	ABDO
124	TYC 7443 1102 1		19.52±0.05	Gaia2	33.45±0.09	-68.39±0.05	Gaia2	-7.2± 0.4	Kis11	-9.9	-15.3	-7.8	BPIC
125	HD 189285	BD-04 4987	13.96±0.05	Gaia2	11.38±0.08	-54.15±0.04	Gaia2	-19.5± 0.5	Des15	-8.9	-25.0	-5.4	ABDO?
126	HIP 98470	HD 189245	45.39±0.09	Gaia2	129.02±0.15	-289.15±0.12	Gaia2	-10.4± 1.3	Des15	-15.7	-27.9	-13.4	
127	HIP 98495	HD 188228	31.04±0.17	VL07	81.78±0.11	-132.16±0.14	VL07	-6.7± 0.7	Zuk11	-21.8	-10.7	-4.5	ARG

Table 6. (continued)

#	Name	other-ID	π (mas)	ref ref	μ_α (mas/yr)	μ_δ (mas/yr)	ref ref	RV (km/s)	ref	U (km/s)	V (km/s)	W (km/s)	MG
128	2M J2001-3313		16.66±0.04	Gaia2	29.30±0.06	-61.24±0.04	Gaia2	-3.7± 0.2	Mal14	-7.2	-15.8	-9.3	BPIC?
129	TYC 8404 0354 1	CD-52 9381	29.36±0.03	Gaia2	88.24±0.05	-143.03±0.04	Gaia2	-13.3± 0.5	SACY	-24.1	-17.2	-5.8	ARG
130	HIP 99742	HD 192425	20.85±0.22	Gaia2	55.14±0.38	58.07±0.34	Gaia2	-23.0± 2.8		-27.7	-9.6	1.0	
131	HIP 102409	HD 197481	102.83±0.05	Gaia2	281.42±0.08	-359.89±0.05	Gaia2	-4.9± 0.2	Des20	-10.3	-16.2	-9.9	BPIC
132	HIP 102626	HD 197890	14.98±0.27	Gaia2	31.49±0.36	-78.56±0.29	Gaia2	-10.3± 0.5	SACY	-13.6	-25.0	-3.9	TUC?
133	TYC 1090 0543 1		13.36±0.05	Gaia2	33.33±0.07	-55.79±0.07	Gaia2	-19.5± 0.5	Des15	-6.2	-27.0	-11.9	ABDO
134	HIP 104365	HD 201184	16.63±0.16	Gaia2	19.33±0.25	-59.43±0.19	Gaia2	-12.0± 3.2		-7.7	-20.1	-0.5	
135	TYC 6351 0286 1	HD 201919	26.15±0.04	Gaia2	79.15±0.07	-146.05±0.05	Gaia2	-7.4± 0.5	SACY	-6.8	-27.3	-13.1	ABDO
136	HIP 105388	HD 202917	21.35±0.04	Gaia2	31.47±0.06	-95.45±0.06	Gaia2	-0.9± 0.5	SACY	-8.0	-20.8	-0.9	TUC
137	TYC 9482 121 1	CD-81 812	30.68±0.03	Gaia2	154.50±0.05	-104.12±0.05	Gaia2						
138	HIP 107345	GSC9116-1363	21.57±0.03	Gaia2	41.47±0.04	-93.52±0.04	Gaia2	2.3± 0.5	SACY	-8.4	-21.0	-1.0	TUC
139	HIP 107350	HD 206860	55.16±0.06	Gaia2	231.09±0.10	-113.13±0.10	Gaia2	-16.8± 0.2	Des20	-14.4	-21.2	-10.5	HELY?
140	HIP 107412	HD 206893	24.51±0.06	Gaia2	93.78±0.09	0.02±0.08	Gaia2	-12.2± 0.2	Des20	-20.2	-7.7	-3.0	
141	2MASS J2202-4210		22.55±0.05	Gaia2	53.17±0.06	-92.51±0.05	Gaia2	-2.8± 0.3	Kra14	-8.4	-20.9	-2.3	TUC
142	TYC 9340 0437 1	CP-72 2713	27.28±0.02	Gaia2	94.80±0.04	-52.46±0.05	Gaia2	8.6± 0.5	SACY	-9.9	-16.2	-8.2	BPIC
143	HIP 112312	GJ 871.1A	47.94±0.05	Gaia2	179.90±0.10	-123.10±0.10	Gaia2	2.2± 1.0	SACY	-10.6	-16.2	-9.7	BPIC
144	HIP 113283	HD 216803	131.44±0.09	Gaia2	329.58±0.12	-158.29±0.10	Gaia2	7.2± 0.2	Des20	-5.5	-8.1	-11.4	CAS?
145	HIP 113368	HD 216956	129.81±0.47	VL07	328.95±0.50	-164.67±0.35	VL07	6.5± 0.5	Mam13	-5.8	-8.3	-11.0	CAS?
146	HIP 114189	HD 218396	24.22±0.09	Gaia2	108.30±0.17	-49.48±0.15	Gaia2	-12.6± 1.4	Gon06	-12.9	-21.8	-7.7	COL
147	HIP 114530	HD 218860A	20.83±0.07	Gaia2	87.47±0.05	-93.50±0.09	Gaia2	9.8± 0.2	Des20	-7.6	-27.8	-10.8	ABDO
148	HIP 114948	HD 219482	48.88±0.06	Gaia2	176.53±0.11	-25.66±0.12	Gaia2	0.7± 0.2	Des20	-14.2	-8.4	-5.2	
149	HIP 115738	HD 220825	20.44±0.22	Gaia2	87.11±0.35	-95.72±0.28	Gaia2	-4.4± 0.6	Zuk11	-7.1	-26.3	-13.3	ABDO
150	HIP 118008	HD 224228	45.61±0.10	Gaia2	206.18±0.10	-185.80±0.13	Gaia2	13.2± 0.2	Des20	-7.3	-27.8	-13.5	ABDO

Parallax and proper motion references: Gaia2: Gaia DR2 Gaia Collaboration et al. (2018), VL07: van Leeuwen (2007). RV references: Des20: this paper; Car18: Carleo et al. (2018); Cha17: Chauvin et al. (2017a); Che18: Cheetham et al. (2018); Che11: Chen et al. (2011); Des15: Desidera et al. (2015); Duf95: Duflot et al. (1995); Ell14: Elliott et al. (2014); Eva67: Evans (1967); Fer08: Fernández et al. (2008); Gaia2: Gaia Collaboration et al. (2018); Gon06: Gontcharov (2006); Kis11: Kiss et al. (2011); Kra14: Kraus et al. (2014); Mal14: Malo et al. (2014); Mam13: Mamajek et al. (2013); Mon01: Montes et al. (2001); Nid02: Nidever et al. (2002); Nor04: Nordström et al. (2004); SACY: Torres et al. (2006); XHIP: Anderson & Francis (2012); Whi07: White et al. (2007); Zuk01: Zuckerman et al. (2001); Zuk11: Zuckerman et al. (2011)

Source of data for previously unpublished RV determinations. ESO Program ID is provided for HARPS spectra: HIP 490: 074.C-0037, 075.C-0202, 076.C-0010, 192.C-0224, 099.C-0205; HIP 1113: 084.C-1039, 192.C-0224; HIP 1481: 074.C-0037, 192.C-0224; HIP 1993: 074.C-0037, 075.C-0202, 077.C-0012; HIP 6276: 192.C-0224, 098.C-0739; HIP 6856: 078.D-0245; HIP 13402: 192.C-0224, 098.C-0739; TYC 5882-1169-1: 074.C-0037, 076.C-0010; TYC 5899-0026-1: 097.C-0864; HIP 23200: 192.C-0224, 097.C-0864, 098.C-0739; HIP 23309: 074.C-0037, 076.C-0010, 192.C-0224; HIP 25283: 072.C-0488, 192.C-0224, 098.C-0739; HIP 30034: 074.C-0037, 076.C-0010, 078.D-0245, 192.C-0224, 098.C-0739; HIP 30314: 083.C-0794, 084.C-1039, 192.C-0224, 098.C-0739; GSC 8894-0426: 097.C-0864; HIP 31878: 192.C-0224, 098.C-0739; HIP 32235: 074.C-0037, 076.C-0010; HIP 36948: 184.C-0815, 192.C-0224, 0102.C-0584; HIP 44526: 192.C-0224; HIP 47135: 074.C-0037, 076.C-0010; HIP 51228: 074.C-0364; HIP 51317: 072.C-0488, 082.C-0718, 183.C-0437, 191.C-0873, 192.C-0224, 099.C-0205; TWA 7: 074.C-0037, 075.C-0202, 076.C-0010, 077.C-0012, 079.C-0046; HIP 54155: 074.C-0037, 075.C-0202, 082.C-0427, 082.C-0390; HIP 66252: 075.C-0202, 192.C-0224; HIP 69989: Borgniet et al. (2019), reduced spectra available on OHP archive; HIP 81084: 097.C-0864; HIP 95270: 083.C-0794, 084.C-1039, 192.C-0224; HIP 102409: 075.C-0202, 192.C-0224, 098.C-0739, 099.C-0205; HIP 107350: 192.C-0224, 099.C-0205; HIP 107412: 098.C-0739, 192.C-0224, 099.C-0205, 1101.C-0557; HIP 113283: 60.A-9036; HIP 114530: 192.C-0224; HIP 114948: 075.C-0689, 077.C-0295, 080.C-0712, 184.C-0815; HIP 118008: 084.C-1039, 192.C-0224, 099.C-0205

Table 7. Summary of target parameters: name, X-ray luminosity, $R_X = \log L_X/L_{bol}$, $\log R_{HK}$, rotation period, $v \sin i$, Lithium 6708 EW, effective temperature, and stellar mass.

#	Name	other-ID	Log LX	R_X	S	$\log R_{HK}$	Ref	P_{rot} (d)	Ampl. mag	Ref	$v\ sini$ (km/s)	Ref	EW Li (mÅ)	R
1	HIP 490	HD 105	29.33	-4.34	0.34	-4.41	Wri04	2.982±0.006	0.018	1a	15.0	SACY	153.0	SAC
2	HIP 682	HD 377	29.50	-4.14	0.38	-4.36	Wri04	3.58±0.05	0.02	1b	13.0	SACY	151.0	SAC
3	HIP 1113	HD 987	30.02	-3.32		-4.21	SPH-C	3.72±0.01	0.10	2,1a	7.3	SACY	202.0	SAC
4	2MASS J00172353-6645124	SCR 0017-6645						6.644±0.027	0.10	3,1a				
5	HIP 1481	HD 1466	29.65	-4.12	0.35	-4.36	Hen96	2.306±0.095	0.01	1a	21.0	SACY	130.0	SAC
6	HIP 1993	GSC8841-1145						4.35±0.34	0.15	2,1a	7.3	SACY	40.0	SAC
7	HIP 2578	HD 3003									115.0	Lag09		
8	HIP 6276	BD-12 243	28.98	-4.30	0.53	-4.32	Wri04	5.88±0.85	0.03	1a	3.0	DaS09	160.0	SAC
9	HIP 6485	HD 8558	30.05	-3.38	0.58	-4.17	SPH-H	3.59±0.01	0.08	2,22,1a	13.8	SACY	196.0	SAC
10	HIP 6856	HD 9054	29.87	-3.30	0.91	-4.26	Gra06	6.25±0.71	0.01	1a	2.7	SACY	168.0	SAC
11	TYC 8047 0232 1	CD-52 381	30.09	-3.04				2.40±0.01	0.11	2,1a	19.8	SACY	339.0	SAC
12	HIP 10602	HD 14228									240.0	DaS09		
13	HIP 11360	HD 15115	29.28	-4.85	0.20	-4.76	Des15	0.865±0.014	0.0004	1a	89.8	Pri14	95.0	Des
14	HIP 12394	HD 16978									96.0	Roy02		
15	HIP 13402	HD 17925	29.08	-4.11		-4.37	Hoj19	6.57±0.05	0.04	4,1a	4.7	Hoj19	194.0	Wic
16	HIP 14551	HD 19545	29.09	-5.37										
17	TYC 7026 0325 1	CD-35 1167	29.27	-3.30				8.48±0.10	0.15	2,1a	6.1	SACY	65.0	SAC
18	HIP 15457	HD 20630	28.89	-4.62		-4.42	Bal95	9.0±0.1	0.03	4,1a	5.2	Mar14	37.7	Tak
19	TYC 8060 1673 1	CD-46 1064	29.60	-3.55	1.80	-4.21	Des15	3.74±0.04	0.09	2,1a	9.7	Des15	227.0	Des
20	HIP 17764	HD 24636	28.79	-5.34				0.839±0.015	0.0003	1a				
21	HD 25284B	TYC 6461 1120 2	30.06	-2.84				4.54±0.39	0.04	1a	6.9	Kra14	207	Kra
22	TYC 5882 1169 1	BD-15 705	29.74	-3.31				3.78±0.04	0.07	2,1a	7.0	Kra14	222.4	SPH
23	HIP 21547	HD 29391						0.651	0.004	5,1a	71.8	Rei03		
24	HIP 22226	HD 30447						0.885±0.015	0.0004	1a	70.0	DaS09		
25	HIP 22295	HD 32195	29.97	-3.86				1.238±0.027	0.03	1a,6	41.0	DaS09		
26	TYC 5899 0026 1	NLTT 14116						1.369±0.035	0.007	1a	5.3	Jef18		
27	HIP 23200	V1005 Ori	29.53	-3.06				4.37±0.03	0.04	2,1a	14.0	SACY	270.0	SAC
28	HIP 23309	CD-57 1054	29.41	-3.30	7.64	-3.89	Gra06	8.60±0.07	0.12	2,1a	5.8	SACY	360.0	SAC
29	HIP 24947	HD 35114	30.09	-3.81				0.768±0.011	0.035	1a	72.0	SACY	140.0	SAC
30	HIP 25283	HD 35650	29.00	-3.60	2.70	-4.26	SPH-F	9.34±0.08	0.07	2,1a	4.0	SACY	12.0	SAC
31	HIP 25544	HD 36435	28.55	-4.78		-4.44	Hen96	7.4±1.0	0.01	1a,5	5.0	SACY	23.0	SAC
32	HIP 27288	HD 38678									229.0	Zor12		
33	HIP 27321	HD 39060									139.0	Zuk01		
34	TYC 7084 0794 1	CD-35 2722	29.22	-3.49				1.717±0.004	0.07	2,1a	13.0	SACY	11.0	SAC
35	HIP 30030	HD 43989	30.13	-3.62	0.45	-4.25	SPH-H	1.361±0.042	0.031	1a,7	40.4	Sch07	214.0	Wic
36	HIP 30034	HD 44627	30.08	-3.25		-4.10	SPH-C	3.85±0.01	0.10	2,1a	11.5	SACY	320.0	SAC
37	HIP 30314	HD 45270	29.51	-4.14	0.40	-4.32	Hen96	3.10±0.23	0.03	1a	17.6	SACY	150.0	SAC
38	GSC 8894-0426	2RE J0625-600						1.033±0.019	0.05	1a,6			0.0	DaS
39	TYC 7617 0549 1	CD-40 2458	29.99	-3.56				4.13±0.02	0.12	2,1a	11.6	SACY	310.0	SAC
40	HIP 31878	CD-61 1439	28.84	-3.73	2.93	-4.24	SPH-F	9.06±0.08	0.07	2,1a	12.0	DaS09	0.0	SAC
41	HIP 32235	HD 49855	29.63	-3.82	0.60	-4.17	SPH-H	3.83±0.01	0.11	2,1a	12.4	SACY	238.0	Des

Table 7. (continued)

#	Name	other-ID	Log LX	R_X	S	$\log R_{HK}$	Ref	P_{rot} (d)	Ampl. mag	Ref	$v\ sini$ (km/s)	Ref	EW Li (mÅ)	R
42	TYC 8118 0871 1	HD 51797	30.39	-3.18				4.38±0.05	0.14	2,1a	15.6	SACY	335.0	SAC
43	HIP 33737	HD 55279	29.88	-3.28				5.10±0.03	0.14	2,1a	9.3	SACY	278.0	SAC
44	2MASS J07065772-5353463							2.85±0.17	0.12	1a	17.1	Mal14		
45	HIP 34899	HD 56022									46.0	Ues70		
46	TYC 1355 214 1	BD+20 1790	29.30	-3.32	4.19	-3.91	SPH-F	2.76±0.04	—	8	13.0	DaS09	102.0	SPH
47	TYC 8128 1946 1	CD-48 2972	30.34	-3.16				1.038±0.004	0.11	9	52.0	SACY	250.0	SAC
48	HIP 36948	HD 61005			0.50	-4.31	Des11	5.04±0.04	0.05	10,1a	8.2	Des11	171.0	Des
49	HIP 37766	YZ CMi	28.66	-2.51				2.77±0.15	0.05	23,1a	4.0	Jef18		
50	HIP 41307	HD 71155									115.0	Lag09		
51	HIP 42637	RECX2												
52	HD 75505	RECX13												
53	HIP 42808	HD 74576	28.67	-4.40		-4.48	MA10	7.8±1.2	0.03	1a	3.9	SACY	70.0	SAC
54	HIP 44526	HD 77825	28.92	-4.06	0.68	-4.41	Gra06	8.65±0.05	0.05	6,1a	4.2	SPH-C	55.0	Zuk
55	HIP 47135	HD 84075	29.37	-4.31	0.38	-4.34	Jen11	2.50±0.05	0.03	1c,1a	20.0	DaS09	170.0	Gue
56	HIP 50191	HD 88955									103.0	Ers03		
57	TWA 6	GSC7183-1477	30.01	-2.76				0.541±0.006	0.09	1a,11	72.0	Ske08	510.0	SAC
58	HIP 51228	HD 90712	29.46	-4.19	0.39	-4.32	Jen06	5.4±0.6	0.008	1a	10.0	Wic03	115.0	Wic
59	HIP 51317	GJ 393	26.83	-4.95				33±6	0.005	1d	1.5	Rei12		
60	TWA 7	GSC7190-2111	29.55	-2.75				5.050	0.11	11,2	4.4	SACY	530.0	SAC
61	HIP 53524	HD 95086												
62	HIP 54155	HD 96064	29.71	-3.62	0.46	-4.37	Gra03	6.9±0.3	0.03	12,1a	5.6	Sch09	130.0	Zik
63	HIP 54231	HD 96338												
64	HIP 57632	HD 102647									128.0	Roy02		
65	HIP 58167	HD 103599				-4.45	Che11	0.4466±0.0033	0.001	1a	180.0	Che11		
66	HIP 58465	HD 104125												
67	HIP 59505	HD 106048												
68	HIP 60183	HD 107301									209.0	Zor12		
69	HIP 60459	HD 107821						0.1168±0.0003	0.0004	1a				
70	HD 108767B		28.53	-4.53				2.49±0.12	0.0001	1a	5.7	Mor01	175.0	Pal
71	HIP 61468	HD 109536									81.0	Ues70		
72	TWA 11	HIP 61498	29.70	-5.24							152.0	Roy02		
73	HIP 61960	HD 110411									154.0	Zor12		
74	HIP 63839	HD 113457									149.0	Dav15		
75	HIP 64892	HD 115470									178.0	Che18		
76	HIP 64995	HD 115600									61.0	Che11	38.0	Che
77	HIP 65426	HD 116434									299.0	Cha17		
78	HIP 66252	HD 118100	29.59	-3.07	3.46	-4.09	Gra03	3.912	0.06	1d	13.6	SPH-F	25.0	Fav
79	HIP 66566	HD 118588												
80	HIP 66651	HD 118697												
81	HIP 68781	HD 122705												
82	TYC 7286 0248 1	CD-31 11053	30.28	-3.05				1.049	0.16	6			470.0	SAC
83	HIP 69989	HD 125451	29.11	-5.03		-4.37	Kin05				40.0	Rei03	0.0	Boe
84	HIP 71724	HD 128819												

Table 7. (continued)

#	Name	other-ID	Log LX	R_X	S	$\log R_{HK}$	Ref	P_{rot} (d)	Ampl. mag	Ref	*v sini* (km/s)	Ref	EW Li (mÅ)	R
85	HIP 71743	HD 128987	28.54	-4.84	0.37	-4.44	Gra06	9.35±0.04		13	3.0	Nor04	26.0	Ga
86	HIP 73145	HD 131835												
87	HIP 73990	HD 133803												
88	HIP 74824	HD 135379												
89	HIP 76063	HD 138204												
90	HIP 77317	HD 140840												
91	HIP 77457	HD 141190												
92	HIP 77464	HD 141378									107.0	Roy07		
93	TYC 7846 1538 1	HD 141943	30.54	-3.37	0.94	-3.95	Isa10	2.26±0.06	0.10	1a,14	40.0	SACY	230.0	SAC
94	HIP 78099	HD 142705												
95	HIP 78196	HD 142851												
96	HIP 78530	HD 143567												
97	HIP 78541	HD 143488												
98	HIP 80324	HD 147553												
99	HIP 80591	HD 148055												
100	HIP 81084	LP 745-70	29.00	-3.34	5.98	-4.21	Gra06	7.04±0.73	0.03	1e	7.0	DaS09	0.0	DaS
101	TYC 7879 0980 1	HD 326277	29.99	-3.48				1.885	0.03	6	31.4	SACY	290.0	SAC
102	HIP 82388	HD 151798	29.31	-4.28		-4.31	Sch09	3.23±0.06	0.05	1g	10.4	Sch09	120.0	Whi
103	HIP 82430	HD 151726												
104	TYC 7362 0724 1	HD 156097	30.76	-3.10				2.02±0.04	0.076	1e,1a	36.7	SACY	270.0	SAC
105	TYC 8728 2262 1	CD-54 7336	30.28	-3.13	1.23	-3.99	Des15	1.775±0.005	0.15	3,1a	35.3	SACY	330.0	SAC
106	BD-13 4687	HD 159911	30.32	-2.35				0.447±0.002	0.19	2	140.0	DaS09	250.0	DaS
107	HIP 86305	HD 159492												
108	HIP 86598	HD 160305	30.21	-3.59				1.341±0.008	0.06	3,1a			130.0	Kis
109	HIP 88399	HD 164249A	29.60	-4.46				1.518±0.044	0.00002	1a	20.0	SACY	107.0	SAC
110	HIP 89829	HD 168210	30.61	-3.15				0.570±0.003	0.19	2	114.7	SACY	290.0	SAC
111	HIP 92024	HD 172555	28.83	-5.63							116.0	DaS09		
112	TYC 9073 0762 1	AC 4357199	29.48	-2.99				5.37±0.04	0.33	2,1a	9.9	SACY	332.0	SAC
113	TYC 7408 0054 1	CD-31 16041	29.83	-2.90				1.089±0.002	0.19	2	49.7	SACY	492.0	SAC
114	HIP 92680	HD 174429	30.35	-3.22	1.72	-3.78	Hen96	0.940±0.002	0.03	15,1a	69.0	SACY	287.0	SAC
115	HIP 92984	HD 175726	29.04	-4.62	0.33	-4.41	Wri04	3.95±0.01		16	12.0	Nor04	100.0	Cut
116	HIP 93375	HD 176367	29.66	-4.08				2.61±0.06	0.02	1c	17.0	SACY	140.0	SAC
117	HIP 93747	HD 177724	28.93	-6.21							317.0	Roy02		
118	TYC 8760 1468 1	CD-54 8168	29.81	-3.17				0.526±0.004	0.09	1a,6	80.0	SACY	270.0	SAC
119	HIP 94114	HD 178253									195.0	Roy07		
120	HIP 95270	HD 181327				-4.55	SPH-H	1.54±0.04	0.001	1a	16.0	SACY	120.0	SAC
121	HIP 95261	HD 181296									330.0	DaS09		
122	HIP 95347	HD 181869	29.52	-6.12										
123	TYC 0486 4943 1		29.73	-3.09				3.75±0.30		17	11.0	DaS09	180.0	DaS
124	TYC 7443 1102 1							11.3±0.2	0.09	3	6.0	Mes17	110.0	Mal
125	HD 189285	BD-04 4987	29.61	-3.85	0.45	-4.33	Des15	2.43±0.06	0.02	1c	8.3	Des15	139.0	Des
126	HIP 98470	HD 189245	29.95	-3.95	0.32	-4.37	Des15	0.8662±0.0003	0.015	1f	100.0	Lag09	90.0	Des
127	HIP 98495	HD 188228									85.0	Zor12		

Table 7. (continued)

#	Name	other-ID	Log LX	R_X	S	$\log R_{HK}$	Ref	P_{rot} (d)	Ampl. mag	Ref	$v\ sini$ (km/s)	Ref	EW Li (mÅ)	R
128	2MASS J20013718-3313139		29.41					12.770	0.13	6	2.6			
129	TYC 8404 0354 1	CD-52 9381	29.75	-2.82				0.830±0.001	0.12	9,1a	42.0	SACY	6[illegible].0	SAC
130	HIP 99742	HD 192425									180.0	Roy07		
131	HIP 102409	HD 197481	29.73	-2.68				4.85±0.02	0.10	2,1a	9.3	SACY	8[illegible].0	SAC
132	HIP 102626	HD 197890	31.43	-2.05				0.380±0.002	0.035	1a,6	132.0	Bar05	50[illegible].0	SAC
133	TYC 1090 0543 1		29.59	-3.12	2.65	-3.97	Des15	2.280±0.007	0.14	2	17.7	Des15	11[illegible].0	Des
134	HIP 104365	HD 201184									212.0	Roy07		
135	TYC 6351 0286 1	HD 201919	29.18	-3.46				4.92±0.07	0.12	2	7.9	SACY	2[illegible].0	SAC
136	HIP 105388	HD 202917	30.10	-3.30	0.54	-4.22	Wri04	3.36±0.01	0.10	2,1a	15.4	SACY	22[illegible].0	SAC
137	TYC 9482 121 1	CD-81 812	28.83	-3.88				8.5±1.3	0.001	1a				
138	HIP 107345	GSC9116-1363	29.42	-3.12				4.50±0.02	0.10	2,1a	8.2	SACY	5[illegible].0	SAC
139	HIP 107350	HD 206860	29.24	-4.39		-4.41	Bal95	4.70		18	10.6	Mar14	12[illegible].8	Eis
140	HIP 107412	HD 206893	29.22	-4.80	0.27	-4.77	Del17	0.996±0.003	0.005	19	32.0	Del17	2[illegible].5	Del
141	2MASS J22021626-4210329							4.514	0.15	6,1a				
142	TYC 9340 0437 1	CP-72 2713	29.93	-2.77				4.48±0.03	0.16	2,1a	7.5	SACY	44[illegible].0	SAC
143	HIP 112312	GJ 871.1A	29.59	-2.13				2.346±0.005	0.09	3	12.1	SACY	[illegible].0	SAC
144	HIP 113283	HD 216803	28.33	-4.51	0.91	-4.47	Wri04	10.2±1.9	0.015	1a,20	1.5	SACY	2[illegible].0	SAC
145	HIP 113368	HD 216956												
146	HIP 114189	HD 218396	28.20	-6.11							49.0	Roy07		
147	HIP 114530	HD 218860A	29.78	-3.62				5.17±0.02	0.07	2,1a	6.6	SACY	22[illegible].0	SAC
148	HIP 114948	HD 219482	29.43	-4.43	0.30	-4.43	SPH-H	2.175±0.085	0.002	1a	7.5	Rei03	6[illegible].0	SPH
149	HIP 115738	HD 220825												
150	HIP 118008	HD 224228	28.66	-4.35	0.62	-4.47	Gra06	7.8±1.1	0.01	1a	2.6	SACY	7[illegible].0	SAC

References for rotation period: 1a: this study (TESS data); 1b: this study (ASAS data); 1c: this study (ROAD data); 1d: this study (K2 data); 1e: this study (PEST data); 1f: this study (Hipparcos data); 1g: this study (YCO data); 2: Messina et al. (2010); 3: Messina et al. (2017); 4: Messina et al. (2001); 5: Koen & Eyer (2002); 6: Kiraga (2012a); 7: Cutispoto et al. (2003); 8: Carleo et al. (2018); 9: Messina et al. (2011); 10: Desidera et al. (2011); 11: Lawson & Crause (2005); 12: Cutispoto et al. (1999); 13: Gaidos et al. (2000); 14: Marsden et al. (2011); 15: Maire et al. (2016); 16: Mosser et al. (2009); 17: Folsom et al. (2016); 18: Noyes et al. (1984); 19: Delorme et al. (2017); 20: Busko & Torres (1978); 21: Donahue et al. (1996); 22: Oelkers et al. (2018) 23: Chugainov (1974)

References for $v \sin i$, EW Li and $\log R_{HK}$ Bal95: Baliunas et al. (1995); Bar05: Barnes (2005); Boe88: Boesgaard et al. (1988); Cha17: Chauvin et al. (2017b); Che18: Cheetham et al. (2018); Che11: Chen et al. (2011); Cut02: Cutispoto et al. (2003); DaS09: da Silva et al. (2009); Dav15: David & Hillenbrand (2015); Del17: Delorme et al. (2017); Des11: Desidera et al. (2011); Des15: Desidera et al. (2015); Eis13: Eisenbeiss et al. (2013); Ers03: Erspamer & North (2003); Fav97: Favata et al. (1997) Gai00: Gaidos et al. (2000); Gra03: Gray et al. (2003); Gra06: Gray et al. (2006); Gue07: Guenther et al. (2007); Hen96: Henry et al. (1996); Hoj19: Hojjatpanah et al. (2019); Jef18: Jeffers et al. (2018); Jen06: Jenkins et al. (2006); Jen11: Jenkins et al. (2011); Kin05: King & Schuler (2005); Kis11: Kiss et al. (2011); Kra14: Kraus et al. (2014); Isa10: Isaacson & Fischer (2010); MA10: Martínez-Arnáiz et al. (2010); Mal13: Malo et al. (2013); Mal14: Malo et al. (2014); Mar14: Marsden et al. (2014); Mes17: Messina et al. (2017); Mor01: Mora et al. (2001); Nor04: Nordström et al. (2004); Pal92: Pallavicini et al. (1992); Pri14: Pribulla et al. (2014); Rei03: Reiners & Schmitt (2003); Rei12: Reiners et al. (2012); Roy02: Royer et al. (2002); Roy07: Royer et al. (2007); SACY: Torres et al. (2006); Sch07: Scholz et al. (2007); Sch09: Schröder et al. (2009); Ske08 Skelly et al. (2008); Tak05: Takeda & Kawanomoto (2005); Ues70: Uesugi & Fukuda (1970); Whi07: White et al. (2007); Wic03: Wichmann et al. (2003) Wri04: Wright et al. (2004); Zik05: Zickgraf et al. (2005); Zor12: Zorec & Royer (2012); Zuk01: Zuckerman et al. (2001); SPH-C: this paper (CORALIE spectra); SPH-F: this paper (FEROS spectra); SPH-H: this paper (HARPS spectra)

Source of data for previously unpublished determinations (ESO Program ID for HARPS and FEROS): HIP 1113: CORALIE RV survey (Udry et al. 2000); HIP 6485: 074.C-0037, 075.C-0202, 076.C-0010, 0103.C-0759 (HARPS); TYC 5882-1169-1: 074.C-0037, 076.C-0010 (HARPS); HIP 25283: 074.D-0016 (FEROS);

HIP 30030: 60.A-9036, 192.C-0224 (HARPS); HIP 30034: CORALIE RV survey (Udry et al. 2000); HIP 31878: 074.D-0016, 083.A-9003 (FEROS); HIP 32235: 074.C-0037, 076.C-0010 (HARPS); TYC 1355-214-1: 083.A-9003 (FEROS); HIP 44526: CORALIE RV survey (Udry et al. 2000); HIP 66252: 074.D-0016 (FEROS) HIP 95270: 083.C-0794, 084.C-1039, 192.C-0224 (HARPS) HIP 114948: 075.C-0689, 077.C-0295, 080.C-0712, 184.C-0815 (HARPS)

Table 8. Summary of target parameters: name, spectral type, effective temperature, stellar mass, and flag on the presence of disks.

#	Name	other-ID	ST	$T_{\rm eff}$ (K)	Mstar $M_\odot$	Disk flag
1	HIP 490	HD 105	G0V	5966± 41	1.13±0.01	RES
2	HIP 682	HD 377	G2V	5851± 39	1.11±0.01	RES
3	HIP 1113	HD 987	G8V	5416± 36	0.93±0.02	IREX
4	2MASS J00172353-6645124	SCR 0017-6645	M2.5Ve	3380± 50	0.56±0.03	NO
5	HIP 1481	HD 1466	F8V	6125± 41	1.19±0.02	IREX2B
6	HIP 1993	GSC8841-1145	M0Ve	3900± 50	0.69±0.03	NO
7	HIP 2578		A0V	9300± 200	2.02±0.02	IREX2B
8	HIP 6276	BD-12 243	G9V	5342± 34	0.92±0.02	IREX2B
9	HIP 6485	HD 8558	G7V	5597± 40	0.98±0.02	IREX
10	HIP 6856	HD 9054	K1V	4965± 31	0.90±0.02	NO
11	TYC 8047 0232 1	CD-52 381	K2V(e)	4777± 30	0.85±0.02	NO
12	HIP 10602	HD 14228	B8IV-V	13200± 500	3.48±0.04	IREX?
13	HIP 11360	HD 15115	F2	6762± 52	1.41±0.01	RES
14	HIP 12394	HD 16978	B9III	10500± 200	2.75±0.01	NO
15	HIP 13402	HD 17925	K1V	5159± 56	0.88±0.01	IREX
16	HIP 14551	HD 19545	A3V	8040± 100	1.66±0.02	NO
17	TYC 7026 0325 1	CD-35 1167	K7Ve	4515± 82	0.65±0.02	NO
18	HIP 15457	HD 20630	G5Vvar	5626± 62	1.02±0.01	NO
19	TYC 8060 1673 1	CD-46 1064	K3V 30	4749± 33	0.83±0.02	IREX?
20	HIP 17764	HD 24636	F3IV/V	6727± 49	1.41±0.01	IREX2B
21	HD 25284B	TYC 6461 1120 2	K5V	4467± 31	0.77±0.02	NO
22	TYC 5882 1169 1	BD-15 705	K3/4	4675± 31	0.82±0.02	NO
23	HIP 21547	HD 29391	F0V	7220± 150	1.55±0.02	IREX
24	HIP 22226	HD 30447	F3V	6783± 52	1.41±0.01	RES
25	HIP 22295	HD 32195	F7V	6156± 48	1.23±0.02	IREX2B
26	TYC 5899 0026 1	NLTT 14116	M3	3390± 50	0.47±0.03	NO
27	HIP 23200	V1005 Ori	M0.5Ve	3860± 50	0.73±0.03	IREX
28	HIP 23309	CD-57 1054	M0Ve	3880± 50	0.79±0.03	NO
29	HIP 24947	HD 35114	F6V	6322± 47	1.26±0.02	IREX2B
30	HIP 25283	HD 35650	K6V	4322± 25	0.65±0.01	RES
31	HIP 25544	HD 36435	G5V	5450± 34	0.94±0.01	NO
32	HIP 27288	HD 38678	A2Vann	8490± 150	1.87±0.04	RES
33	HIP 27321	HD 39060	A3V	8000± 100	1.70±0.04	RES
34	TYC 7084 0794 1	CD-35 2722	M1Ve	3780± 50	0.57±0.03	NO
35	HIP 30030	HD 43989	G0	5967± 41	1.18±0.02	IREX2B
36	HIP 30034	HD 44627	K1V(e)	5085± 32	0.91±0.02	IREX
37	HIP 30314	HD 45270	G1V	5867± 38	1.10±0.01	NO
38	GSC 8894-0426	2RE J0625-600	M2	3230± 50	0.35±0.03	NO
39	TYC 7617 0549 1	CD-40 2458	K0V	5245± 37	1.10±0.05	NO
40	HIP 31878	CD-61 1439	K7V(e)	4246± 25	0.64±0.01	NO
41	HIP 32235	HD 49855	G6V	5587± 46	0.99±0.03	IREX
42	TYC 8118 0871 1	HD 51797	K0V(e)	5208± 40	1.15±0.05	IREX

Table 8. (continued)

#	Name	other-ID	ST	$T_{\rm eff}$ (K)	Mstar $M_{\odot}$	Disk flag
43	HIP 33737	HD 55279	K2V	4850± 31	0.86±0.02	NO
44	2MASS J07065772-5353463		M0	3890± 50	0.71±0.03	NO
45	HIP 34899	HD 56022	Ap	9700± 200	2.30±0.05	NO
46	TYC 1355 214 1	BD+20 1790	K3	4356± 28	0.67±0.01	NO
47	TYC 8128 1946 1	CD-48 2972	G8V	5429± 42	0.97±0.02	NO
48	HIP 36948	HD 61005	G3/G5V	5460± 36	0.96±0.02	RES
49	HIP 37766	YZ CMi	M4.5Ve	3150± 50	0.14±0.03	IREX
50	HIP 41307	HD 71155	A0V	9900± 200	2.35±0.05	RES
51	HIP 42637	RECX2	B9IV	12000± 500	3.24±0.03	IREX2B
52	HD 75505	RECX13	A1V	8000± 150	1.68±0.02	IREX
53	HIP 42808	HD 74576	K3V	4990± 30	0.83±0.01	NO
54	HIP 44526	HD 77825	K2V	4861± 30	0.80±0.02	NO
55	HIP 47135	HD 84075	G2V	5937± 38	1.14±0.02	IREX2B
56	HIP 50191	HD 88955	A2V	8840± 200	2.06±0.04	IREX
57	TWA 6	GSC7183-1477	M0Ve	3980± 50	0.69±0.03	IREX?
58	HIP 51228	HD 90712	G2/G3V	5889± 39	1.11±0.01	NO
59	HIP 51317	GJ 393	M2	3530± 50	0.44±0.03	IREX
60	TWA 7	GSC7190-2111	M2Ve	3380± 50	0.55±0.03	RES
61	HIP 53524	HD 95086	A8III	7650± 150	1.60±0.02	RES
62	HIP 54155	HD 96064	G5	5393± 34	0.94±0.01	NO
63	HIP 54231	HD 96338	A0V	9200± 200	2.08±0.05	NO
64	HIP 57632	HD 102647	A3Vvar	8550± 150	1.92±0.02	RES
65	HIP 58167	HD 103599	F3IV	6859± 53	1.52±0.04	NO
66	HIP 58465	HD 104125	A2V	8000± 200	1.94±0.02	NO
67	HIP 59505	HD 106048	A9V	7000± 200	1.45±0.04	IREX?
68	HIP 60183	HD 107301	B9V	10500± 200	2.37±0.04	IREX2B
69	HIP 60459	HD 107821	G6IV	8200± 200	1.76±0.02	NO
70	HD 108767B		K0V	4935± 32	0.83±0.01	IREX
71	HIP 61468	HD 109536	A7III	7700± 200	1.65±0.03	NO
72	TWA 11	HIP 61498	A0V	9700± 200	2.19±0.05	RES
73	HIP 61960	HD 110411	A0V	8840± 150	1.88±0.03	RES
74	HIP 63839	HD 113457	A0V	9700± 200	2.19±0.01	IREX2B
75	HIP 64892	HD 115470	B9V	10400± 300	2.35±0.09	NO
76	HIP 64995	HD 115600	F2IV/V	6855± 55	1.53±0.04	RES
77	HIP 65426	HD 116434	A2V	8877± 87	1.96±0.04	NO
78	HIP 66252	HD 118100	K7V	4299± 27	0.67±0.01	NO
79	HIP 66566	HD 118588	A1V	8550± 300	1.96±0.03	IREX2B
80	HIP 66651	HD 118697	B9.5V	9800± 300	2.09±0.01	NO
81	HIP 68781	HD 122705	A2V	8400± 300	1.78±0.02	IREX2B
82	TYC 7286 0248 1	CD-31 11053	K3Ve	4465± 27	1.02±0.05	NO
83	HIP 69989	HD 125451	F5IV	6640± 100	1.35±0.03	IREX
84	HIP 71724	HD 128819	B8/B9V	10700± 300	2.86±0.03	NO
85	HIP 71743	HD 128987	G6V	5554± 35	0.97±0.01	IREX?

Table 8. (continued)

#	Name	other-ID	ST	$T_{\rm eff}$ (K)	Mstar $M_\odot$	Disk flag
86	HIP 73145	HD 131835	A2IV	8400± 300	1.94±0.04	RES
87	HIP 73990	HD 133803	A9V	6920± 150	1.56±0.03	IREX2B
88	HIP 74824	HD 135379	A3V	8600± 150	1.95±0.04	IREX2B
89	HIP 76063	HD 138204	A3III	7800± 150	1.63±0.03	IREX?
90	HIP 77317	HD 140840	B9.5V	9800± 300	2.22±0.02	IREX2B
91	HIP 77457	HD 141190	A7IV	7400± 200	1.61±0.04	NO
92	HIP 77464	HD 141378	A5IV	8410± 200	1.86±0.04	RES
93	TYC 7846 1538 1	HD 141943	G2	5728± 40	1.24±0.03	RES
94	HIP 78099	HD 142705	A0V	9700± 400	2.30±0.07	NO
95	HIP 78196	HD 142851	A0V	9800± 300	2.35±0.07	NO
96	HIP 78530	HD 143567	B9V	10700± 300	2.59±0.09	NO
97	HIP 78541	HD 143488	A0V	9700± 300	2.23±0.05	NO
98	HIP 80324	HD 147553	A0V+...	10111± 138	2.62±0.05	NO
99	HIP 80591	HD 148055	A5V	7900± 200	1.65±0.02	IREX
100	HIP 81084	LP 745-70	M0.5	3900± 50	0.61±0.03	NO
101	TYC 7879 0980 1	HD 326277	K0IV	5354± 39	1.05±0.02	NO
102	HIP 82388	HD 151798	G3V	5856± 38	1.07±0.01	NO
103	HIP 82430	HD 151726	B9V	10100± 300	2.56±0.02	NO
104	TYC 7362 0724 1	HD 156097	G5V	5562± 38	1.31±0.05	NO
105	TYC 8728 2262 1	CD-54 7336	K1V	5040± 33	1.02±0.02	IREX
106	BD-13 4687	HD 159911	K3/K4III	4270± 25	0.70±0.01	NO
107	HIP 86305	HD 159492	A7V	7900± 100	1.72±0.03	RES
108	HIP 86598	HD 160305	F8/G0V	6045± 42	1.17±0.04	RES
109	HIP 88399	HD 164249A	F6V	6490± 48	1.39±0.02	IREX2B
110	HIP 89829	HD 168210	G5V	5453± 40	1.18±0.01	IREX?
111	HIP 92024	HD 172555	A7V	7950± 150	1.66±0.01	RES
112	TYC 9073 0762 1	AC 4357199	M1Ve	3640± 50	0.73±0.03	NO
113	TYC 7408 0054 1	CD-31 16041	K8Ve	3910± 50	0.81±0.03	IREX?
114	HIP 92680	HD 174429	G9IV	5303± 35	1.08±0.02	BKG
115	HIP 92984	HD 175726	G5	6012± 41	1.11±0.01	IREX
116	HIP 93375	HD 176367	G1V	6082± 44	1.15±0.01	NO
117	HIP 93747	HD 177724	A0Vn	9600± 200	2.32±0.05	IREX
118	TYC 8760 1468 1	CD-54 8168	K2V(e)	4765± 29	0.78±0.02	NO
119	HIP 94114	HD 178253	A0/A1V	9200± 200	2.18±0.05	IREX2B
120	HIP 95270	HD 181327	F6V	6436± 53	1.36±0.03	RES
121	HIP 95261	HD 181296	A0Vn	9500± 200	2.09±0.03	RES
122	HIP 95347	HD 181869	B8V	12500± 300	3.17±0.03	IREX
123	TYC 0486 4943 1		K3V	4640± 28	0.74±0.01	NO
124	TYC 7443 1102 1		M0.0V	3770± 50	0.74±0.03	BKG
125	HD 189285	BD-04 4987	G5	5655± 38	1.00±0.01	NO
126	HIP 98470	HD 189245	F7V	6330± 47	1.25±0.01	NO
127	HIP 98495	HD 188228	A0V	10000± 300	2.21±0.04	RES
128	2MASS J20013718-3313139		M1	3740± 50	0.72±0.03	NO

Table 8. (continued)

#	Name	other-ID	ST	$T_{\rm eff}$ (K)	Mstar $M_\odot$	Disk flag
129	TYC 8404 0354 1	CD-52 9381	K6Ve	4254± 27	0.64±0.01	NO
130	HIP 99742	HD 192425	A2V	8840± 150	2.01±0.04	RES
131	HIP 102409	HD 197481	M1Ve	3640± 50	0.64±0.03	RES
132	HIP 102626	HD 197890	K0V	4733± 30	1.08±0.05	IREX
133	TYC 1090 0543 1		K4Ve	4462± 30	0.71±0.01	NO
134	HIP 104365	HD 201184	A0V	9700± 200	2.19±0.06	NO
135	TYC 6351 0286 1	HD 201919	K6Ve	4338± 25	0.67±0.01	NO
136	HIP 105388	HD 202917	G7V	5464± 36	0.95±0.03	RES
137	TYC 9482 121 1	CD-81 812		4333± 80	0.68±0.01	NO
138	HIP 107345	GSC9116-1363	M0Ve	3890± 50	0.69±0.03	NO
139	HIP 107350	HD 206860	G0V	5953± 49	1.09±0.01	IREX
140	HIP 107412	HD 206893	F5V	6517± 48	1.32±0.02	RES
141	2MASS J22021626-4210329		M1	3660± 50	0.65±0.03	NO
142	TYC 9340 0437 1	CP-72 2713	K7Ve	3930± 50	0.79±0.03	RES
143	HIP 112312	GJ 871.1A	M4IVe	3170± 50	0.42±0.03	NO
144	HIP 113283	HD 216803	K4V	4612± 49	0.75±0.01	IREX
145	HIP 113368	HD 216956	A3V	8590± 73	1.92±0.03	RES
146	HIP 114189	HD 218396	A5V	7400± 60	1.53±0.02	RES
147	HIP 114530	HD 218860A	G8V	5510± 37	0.97±0.01	IREX
148	HIP 114948	HD 219482	F7V	6274± 41	1.21±0.01	IREX2B
149	HIP 115738	HD 220825	A0p	9400± 200	2.14±0.02	IREX2B
150	HIP 118008	HD 224228	K3V	4896± 30	0.81±0.01	IREX

Disk flags: RES: spatially resolved disks (not only with SPHERE, only at longer wavelength in several cases); IREX: IR excess from SED fitting; IREX2B: IR excess with double components from SED fitting, typically from Chen et al. (2014a); IREX? possible IR excess; NO: no detectable IR excess; BCK: IR excess is most likely due to background sources.

Table 9. Summary of target parameters: stellar ages. References: MG: age from membership to groups; Des20: this paper; Boc19: Boccaletti et al. (2019); Cha17: Chauvin et al. (2017a); Del17: Delorme et al. (2017) Laz18: Lazzoni et al. (2018); Mam12: Mamajek (2012), Vig17: Vigan et al. (2017).

#	Name	other-ID	other-ID	age Myr	min age Myr	max age Myr	source
1	HIP 490	HD 105		45	35	50	MG
2	HIP 682	HD 377		150	100	200	Des20
3	HIP 1113	HD 987		45	35	50	MG
4	2MASS J00172353-6645124	SCR 0017-6645		24	19	29	MG
5	HIP 1481	HD 1466		45	35	50	MG
6	HIP 1993	GSC8841-1145	CT Tuc	45	35	50	MG
7	HIP 2578	HD 3003		45	35	50	MG
8	HIP 6276	BD-12 243		149	100	180	MG
9	HIP 6485	HD 8558		45	35	50	MG
10	HIP 6856	HD 9054	CC Phe	45	35	50	MG
11	TYC 8047 0232 1	CD-52 381		42	35	50	MG
12	HIP 10602	HD 14228		45	35	50	MG
13	HIP 11360	HD 15115		45	35	50	MG
14	HIP 12394	HD 16978	eps Hyi	45	35	50	MG
15	HIP 13402	HD 17925	EP Eri	150	70	300	Vig17
16	HIP 14551	HD 19545	HR 943	42	35	50	MG
17	TYC 7026 0325 1	CD-35 1167		45	35	50	MG
18	HIP 15457	HD 20630	kap Cet	600	450	750	Des20
19	TYC 8060 1673 1	CD-46 1064		45	35	50	MG
20	HIP 17764	HD 24636		45	35	50	MG
21	HD 25284B	TYC 6461 1120 2		45	35	50	MG
22	TYC 5882 1169 1	BD-15 705	PPM 213757	45	35	50	MG
23	HIP 21547	HD 29391	51 Eri	24	19	29	MG
24	HIP 22226	HD 30447		42	35	50	MG
25	HIP 22295	HD 32195		45	35	50	MG
26	TYC 5899 0026 1	NLTT 14116	LP 776-25	149	100	180	MG
27	HIP 23200	V1005 Ori	GJ 182	24	19	29	MG
28	HIP 23309	CD-57 1054		24	19	29	MG
29	HIP 24947	HD 35114	AS Col	42	35	50	MG
30	HIP 25283	HD 35650		149	100	180	MG
31	HIP 25544	HD 36435	GJ 9180	700	550	850	Des20
32	HIP 27288	HD 38678	zeta Lep	350	19	500	Des20
33	HIP 27321	HD 39060	bet Pic	24	19	29	MG
34	TYC 7084 0794 1	CD-35 2722		149	100	180	MG
35	HIP 30030	HD 43989	V1358 Ori	42	35	50	MG
36	HIP 30034	HD 44627	AB Pic	45	35	50	MG
37	HIP 30314	HD 45270		149	100	180	MG
38	GSC 8894-0426	2RE J0625-600		149	100	180	MG
39	TYC 7617 0549 1	CD-40 2458		42	35	50	MG

Table 9. (continued)

#	Name	other-ID	other-ID	age Myr	min age Myr	max age Myr	source
40	HIP 31878	CD-61 1439		149	100	180	MG
41	HIP 32235	HD 49855		45	35	50	MG
42	TYC 8118 0871 1	HD 51797		42	35	50	MG
43	HIP 33737	HD 55279		45	35	50	MG
44	2MASS J07065772-5353463			45	35	50	MG
45	HIP 34899	HD 56022	OU Pup	295	185	405	Des20
46	TYC 1355 214 1	BD+20 1790	V429 Gem	149	100	180	MG
47	TYC 8128 1946 1	CD-48 2972		50	40	70	MG
48	HIP 36948	HD 61005		50	40	70	MG
49	HIP 37766	YZ CMi	GJ 285	100	20	200	Des20
50	HIP 41307	HD 71155	30 Mon	260	185	335	Laz18
51	HIP 42637	RECX2	eta Cha	11	8	14	MG
52	HD 75505	RECX13		11	8	14	MG
53	HIP 42808	HD 74576		250	120	400	Des20
54	HIP 44526	HD 77825	V405 Hya	300	200	450	Des20
55	HIP 47135	HD 84075		50	40	70	MG
56	HIP 50191	HD 88955	q Vel	460	40	650	Des20
57	TWA 6	GSC7183-1477	BX Ant	10	7	13	Des20
58	HIP 51228	HD 90712		150	70	200	Des20
59	HIP 51317	GJ 393	BD+01 2447	149	100	180	MG
60	TWA 7	GSC7190-2111	CE Ant	10	7	13	MG
61	HIP 53524	HD 95086		26	12	50	Des20
62	HIP 54155	HD 96064	HH Leo	250	200	400	Vig17
63	HIP 54231	HD 96338		16	12	380	Des20
64	HIP 57632	HD 102647	bet Leo	50	40	70	MG
65	HIP 58167	HD 103599		16	12	20	MG
66	HIP 58465	HD 104125		16	12	20	MG
67	HIP 59505	HD 106048		16	12	20	MG
68	HIP 60183	HD 107301	HR 4692	16	12	90	MG
69	HIP 60459	HD 107821		16	12	20	MG
70	HD 108767B		delCrvB	180	100	350	Vig17
71	HIP 61468	HD 109536		430	110	750	Des20
72	TWA 11	HIP 61498	HD 109573	10	7	13	MG
73	HIP 61960	HD 110411	rho Vir	100	20	180	Laz18
74	HIP 63839	HD 113457		16	12	20	MG
75	HIP 64892	HD 115470		16	12	20	MG
76	HIP 64995	HD 115600		16	12	20	MG
77	HIP 65426	HD 116434		14	10	18	Cha17
78	HIP 66252	HD 118100	EQ Vir	150	100	200	Vig17
79	HIP 66566	HD 118588		17	15	20	MG
80	HIP 66651	HD 118697		17	12	20	MG
81	HIP 68781	HD 122705		17	15	20	MG
82	TYC 7286 0248 1	CD-31 11053		17	15	20	MG

Table 9. (continued)

#	Name	other-ID	other-ID	age Myr	min age Myr	max age Myr	source
83	HIP 69989	HD 125451	18 Boo	500	400	1900	MG
84	HIP 71724	HD 128819		17	15	20	MG
85	HIP 71743	HD 128987	KU Lib	700	600	800	Des20
86	HIP 73145	HD 131835		17	15	20	MG
87	HIP 73990	HD 133803		17	15	20	MG
88	HIP 74824	HD 135379	beta cir	450	250	650	Des20
89	HIP 76063	HD 138204		220	15	400	Des20
90	HIP 77317	HD 140840		17	15	20	MG
91	HIP 77457	HD 141190		750	4	1200	Des20
92	HIP 77464	HD 141378		380	190	570	Laz18
93	TYC 7846 1538 1	HD 141943	NZ Lup	16	14	18	Boc19
94	HIP 78099	HD 142705		11	4	12	MG
95	HIP 78196	HD 142851		17	4	20	MG
96	HIP 78530	HD 143567		11	4	12	MG
97	HIP 78541	HD 143488		17	15	290	Des20
98	HIP 80324	HD 147553		17	15	20	MG
99	HIP 80591	HD 148055		17	15	20	MG
100	HIP 81084	LP 745-70		149	100	180	MG
101	TYC 7879 0980 1	HD 326277		17	15	20	MG
102	HIP 82388	HD 151798		150	100	300	Des20
103	HIP 82430	HD 151726		17	15	20	MG
104	TYC 7362 0724 1	HD 156097		11	8	20	Des20
105	TYC 8728 2262 1	CD-54 7336		24	19	29	MG
106	BD-13 4687	HD 159911		150	100	180	Des20
107	HIP 86305	HD 159492	pi Ara	570	360	780	Des20
108	HIP 86598	HD 160305		24	19	29	MG
109	HIP 88399	HD 164249A		24	19	29	MG
110	HIP 89829	HD 168210		24	19	29	MG
111	HIP 92024	HD 172555	HR 7012	24	19	29	MG
112	TYC 9073 0762 1	AC 4357199		24	19	29	MG
113	TYC 7408 0054 1	CD-31 16041		24	19	29	MG
114	HIP 92680	HD 174429	PZ Tel	24	19	29	MG
115	HIP 92984	HD 175726		400	200	600	Des20
116	HIP 93375	HD 176367		150	100	180	Des20
117	HIP 93747	HD 177724	zeta Aql	350	220	480	Des20
118	TYC 8760 1468 1	CD-54 8168		40	20	100	Des20
119	HIP 94114	HD 178253	alf CrA	380	290	470	Laz18
120	HIP 95270	HD 181327		24	19	29	MG
121	HIP 95261	HD 181296	eta Tel	24	19	29	MG
122	HIP 95347	HD 181869	alf Sgr	149	100	180	MG
123	TYC 0486 4943 1			150	100	200	Des20
124	TYC 7443 1102 1			24	19	29	MG
125	HD 189285	BD-04 4987		150	100	200	Des20

Table 9. (continued)

#	Name	other-ID	other-ID	age Myr	min age Myr	max age Myr	source
126	HIP 98470	HD 189245		150	80	300	Des20
127	HIP 98495	HD 188228	eps Pav	50	40	70	MG
128	2MASS J20013718-3313139			24	19	29	MG
129	TYC 8404 0354 1	CD-52 9381		50	40	70	MG
130	HIP 99742	HD 192425	rho Aql	400	250	550	Des20
131	HIP 102409	HD 197481	AU Mic	24	19	29	MG
132	HIP 102626	HD 197890	BO Mic	45	10	100	Vig17
133	TYC 1090 0543 1			150	100	200	MG
134	HIP 104365	HD 201184	chi Cap	140	35	240	Des20
135	TYC 6351 0286 1	HD 201919		149	100	180	MG
136	HIP 105388	HD 202917		45	35	50	MG
137	TYC 9482 121 1	CD-81 812		250	150	400	Des20
138	HIP 107345	GSC9116-1363	BPM14269	45	35	50	MG
139	HIP 107350	HD 206860	HN Peg	300	200	1000	Vig17
140	HIP 107412	HD 206893		250	50	650	Del17
141	2MASS J22021626-4210329			45	35	50	MG
142	TYC 9340 0437 1	CP-72 2713		24	19	29	MG
143	HIP 112312	GJ 871.1 A		24	19	29	MG
144	HIP 113283	HD 216803	TW PsA	440	40	40	Mam12
145	HIP 113368	HD 216956	Fomalhaut	440	40	40	Mam12
146	HIP 114189	HD 218396	HR 8799	42	19	50	Des20
147	HIP 114530	HD 218860A		149	100	180	MG
148	HIP 114948	HD 219482	GJ 1282	300	150	500	Des20
149	HIP 115738	HD 220825	kap Psc	149	100	180	MG
150	HIP 118008	HD 224228		149	100	180	MG

Flags or references: MG: age from membership to moving groups, associations or open cluster; Des20: this paper; Boc19: Boccaletti et al. (2019); Cha17: Chauvin et al. (2017b); Del17: Delorme et al. (2017); Laz18: Lazzoni et al. (2018); Mam12: Mamajek (2012); Vig17: Vigan et al. (2017).

Table 10. Wide companions to targets in the sample. Negative Δ mag means that the companion is brighter than the SPHERE target. When both components are included in the sample, separate entries are provided. For hierarchical multiple systems the sum of the masses of the components is listed as the mass of the companion to the SPHERE target.

#	Name SPH target	Name companion	rho arcsec	rho au	Δ mag mag	band	Mass target $M_\odot$	Mass companion $M_\odot$	remarks
	HIP 2578	HIP 2484/2487	552.3	25350			2.02	8.94	HIP 2484/HIP2487 quadruple
	HIP 14551	UCAC4 311-003056	59.3	3220	8.00	G	1.66	0.28	
	HD 25284B	HD 25284A	11.6	566	-0.02	V	0.77	0.77	
	51 Eri	GJ 3305	66.0	1966	4.60	G	1.55	1.11	GJ 3305 close bin
	HIP 22226	2MASS J04463413-262755	6220.0	50100			1.41	0.40	2M J0446-2627 close bin
	HIP 31878	HIP 31711	809.3	18000			0.64	1.83	HIP 31711 close bin
	TYC 8128-1946-1	HIP 36312	81.7	7150	-0.96	G	0.97	1.22	
	η Cha	EK Cha	194.1	19330	8.32	G	3.24	0.15	
	HD 75505	EH Cha	43.2	4320	5.75	G	1.68	0.25	
		EI Cha	131.2	13120	4.57	G	1.68	0.46	
	HIP 44526	UCAC4 371-053521	220.0	6020	3.31	G	0.80	0.40	
	HIP 51228	2MASS J10275043-3423521	33.1	1250	-4.62	G	1.11	0.50	
	HIP 54155	HD 96064B / C	11.5	301			0.94	1.20	HD 96064B/C close pair
	HIP 58167	2MASS J11551267-5406215	382.0	41250	10.32	G	1.52	0.02	BD companion
	HD 108767B	δ Crv A	23.4	625	-5.57	V	0.83	2.39	
	HIP 61468	2MASS J12354637-4101315	15.6	544	8.82	G	1.65	0.26	
	TWA 11	TWA 11B	7.8	560	6.19	G	2.19	0.62	
		TWA 11C	174.8	12570	7.19	G		0.40	
	HIP 68781	2MASS J14043341-5003571	86.5	10600	10.41	G	1.78	0.050	
	HIP 71724	HD 128819B	8.7	1430	2.91	Ks	2.86	1.06	
	KU Lib	α Lib	9348.0	233000			0.97	5.70	α Lib quadruple
	HIP 73990	2MASS J15071795-2929501	47.2	5230	6.59	G	1.56	0.28	
	β Cir	β Cir B	217.6	6660	15.46	G	1.95	0.056	BD companion
	HIP 77317	HIP 77315	34.7	5140	-0.34	V	2.22	3.90	HIP 77315 close bin
	HIP 77464	2MASS J15490081-0348147	79.2	4240	10.03	G	1.86	0.20	
	HIP 78099	2MASS J15564019-2309291	141.1	20360	8.61	G	2.30	0.15	
	HIP 80324	HD 147553B	6.2	860	0.35	V	2.62	2.06	
	HIP 80591	2MASS J16271281-3949144	21.9	3210	7.88	G	1.65	0.16	
	HIP 88399	HD 164249B	6.5	320	5.50	V	1.39	0.60	
	HIP 92024	TYC 9077 2489 1	71.5	2040	4.66	V	1.66	1.31	TYC 9077 2489 1 close bin
	TYC 9073-0762-1	HD 173167	550.3	27820	4.55	V	0.73	1.32	
	ζ Aql	ADS 12026 B	7.3	185	4.87	K	2.32	0.50	
	HIP 95270	η Tel	416.3	20070	-1.92	V	1.36	2.09	η Tel has BD companion
	η Tel	HIP 95270	416.3	20070	1.92	V	2.09	1.36	η Tel has BD companion
	TYC 0486 4943 1	2MASS J19330197+0345484	28.0	1970	1.86	G	0.74	0.62	
	TYC 7443 1102 1	U0578-1079977	26.0	1330	1.07	G	0.74	0.71	
	TYC 1090-0543-1	HD 199058	245.1	18340	-2.80	G	0.71	1.90	HD 199058 close bin

Table 10. (continued)

#	Name SPH target	Name companion	rho arcsec	rho au	Δ mag mag	band	Mass target $M_\odot$	Mass companion $M_\odot$	remarks
	AU Mic	AT Mic	4680.1	45500	1.73	V	0.64	0.50	AT Mic close bin
	HIP 104365	WDS 21086-2112E / F	9.5	570	7.40	CH4	2.19	0.22	WDS 21086-2112 EF close bin
	HIP 107350	HN Peg B	42.9	780	10.56	Ks	1.09	0.021	BD companion
	HIP 112312	TX PsA	35.9	750	1.10	G	0.42	0.22	
	Fomalhaut	Fomalhaut B	7062.7	54400	5.33	V	1.92	0.75	
		Fomalhaut C	20407.6	157200	11.46	V		0.18	
	Fomalhaut B	Fomalhaut	7062.7	54400	-5.33	V	0.75	1.92	
		Fomalhaut C			6.13	V		0.18	
	HIP 114530	HD 218860B	19.6	940	4.20	V	0.97	0.54	

Table 11. Parameters adopted in the original selection. MF15, MF30, and MF50 are the merit functions for cut-offs of planet distribution to 15, 30, and 50 au, respectively.

#	Name	other-ID	other-ID	Mass	Distance (pc)	Age (Myr)	MG	Priority	MF15	MF30	MF50
1	HIP 490	HD 105		1.13	39.4	30	TUC	1	0.0397	0.0816	
2	HIP 682	HD 377		1.12	39.1	150	–	2	0.0218	0.0434	
3	HIP 1113	HD 987		0.98	44.4	30	TUC	1	0.0323	0.0674	
4	2M J0017-6645	SCR 0017-6645		0.53	39.0	16	BPIC	1	0.0254	0.0480	
5	HIP 1481	HD 1466		1.16	41.5	30	TUC	1	0.0384	0.0752	
6	HIP 1993	GSC8841-1145	CT Tuc	0.65	42.0	30	TUC	1	0.0229	0.0465	
7	HIP 2578	HD 3003		1.87	45.6	30	TUC	1	0.0471	0.1026	
8	HIP 6276	BD-12 243		0.95	34.4	100	ABDO	1	0.0255	0.0474	
9	HIP 6485	HD 8558		1.05	49.5	30	TUC	1	0.0306	0.0642	
10	HIP 6856	HD 9054	CC Phe	0.88	36.0	30	TUC	1	0.0367	0.0681	
12	HIP 10602	HD 14228		2.83	47.1	30	TUC	1	0.0078	0.0174	
13	HIP 11360	HD 15115		1.33	45.2	30	TUC	1	0.0384	0.0790	
14	ϵ Hyi	HIP 12394	HD 16978	2.39	46.6	30	TUC	1	0.0298	0.0650	
15	HIP 13402	HD 17925	EP Eri	0.92	10.4	120	–	1	0.0416	0.0427	
16	HIP 14551	HD 19545	HR 943	1.65	57.6	30	TUC	1	0.0341	0.0801	
17	TYC 7026 0325 1	CD-35 1167		0.78	56.4	30	TUC	1	0.0206	0.0449	
18	κ Cet	HIP 15457	HD 20630	1.05	9.2	456	–	2	0.0222	0.0212	
19	TYC 8060 1673 1	CD-46 1064		0.84	40.4	30	TUC	1	0.0313	0.0618	
20	HIP 17764	HD 24636		1.35	54.9	30	TUC	1	0.0301	0.0710	
21	HD 25284B	TYC 6461 1120 2		0.79	50.2	40	TUC	1	0.0199	0.0447	
22	TYC 5882 1169 1	BD-15 705	PPM 213757	0.85	53.2	30	COL	1	0.0237	0.0523	
23	51 Eri	HIP 21547	HD 29391	1.49	29.4	16	BPIC	1	0.0735	0.1233	
24	HIP 22226	HD 30447		1.38	80.3	30	COL	2	0.0183	0.0526	
25	HIP 22295	HD 32195		1.19	61.0	30	TUC	1	0.0272	0.0621	
26	TYC 5899 0026 1	NLTT 14116	LP 776-25	0.50	12.9	100	ABDO	1	0.0266	0.0297	
27	HIP 23200	V1005 Ori	GJ 182	0.69	25.9	16	BPIC	1	0.0451	0.0700	
28	HIP 23309	CD-57 1054		0.70	26.8	16	BPIC	1	0.0446	0.0693	
29	HIP 24947	HD 35114	AS Col	1.25	48.3	30	COL	1	0.0357	0.0723	
30	HIP 25283	HD 35650		0.71	18.0	100	ABDO	1	0.0317	0.0404	
31	HIP 25544	HD 36435	GJ 9180	0.98	19.6	526	–	3	0.0170	0.0239	
32	HIP 27288	HD 38678	zeta Lep	1.83	21.6	320	CAS	2	0.0349	0.0519	
33	β Pic	HIP 27321	HD 39060	1.64	19.4	16	BPIC	1	0.0993	0.1308	
34	TYC 7084 0794 1	CD-35 2722		0.55	21.3	100	ABDO	1	0.0237	0.0314	
35	HIP 30030	HD 43989	V1358 Ori	1.14	49.2	30	TUC	1	0.0306	0.0674	
36	AB Pic	HIP 30034	HD 44627	0.94	46.1	30	CAR	1	0.0305	0.0635	
37	HIP 30314	HD 45270		1.11	23.8	100	ABDO	1	0.0364	0.0572	
38	GSC 8894-0426	2RE J0625-600		0.50	23.0	100	ABDO	1	0.0187	0.0273	
39	TYC 7617 0549 1	CD-40 2458		0.97	77.8	30	COL	1	0.0155	0.0416	
40	HIP 31878	CD-61 1439		0.69	22.4	100	ABDO	1	0.0268	0.0392	
41	HIP 32235	HD 49855		1.04	58.2	30	CAR	1	0.0246	0.0575	
42	HD 51797	TYC 8118 0871 1		0.97	71.7	30	COL	1	0.0181	0.0465	

Table 11. (continued)

#	Name	other-ID	other-ID	Mass	Distance (pc)	Age (Myr)	MG	Priority	MF15	MF30	MF50
43	HIP 33737	HD 55279		0.89	58.8	30	TUC	1	0.0220	0.0495	
44	2M J0706-5353										
45	HIP 34899	HD 56022	OU Pup	2.18	55.6	281	–	3	0.0138	0.0358	
46	TYC 1355 214 1	BD+20 1790	V429 Gem	0.78	28.3	100	ABDO	1	0.0278	0.0444	
47	TYC 8128 1946 1	CD-48 2972		1.05	89.7	40	ARG	2	0.0117	0.0365	
48	HIP 36948	HD 61005		0.99	35.3	40	ARG	1	0.0364	0.0680	
49	HIP 37766	YZ CMi	GJ 285	0.26	6.0	100	–	2	0.0114	0.0119	
50	HIP 41307	HD 71155	30 Mon	2.23	37.5	170	–	2	0.0238	0.0506	
51	η Cha	HIP 42637	RECX2	2.57	97.0	7	ETAC	1	0.0104	0.0370	
52	HD 75505	RECX13		1.81	97.0	7	ETAC	1	0.0287	0.0904	
53	HIP 42808	HD 74576		0.88	11.1	200	–	2	0.0328	0.0332	
54	HIP 44526	HD 77825	V405 Hya	0.86	28.3	320	CAS	3	0.0162	0.0286	
55	HIP 47135	HD 84075		1.12	63.0	40	ARG	1	0.0212	0.0516	
56	HIP 50191	HD 88955	q Vel	2.06	31.5	45	ARG?	1	0.0561	0.1072	
57	TWA 6	GSC7183-1477	BX Ant	0.69	62.4	8	TWA	1	0.0246	0.0552	
58	HIP 51228	HD 90712		1.13	39.0	100	–	2	0.0243	0.0500	
59	HIP 51317	GJ 393	BD+01 2447	0.44	7.1	100	ABDO	1	0.0216	0.0222	
60	TWA 7	GSC7190-2111	CE Ant	0.59	34.5	8	TWA	1	0.0367	0.0643	
61	HIP 53524	HD 95086		1.59	91.6	16	LCC	1			0.1153
62	HIP 54155	HD 96064	HH Leo	0.98	26.3	200	–	2	0.0248	0.0392	
63	HIP 54231	HD 96338		1.93	108.3	16	LCC	1			0.1207
64	β Leo	HIP 57632	HD 102647	1.81	11.1	40	ARG	1	0.0842	0.0872	
65	HIP 58167	HD 103599		1.36	90.9	16	LCC	1			0.1041
66	HIP 58465	HD 104125		1.84	96.7	16	LCC	1			0.1146
67	HIP 59505	HD 106048		1.35	108.6	16	LCC	3			0.0914
68	HIP 60183	HD 107301	HR 4692	2.13	99.0	16	LCC	1			0.1097
69	HIP 60459	HD 107821		1.62	97.9	16	LCC	1			0.1135
70	HD 108767B		δ CrvB	0.87	26.6	180	–	2	0.0237	0.0389	
71	HIP 61468	HD 109536		1.65	35.5	421	–	3	0.0180	0.0410	
72	TWA 11	HIP 61498	HD 109573	1.93	67.1	8	TWA	1	0.0468	0.1207	
73	ρ Vir	HIP 61960	HD 110411	1.76	36.9	27	–	1	0.0600	0.1201	
74	HIP 63839	HD 113457		1.88	95.1	16	LCC	1			0.1290
75	HIP 64892	HD 115470		1.95	110.4	16	LCC	1			0.1161
76	HIP 64995	HD 115600		1.46	111.2	16	LCC	3			0.0913
77	HIP 65426	HD 116434		1.83	105.9	16	LCC	1			0.1153
78	HIP 66252	HD 118100	EQ Vir	0.72	20.2	90	–	2	0.0308	0.0415	
79	HIP 66566	HD 118588		1.70	116.0	16	LCC	1			0.1085
80	HIP 66651	HD 118697		1.79	117.6	16	LCC	1			0.1081
81	HIP 68781	HD 122705		1.61	106.7	17	UCL	1			0.1036
82	TYC 7286 0248 1	CD-31 11053		0.79	62.1	15	–	2	0.0231	0.0505	
83	HIP 69989	HD 125451	18 Boo	1.38	26.1	500	UMA	3	0.0197	0.0337	
84	HIP 71724	HD 128819		2.14	122.7	17	UCL	3			0.0907
85	HIP 71743	HD 128987	KU Lib	1.00	23.6	589	–	4	0.0153	0.0233	

Table 11. (continued)

#	Name	other-ID	other-ID	Mass	Distance (pc)	Age (Myr)	MG	Priority	MF15	MF30	MF50
86	HIP 73145	HD 131835		1.56	111.1	17	UCL	2			0.0976
87	HIP 73990	HD 133803		1.41	97.2	17	UCL	2			0.0971
88	β Cir	HIP 74824	HD 135379	1.90	29.6	166	–	1	0.0394	0.0715	
89	HIP 76063	HD 138204		1.58	53.6	274	–	3	0.0134	0.0342	
90	HIP 77317	HD 140840		1.79	118.3	17	UCL	1			0.1045
91	HIP 77457	HD 141190		1.72	144.7	11	US	2			0.0905
92	HIP 77464	HD 141378		1.75	49.2	203	–	2	0.0194	0.0482	
93	HD 141943	TYC 7846 1538 1	NZ Lup	1.09	52.9	16	UCL?	2	0.0333	0.0709	
94	HIP 78099	HD 142705		1.69	125.3	11	US	1			0.1023
95	HIP 78196	HD 142851		1.86	111.4	11	US	1			0.1295
96	HIP 78530	HD 143567		1.95	131.9	11	US	1			0.1107
97	HIP 78541	HD 143488		2.02	129.0	17	UCL	1			0.1028
98	HIP 80324	HD 147553		2.19	116.8	11	US	1			0.1107
99	HIP 80591	HD 148055		1.47	117.6	17	UCL	2			0.0873
100	HIP 81084	LP 745-70		0.60	30.7	100	ABDO	1	0.0184	0.0320	
101	HD 326277	TYC 7879 0980 1		1.00	89.5	30	–	3	0.0126	0.0381	
102	HIP 82388	HD 151798		1.08	41.4	170	–	3	0.0186	0.0379	
103	HIP 82430	HD 151726		1.91	129.4	17	UCL	2			0.1027
104	HD 156097	TYC 7362 0724 1		1.06	81.8	20	–	2	0.0172	0.0483	
105	TYC 8728 2262 1	CD-54 7336		0.93	70.4	16	BPIC	1	0.0204	0.0527	
106	HD 159911	BD-13 4687		0.77	26.2	100	ABDO	1	0.0306	0.0452	
107	π Ara	HIP 86305	HD 159492	1.73	42.2	50	–	1	0.0399	0.0841	
108	HIP 86598	HD 160305		1.25	76.0	16	BPIC	1	0.0240	0.0645	
109	HIP 88399	HD 164249A		1.32	48.1	16	BPIC	1	0.0433	0.0938	
110	HIP 89829	HD 168210		1.13	72.6	16	BPIC	1	0.0231	0.0621	
111	HIP 92024	HD 172555	HR 7012	1.61	28.5	16	BPIC	1	0.0778	0.1301	
112	TYC 9073 0762 1	AC 4357199		0.61	45.9	16	BPIC	1	0.0251	0.0513	
113	TYC 7408 0054 1	CD-31 16041		0.67	45.5	16	BPIC	1	0.0276	0.0536	
114	PZ Tel	HIP 92680	HD 174429	1.10	51.5	16	BPIC	1	0.0350	0.0794	
115	HIP 92984	HD 175726		1.13	27.0	424	–	3	0.0175	0.0293	
116	HIP 93375	HD 176367		1.12	58.8	100	ABDO	1	0.0164	0.0387	
117	ζ Aql	HIP 93747		2.28	25.5	260	–	2	0.0262	0.0441	
118	TYC 8760 1468 1	CD-54 8168		0.86	57.7	40	–	2	0.0203	0.0449	
119	α CrA	HIP 94114	HD 178253	2.19	39.8	254	–	2	0.0193	0.0468	
120	HIP 95270	HD 181327		1.35	51.8	16	BPIC	1	0.0410	0.0894	
121	η Tel	HIP 95261	HD 181296	1.94	48.2	16	BPIC	1	0.0561	0.1266	
122	α Sgr	HIP 95347	HD 181869	2.68	52.1	100	ABDO	1	0.0083	0.0214	
123	TYC 0486 4943 1			0.82	75.8	100	ABDO	2	0.0095	0.0231	
124	TYC 7443 1102 1			0.55	51.1	16	BPIC	1	0.0186	0.0396	
125	HD 189285	BD-04 4987		1.06	77.8	100	ABDO	2	0.0108	0.0277	
126	HIP 98470	HD 189245		1.23	21.2	100	–	1	0.0424	0.0570	
127	ϵ Pav	HIP 98495	HD 188228	2.03	32.2	40	ARG	1	0.0571	0.1089	
128	2M J2001-3313			0.50	61.3	16	BPIC?	2	0.0137	0.0308	

Table 11. (continued)

#	Name	other-ID	other-ID	Mass	Distance (pc)	Age (Myr)	MG	Priority	MF15	MF30	MF50
129	TYC 8404 0354 1	CD-52 9381		0.72	43.3	40	ARG	1	0.0227	0.0458	
130	ρ Aql	HIP 99742	HD 192425	1.96	47.1	370	–	2	0.0170	0.0442	
131	AU Mic	HIP 102409	HD 197481	0.61	9.9	16	BPIC	1	0.0505	0.0545	
132	BO Mic	HIP 102626	HD 197890	0.94	52.2	30	TUC	1	0.0244	0.0538	
133	TYC 1090 0543 1	QV Del		0.73	66.1	100	ABDO	2	0.0102	0.0239	
134	HIP 104365	HD 201184	χ Cap	2.01	58.6	149	–	2	0.0200	0.0539	
135	HD 201919	TYC 6351 0286 1		0.74	38.5	100	ABDO	1	0.0189	0.0370	
136	HIP 105388	HD 202917		0.98	43.0	30	TUC	1	0.0341	0.0676	
137	TYC 9482 121 1	CD-81 812		0.73	21.7	200	–	2	0.0245	0.0326	
138	HIP 107345	GSC9116-1363	BPM14269	0.65	43.6	30	TUC	1	0.0237	0.0459	
139	HIP 107350	HD 206860	HN Peg	1.11	17.9	300	–	2	0.0277	0.0351	
140	HIP 107412	HD 206893		1.28	38.9	556	–	4	0.0113	0.0252	
141	2M J2202-4210										
142	TYC 9340 0437 1	CP-72 2713		0.67	35.6	16	BPIC	1	0.0347	0.0639	
143	HIP 112312	GJ 871.1A		0.46	23.3	16	BPIC	1	0.0318	0.0452	
144	HIP 113283	HD 216803	TW PsA	0.79	7.6	440	–	3	0.0203	0.0215	
145	Fomalhaut	HIP 113368	HD 216956	1.89	7.7	440	–	2	0.0340	0.0351	
146	HR 8799	HIP 114189	HD 218396	1.46	39.4	30	COL	1	0.0466	0.0927	
147	HIP 114530	HD 218860A		1.02	49.4	100	ABDO	1	0.0183	0.0439	
148	HIP 114948	HD 219482	GJ 1282	1.22	20.6	400	–	2	0.0245	0.0366	
149	κ Psc	HIP 115738	HD 220825	2.01	49.7	100	ABDO	1	0.0308	0.0722	
150	HIP 118008	HD 224228		0.86	22.0	100	ABDO	1	0.0355	0.0467	

[1] INAF-Osservatorio Astronomico di Padova, Vicolo dell'Osservatorio 5, 35122 Padova, Italy
[2] Univ. Grenoble Alpes, CNRS, IPAG, F-38000 Grenoble, France
[3] SUPA, Institute for Astronomy, University of Edinburgh, Blackford Hill, Edinburgh EH9 3HJ, UK
[4] Centre for Exoplanet Science, University of Edinburgh, Edinburgh EH9 3HJ, UK
[5] INAF - Osservatorio Astrofisico di Catania, Via S. Sofia 78, I-95123, Catania, Italy
[6] Aix Marseille Univ, CNRS, CNES, LAM, Marseille, France
[7] Hamburger Sternwarte, Gojenbergsweg 112, D-21029 Hamburg, Germany
[8] LESIA, Observatoire de Paris, Université PSL, CNRS, Sorbonne Université, Université de Paris, 5 place Jules Janssen, 92195 Meudon, France
[9] Dipartimento di Fisica e Astronomia Galileo Galilei, Universitá di Padova, Vicolo dell'Osservatorio 3, I-35122, Padova, Italy
[10] Department of Astronomy, University of Michigan, Ann Arbor, MI 48109, USA
[11] Institute for Particle Physics and Astrophysics, ETH Zurich, Wolfgang-Pauli-Strasse 27, 8093 Zurich, Switzerland
[12] Exoplanets and Stellar Astrophysics Laboratory, Code 667, NASA Goddard Space Flight Center, 8800 Greenbelt Rd., Greenbelt, MD 20771, USA
[13] Max Planck Institute for Astronomy, Königstuhl 17, D-69117 Heidelberg, Germany
[14] Geneva Observatory, University of Geneva, Chemin des Mailettes 51, 1290 Versoix, Switzerland
[15] CRAL, CNRS, Université Lyon 1, Université de Lyon, ENS, 9 avenue Charles Andre, 69561 Saint Genis Laval, France
[16] Perth Exoplanet Survey Telescope, Western Australia, Australia
[17] Remote Observatory Atacama Desert, Chile
[18] York Creek Observatory, Georgetown, Tasmania, Australia
[19] INAF - Osservatorio Astronomico di Capodimonte, Salita Moiariello 16, 80131 Napoli, Italy
[20] INAF - Osservatorio Astronomico di Palermo, Piazza del Parlamento, 1, I-90134 Palermo, Italy
[21] College of Charleston, Department of Physics & Astronomy, 66 George St, Charleston, SC 29424 USA
[22] Department of Astronomy, Stockholm University, SE-10691 Stockholm, Sweden
[23] Anton Pannekoek Institute for Astronomy, Science Park 9, NL-1098 XH Amsterdam, The Netherlands
[24] Center for Space and Habitability, University of Bern, 3012 Bern, Switzerland
[25] Universite Cote d'Azur, OCA, CNRS, Lagrange, France
[26] INAF - Osservatorio Astronomico di Brera, Via E. Bianchi 46, 23807 Merate, Italy
[27] STAR Institute, University of Liège, Allée du Six Août 19c, B-4000 Liège, Belgium
[28] Núcleo de Astronomía, Facultad de Ingeniería y Ciencias, Universidad Diego Portales, Av. Ejercito 441, Santiago, Chile
[29] Escuela de Ingeniería Industrial, Facultad de Ingeniería y Ciencias, Universidad Diego Portales, Av. Ejercito 441, Santiago, Chile
[30] DKFZ, Heidelberg, Germany
[31] Ural Federal University, Yekaterinburg, 620002, Russia
[32] INAF-Osservatorio Astrofisico di Arcetri Largo Enrico Fermi 5, I-50125 Firenze, Italy
[33] ONERA (Office National dEtudes et de Recherches Arospatiales),B.P.72, F-92322 Chatillon, France
[34] European Southern Observatory (ESO), Karl-Schwarzschild-Str. 2, D-85748 Garching, Germany
[35] NOVA Optical Infrared Instrumentation Group, Oude Hoogeveensedijk 4, 7991 PD Dwingeloo, The Netherlands